UNIVERSITY OF CALIFORNIA
RIVERSIDE

Engineering of Silver Nanoparticles for Enhanced Raman Spectroscopy

A Dissertation submitted in partial satisfaction
of the requirements for the degree of

Doctor of Philosophy

in

Chemical and Environmental Engineering

by

Ning Yu

December 2022

Dissertation Committee:
Dr. Ruoxue Yan, Chairperson
Dr. Juchen Guo
Dr. Bryan Wong

The Dissertation of Ning Yu is approved:

_____

_____

_____

Committee Chairperson

University of California, Riverside

ACKNOWLEDGEMENTS

First and foremost, I want to express my most profound appreciation to my Ph.D. advisor, Prof. Ruoxue Yan, for her constant support and valuable guidance along this journey. It has been a great honor getting my Ph.D. training in her research group, where I was not only allowed to conduct pioneering research in the field of nanomaterial synthesis and their application in enhanced Raman spectroscopy but also I get to learn how to tackle challenging problems systematically which is more important as an independent researcher. She is a knowledgeable, talented scientist and a supportive, thoughtful mentor. Without her, I will never have come this far in my research.

I sincerely thank my committee members, Prof. Juchen Guo and Prof. Bryan Wong, for their valuable insights and precious time and patience. They are the perfect examples of outstanding researchers who work diligently and smartly.

I also want to thank Prof. Ming Liu for his guidance and many helpful discussions when a chemical engineer gets lost in the field of optics. His insights into my research and recommendations are really appreciated. Prof. Liu has always been so supportive that he comes to the lab in minutes when help is needed.

You cannot choose who you work with, but I was lucky enough to work with a group of wonderful lab mates. I want to thank everyone I have worked with from Yan and Liu groups. I want to thank Dr. Sanggon Kim for his valuable training when I joined the Yan group without any knowledge of near-field scanning optical microscopy. I want to thank Dr. Yangzhi Zhu for his training on silver nanowire synthesis and his continuous helpful discussions even after he graduated from UC Riverside. I also want to thank Dr. Qiushi Liu, Dr. Xuezhi Ma, Da Xu, Yaodong Xu, Boqun Liang, and Zhaoxi Yang for their many

valuable discussions and assistance on my projects. Without the help from my lab mates and collaborators, it would have been impossible for me to complete all the work in this dissertation.

I am highly grateful to my family. My parents, Mr. Fagao Yu and Mrs. Yun Song have always been supportive when I seek higher education abroad. Their unconditional love and support keep me continuing with my dream. My sister, Mrs. Haixia Yu, gives me so much support that knowing she is there taking good care of my parents gives me a peaceful mind, especially during the COVID-19 pandemic.

Last but not least, I would like to dedicate this work to my lovely, beautiful wife, Yan Liu. She is so amazingly supportive, and I could not imagine a day without her love and faith in me. Along this journey, I have faced so many difficulties and frustration. Whenever I doubted myself, her love and encouragement gave me the power to carry on. I am the luckiest person in the world to have her standing by me.

ABSTRACT OF THE DISSERTATION

Engineering of Silver Nanoparticles for Enhanced Raman Spectroscopy

by

Ning Yu

Doctor of Philosophy, Graduate Program in Chemical and Environmental Engineering
University of California, Riverside, December 2022
Dr. Ruoxue Yan, Chairperson

While Raman is a powerful tool that can be used to identify chemicals in a mixed environment, two of the major issues with the conventional Raman are weak signal intensity and low spatial resolution. To resolve these issues, surface and tip-enhanced Raman spectroscopy have been developed that surface-enhanced Raman spectroscopy (SERS) mainly focuses on solving the problem of weak Raman signal, while tip-enhanced Raman spectroscopy (TERS) can improve the spatial resolution overcoming the diffraction limit while enhancing Raman signal. In this work, we report a one-pot synthesis method for monodispersed silver nanocubes with tunable sizes ranging from 60 to 180 nm and investigate the size effect of silver nanocubes when monolayer close-packed silver nanocubes are used as SERS substrate. With the tunable size of silver nanocubes, the size-dependent of SERS substrate was demonstrated. TERS combines traditional Raman spectroscopy and near-field scanning optical microscopy that overcomes the diffraction limit, enabling to obtain of Raman spectroscopy and topological image simultaneously at the nanoscale. Chemically

synthesized silver nanowires (AgNWs) have been reported to be used as scanning probes. Specifically, AgNW with sharp tips can significantly improve the Raman signals and spatial resolution. Here a two-step polyol synthetic method was developed to promote oxidative etching selectively to the ends of AgNWs, which eventually produced sharp-tip AgNWs with over 96% selectivity and an average tip radius of 7.87 nm. Among atomic force microscope (AFM) probes fabricated by mounting silver nanowires with different tip sharpness onto commercial AFM cantilevers, the probe based on ultra-sharp AgNW showed significant improvement in spatial resolution in topographic scanning and enhancement factor of TERS tests over the same carbon nanotube sample compared to the probes based on AgNWs with pentagonal pyramid or rounded ends. To broaden the application of TERS in the catalysis field, a second noble metal (Pd, Pt) was grown onto ultra-sharp AgNWs creating a uniform core-shell structure with tunable shell thickness. The resulting nanowires show minimal light scattering and strong tip emission when mounted onto optical fiber under excitation light of 532 nm and 650 nm wavelength suggesting feasibility as TERS probes.

Table of Content

List of Figures

List of Tables

Chapter 1. Introduction

1.1 Raman Spectroscopy

Vibrational spectroscopy such as Raman and infrared spectroscopy are important tools in chemical identification that providing “fingerprints” information of particular molecules as the frequencies of molecular vibrations depend on the masses of atoms, the geometric arrangement and the strength of chemical bonds. Both Raman and IR spectroscopy deals with same vibrational energy levels of the same materials and can provide useful information to identify chemical bonds, but they are different in the fundamental principle that while IR spectroscopy depends on dipole movement change, Raman scattering mainly depends on the polarization change of chemical bonds. Compared with IR, Raman spectroscopy has the advantage in identifying different components in mixtures as it has narrower bandwidth.[1] Also, Raman measurement needs minimum preparation of the sample and due to weak water spectrum, Raman measurements can be carried out in biological fluids.[2]

For Raman spectroscopy, a monochromatic light source is used which is usually from a laser in the visible, near infrared, or near ultraviolet. When photons of incident light interact with a molecule, an electron may be excited to a higher energy level (i.e., an excited virtual state) but not fully undergo an electronic transition. The electron then can relax to a vibrational energy level that is different from that of the incident energy. The difference between the energy of the incident photon and the energy of the scattered photon is called the Raman shift. The molecule's interaction with light can induce a shifting of the molecule's electron cloud that results in a change in polarizability. A molecule has specific energy transitions related to its intramolecular bonds in which a

change of polarizability occurs, and these changes give rise to Raman active modes. The frequency of the Raman shift is related to the type of bond being excited and the intensity of this Raman peak is proportional to the number of those bonds.

While Raman is a powerful tool that can be used to identify chemicals in a mixed environment, two of the major issues with the conventional Raman are weak signal intensity and low spatial resolution. The Raman effect is weak (often referred to as a one in ten million event), resulting from an energy event when photons of monochromatic light (laser) interact with a molecule that leads to a release of inelastic photons. In terms of spatial resolution, similar to other optical microscopies, the best spatial resolution Raman can achieve is half of the excitation wavelength because of diffraction limit. These two issues significantly impede the wider application of Raman in research. To resolve these issues, surface and tip enhanced Raman spectroscopy has been developed that surface-enhanced Raman spectroscopy (SERS) mainly focused on solving the issue of weak Raman signal while tip-enhanced Raman can improve the spatial resolution overcoming the diffraction limit while enhancing Raman signal.

1.2 Surface-Enhanced Raman Spectroscopy

1.2.1 Mechanism of SERS

When photons interact with materials, they can scatter inelastically, losing energy when a molecule moves from the ground state to its first excited vibrational state (Stokes Raman scattering), or gaining energy when a molecule moves in the other direction (anti-Stokes Raman scattering). Inelastically scattered photons carry information about the vibrational modes of the materials they interact with in the form of energy changes that can be used to identify the materials.[3] Raman is an intrinsically very weak phenomena, around six to

ten orders of magnitude less effective than fluorescence even though Raman spectra typically report Stocks scattering due to their noticeably greater intensity relative to the anti-Stokes.[4] However, the Raman scattering generated by molecules can be strongly amplified by placing them near the surface of suitably nanostructured substrates which is called surface-enhanced Raman scattering (SERS). Surface-enhanced Raman scattering (SERS), initially reported by Fleischmann *et al*. in 1974[5] and explained by Van Duyne[6] and Albrecht[7] in 1977, uses the localized surface plasmon resonance (LSPR) at the surface of an amorphous metal film to increase the Raman scattering cross-sections of the specimen. After a few decades of development, SERS has pushed the chemical sensitivity down to the single-molecule level[8, 9] and has been applied to a broad range of applications, such as biomolecule detections[10] and chemical reaction mechanism study.[11] Over the years, the origin of SERS has been attributed to the electromagnetic and chemical effect. [4, 12-16]

When a molecule is placed on the surface of a metallic substrate, surface plasmons are excited and produced an increased electromagnetic field when irradiated with laser light. The electromagnetic enhancement possesses two distinct contributions: the local field (or near field) enhancement and re-radiation enhancement. Local field enhancement refers to the hot spot caused by stimulation of surface plasmons that is localized at smack regions where the laser light is magnified. Because of the metallic substrate, the electromagnetic field that molecules in hot spots experience is substantially stronger than it would be otherwise. The presence of the metallic structure nearby the molecule also modifies the efficiency with which the molecule radiates Raman power; this occurs because the power radiated by a dipole depends on the environment in which it is embedded.

Even though the chemical enhancement is significantly smaller in magnitude than the electromagnetic enhancement, it still has a substantial influence in determining the spectrum pattern of the SERS spectra such as the Raman shifts and the band intensity ratios. The adsorption of a molecule on a substrate can be classified on the basis of the strength of the interaction. When a molecule is absorbed on substrate surface by physisorption, Van der Waals forces drive the adsorption process and therefore, the structure of the molecule is only slightly modified. For chemisorption, a chemical bond is formed between the molecule and the surface which is a much stronger form of interaction. In both situations, although at a different extent, the electronic and geometrical structure of the molecule is altered by the interaction with the surface and, hence, the Raman cross-sections of its vibrational modes will be different with respect to those of the free molecule. Two different mechanisms can contribute to the chemical enhancement which are non-resonant chemical effect and resonant charge transfer chemical effect.[17] For non-resonant chemical effects, the molecule's interaction with the metal does not result in the formation of a new electronic state because the molecular orbitals are not located at energies close enough to the metal's Fermi level. However, this interaction may cause a significant alteration to the molecule's geometrical and electronic structure, which arises as a slight modification to the Raman shifts and the strength of the vibrational modes. For resonant charge transfer chemical effect, a metal-molecule charge transfer (CT) state is produced as a result of the contact between the molecule and the metal. Some Raman modes, especially those related to the allowed electronic transitions (resonant Raman scattering[18]), may be greatly amplified if the Raman scattering is generated with a laser source in resonance or pre-resonance with this state.

With SERS the issue of weak signal intensity associated with normal Raman is resolved and enhancement factor (EF) is usually used to characterize the SERS performance. Theoretically, EF is derived by often-stated E^4 enhancement approximation. However, in practical use, it is often simpler to experimentally measure the EF analytically than to predict it theoretically. The EF for a SERS system can be described by

$$EF = \frac{I_{SERS}/N_{surf}}{I_{NRS}/N_{vol}}$$

which evaluated at a single excitation wavelength, describes the average Raman enhancement, where I_{SERS} is the surface-enhanced Raman intensity, N_{surf} is the number of molecules bound to the enhancing metallic substrate, I_{NRS} is the normal Raman intensity, and N_{vol} is the number of molecules in the excitation volume.[19, 20] Practically, for a given molecule, one must measure I_{SERS} and I_{NRS} independently and be careful when evaluating spot size and probe volume to determine the EF analytically.

1.2.2 Materials for SERS

Plasmonic resonance-supporting materials, mostly gold and silver, sometimes copper and aluminum, are used to create SERS substrates. When electromagnetic radiation directly impacts on a metal nanoparticle, the system becomes polarized displacing the conduction electrons from the positive ions that make up the lattice; nevertheless, the Coulombic attraction between the displaced negative and positive charges serves as a restoring force. The nanoparticle can therefore be represented as a simple mass-spring oscillator, in which the conduction electrons within the nanoparticle (mass) oscillate coherently under the influence of the periodic electric field's driving force and the restoring force created by the Coulombic attraction between the positive and negative charges (spring) as illustrated in **Figure 1.1**.[21] This coherent oscillation is referred to as localized surface

plasmon resonance. The term "localized" refers to the electron oscillations being spatially isolated in three dimensions and not propagating due to their tiny size, which is much smaller than the wavelength of light.

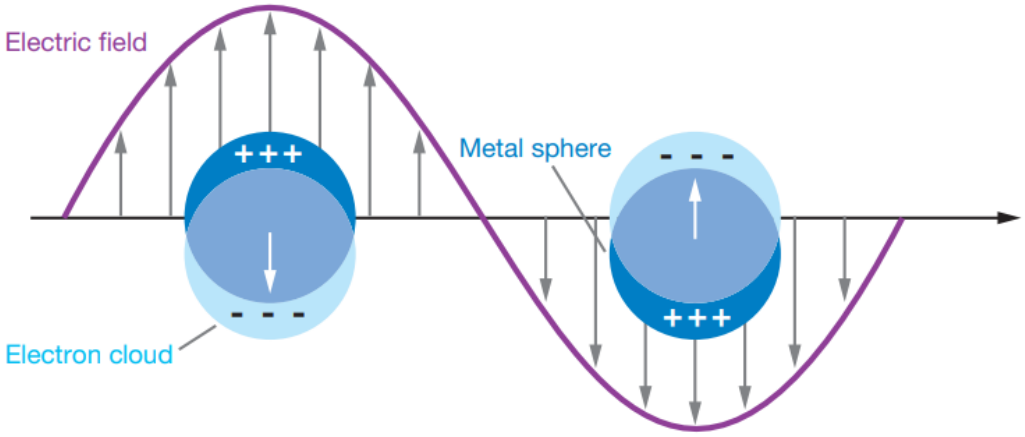

Figure 1.1 Illustration of the excitation of localized surface plasmon resonance. Reproduced with permission from ref. 22.

The dielectric constant of a material is generally a complex quantity that describes how the material behaves when it interacts with an external electromagnetic field.

$$\varepsilon(\omega) = \varepsilon'(\omega) + i\varepsilon''(\omega)$$

The real part of the above equation describes how the system polarized by the external field and the imaginary part accounts for the losses during the process. [23] The local field inside a nanoparticle (E_{in}) is a function of the incident electric field (E_0) that

$$E_{in} = \frac{3\varepsilon_d}{\varepsilon(\omega) + 2\varepsilon_d} E_0$$

where ε_d is the dielectric constant of the medium surrounding the nanoparticle. To produce strong enhancement ($|E_{in}| >> |E_0|$), the denominator of the above equation should be close to zero which means that the real part of dielectric constant $\varepsilon'(\omega)$ is about $-2\varepsilon_d$. As the surrounding medium around the nanoparticle is supposed to be non-absorbing, ε_d

is positive so that to fulfill resonance conditions, the real part of nanoparticle dielectric constant should be negative so that

$$E_{in} = \frac{3\varepsilon_d}{i\varepsilon''(\omega)} E_0$$

The above equation indicates a smaller imaginary part would lead to stronger enhancement. Therefore, metal nanoparticles which have dielectric constant with negative real part and relatively low imaginary part would serve as ideal candidate for SERS materials. Among the metals, silver has the lowest losses in the visible region and is the material expected to provide the largest enhancement.

The choice of materials for SERS is not simply decide by their ability to enhance Raman signal itself, but also by the specific applications considering the cost, the fabrication, chemical stability, and the biocompatibility. While silver and gold are mostly used due to their chemical stability and low toxicity, silver can easily get oxidized and react with sulfur compounds.[24-27] Copper is a low-cost alternative to gold and silver in some studies, but the oxidation to copper can form a layer of oxide that affects the plasmonic performance.[28-30] Aluminum has been reported in the UV region for biomolecules such as amino acids and proteins which absorb in the UV.[31-34]

Although metallic materials are used in the majority of SERS experiments, non-metallic materials such as dielectric and semiconductor materials are sometimes preferred.[35-38] For instance, heat may be released as a consequence of the absorption and dissipation processes in metals, which might alter or harm the sample. According to Mahmoudi *et al*.[39], plasmonic heating may alter the composition of the protein corona, resulting in unexpected alterations in the material being studied. It is theoretically possible to raise the laser power to enhance the Raman signal since the molecule in non-absorbing

materials does not overheat when subjected to strong electromagnetic fields. In addition, the band edges' positions and band gap width, as well as the nanoparticles' size, shape, and positioning, may be changed to alter the enhancement in semiconductors and dielectrics. These materials offer a richer variety of functional groups that can be linked to the surface. [40]

In non-metallic materials, the Raman signal is also enhanced by electromagnetic and chemical mechanisms, albeit there are some distinctions from metals. It is challenging to create electromagnetic enhancement based on the activation of the surface plasmon resonance in dielectrics and semiconductors. In contrast, it generally requires a significant number of free electrons in the conduction band, which is often sparsely populated in dielectrics. It has been suggested that heavily doping semiconductors would increase the electron density in the conduction band and, as a result, enable the activation of plasmonic resonances in the visible or near-infrared. However, the required level of doping is very high, and the solid solubility of dopants poses a challenging problem for silicon, germanium, and III-V semiconductors. In the study of transparent conductive oxides (TCOs)[35], the plasmonic properties of indium tin oxide (ITO), aluminum-doped ZnO (AZO), and gallium-doped ZnO (GZO) were investigated and TCO nanoparticles were found to exhibit a plasmonic resonance in between 1500 and 2000 nm. According to calculations, the plasmonic properties (absorption and field enhancement) of titanium nitride (TiN) and zirconium nitride (ZrN) nanoparticles are equivalent to those of gold. Since these nitrides are non-stoichiometric and may be adjusted for composition and optical characteristics, they could be feasible as SERS materials.[41, 42] Additionally, TiN

has excellent biocompatibility, hardness, and thermal stability so it has great potential as SERS substrate for wide applications.[43-45]

Two mechanisms of non-plasmonic electromagnetic enhancement in dielectric nanoparticles are illustrated in **Figure 1.2**. In the first case, the dielectric nanoparticle acts as a microlens, focusing the incident light in a small volume. The second case is based on the phenomenon of Mie scattering.[46] Rayleigh scattering happens when light impinges on objects smaller than about 1/10 of the wavelength. Mie scattering, on the other hand, occurs when light impinges on objects with a size similar to the wavelength.[40] The diffusion pattern and the relative scattered irradiance as a function of wavelength are different between these two processes, despite the fact that they are both elastic. Photons may be trapped within a dielectric particle and run for hundreds of meters before the internal electric field is appreciably weakened. Evanescent waves are produced at the particle's exterior surface and travel hundreds of nanometers into the space. As a result, molecules that are near to a particle's surface may have their optical characteristics amplified. In a Raman experiment, these two processes are likely to operate concurrently, with the first or the second taking precedence depending on the particle size and the disparity in refractive indices between the exterior medium and the particle size.

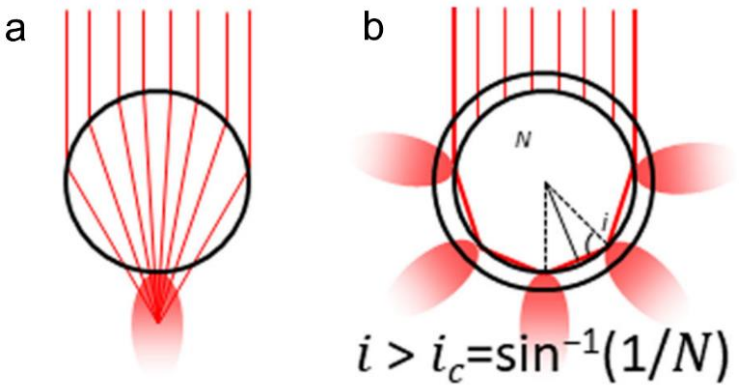

Figure 1.2 (a) Scheme of a dielectric sphere utilized as a microlens: Light is focused through the sphere generating a photonic nano beam that concentrates the electromagnetic field on the shadow-side of the sphere;(b) Scheme of a core/shell dielectric resonator resulting fromthe combination of a low-refractive-index core and high-refractive-index shell: Light is partially trapped within the sphere by internal reflections. Reproduced with permission from ref. 47.

Similar to metals, the chemical enhancement consists of non-resonant and resonant components. The development of a charge transfer state is different from the situation of metals in two aspects. Instead of to or from the Fermi level, the charge is transferred to or from the edges of the conduction or valence band. The selection rules and relative intensities of Raman bands are affected by the exciton transition in the semiconductor. It is important to note that a broad range of semiconductors are available with various band edges and band gaps, enabling for the chemical enhancement to be specifically tailored to the desired analyte.

1.2.3 Hot Spots

The field enhancement distribution at the surface of a plasmonic substrate is highly inhomogeneous and mainly localized in very small spatial regions called “hot spots”. From a structural point of view, these hot spots are often identified as very sharp tips or as nanogaps between nanoparticles or between a nanoparticle and a surface with the nanogaps remarkably more efficient in amplifying the optical signals than the sharp tips.

As shown in **Figure 1.3**, when two nanoparticles are brought together and with polarized external electric field, the nanoparticles get polarized, generating an excess of positive and negative charges on opposite sides of the nanoparticles themselves. When the distance between two nanoparticles is close enough, the high density of charges increases the electric field in between them. Moreover, the reciprocal interaction between the nanoparticles leads to an increase of their polarizations. In fact, each nanoparticle feels the effect of the external field plus the polarizing effect of the charges induced in the nearby nanoparticle. In other words, not only the external field, but also the induced dipole in one nanoparticle, contribute to the polarization of the other nanoparticle at the same time.

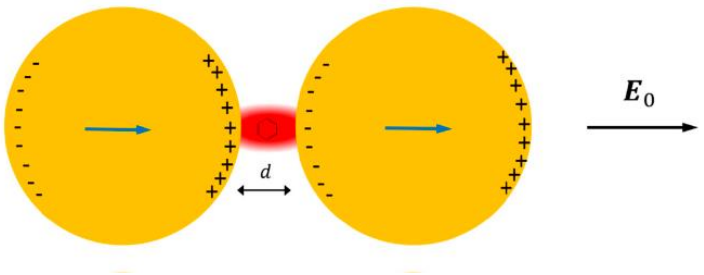

Figure 1.3 A dimer formed by two nanoparticles, separated by a gap d, is polarized by the action of an external electric field E_0, a molecule is placed in the middle of the gap. E_0 is polarized along the main axis of the dimer. The blue arrows inside the nanoparticles represent the induced dipoles. Reproduced with permission from ref.48.

A recent study in the Van Duyne group[49] has observed SERS spectra for non-resonant scatterers adsorbed onto dimers and other small clusters of ~90 nm spherical gold nanoparticles. They observed that neither SERS intensities nor plasmon resonance wavelengths or cluster size are linked to SERS intensity. Instead, they deduced that the distance between the particles, or the radius of curvature at the site of junction, if the particles are fused, is the primary element in determining the SERS enhancement factor.

In the work of Le Ru et al.[4], the dimer formed by two gold nanoparticles with radius of 25 nm immersed in water and separated by a variable gap g was studied and enhancement factor is numerically calculated for different gap sizes. The laser is polarized along the main axis and the probe molecule is placed at the surface of one of the two nanoparticles, along the main axis. The extinction and the enhancement spectra of a single nanoparticle and of the dimer (with different gaps) are shown in **Figure 1.4 b** and **c**, respectively.
It was found that enhancement factor strongly increases by reducing the gap size. With a gap of 10 nm, the enhancement factor was around 5×10^5, when the gap distance was decreased to 2 nm, the enhancement factor is 4 orders of magnitude higher to 3×10^9. The power law dependence is reported to be approximately $EF\sim1/g^2$.[50-52] A single gold sphere is limited to around 2×10^3. Because of this characteristic, SERS is often seen on aggregated nanoparticles but seldom on solitary nanoparticles. Aggregation very rarely inhibits or mildly improves Raman scattering; an example of this would be hollow nanoparticles, where the field enhancement created between the particles might be countered by a decrease in the field inside the particles.[53, 54] For very small gaps ($g < 1$ nm), field enhancement increases are constrained by quantum mechanical processes like electron tunneling.[40, 55] The electromagnetic enhancement and point enhancement factor are strongly dependent on the distance from the substrate surface. The analyte should typically be positioned no farther than 10 nm from the surface in order to effectively use the plasmonic effect. Excitation of the LSPR produces enhanced fields that extend beyond the substrate's surface, generating a volume where molecules may be identified within a few nanometers of the surface. It has been shown that SERS intensity scales as r^{-10}:

$$I_{SERS} = (\frac{a+r}{a})^{-10}$$

where I_{SERS} is the intensity of a particular Raman mode, a is the average size of the field-enhancing features on the surface, and r is the distance from the enhancing surface to the adsorbate. While retaining the enhancing qualities of the underlying substrate, the distance dependency enables one to stabilize or functionalize a SERS substrate with materials of interest, however care must be made to utilize ultrathin modifiers to reduce signal losses.

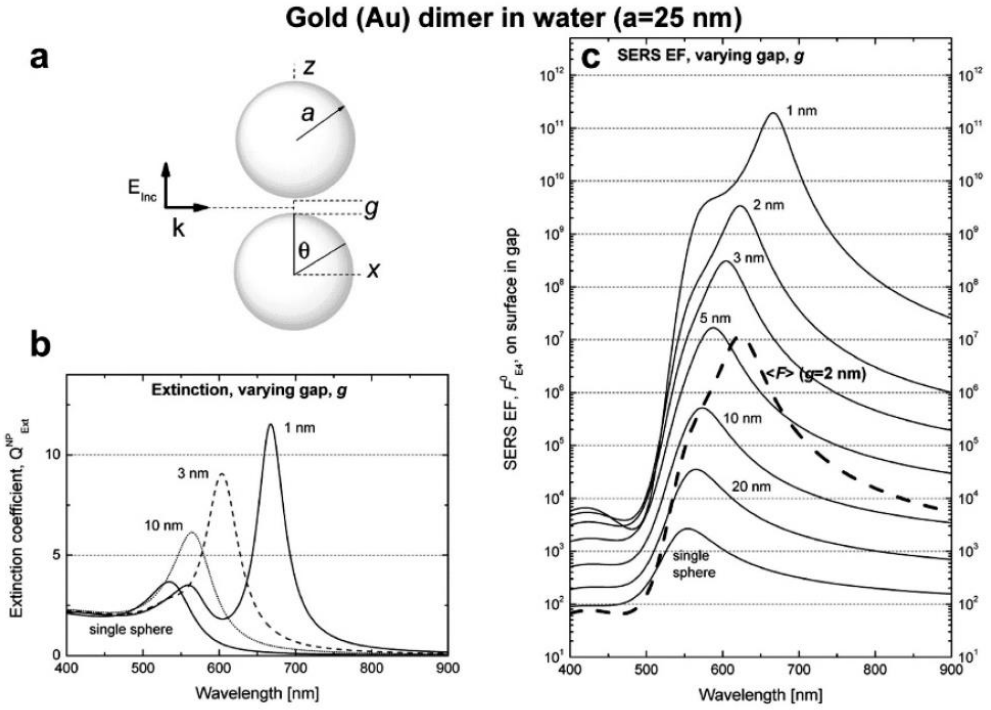

Figure 1.4 (a) The dimer under investigation is formed by two gold nanoparticles with radius a and separated by a gap g; the laser is polarized along the main axis. (b) Extinction coefficient for a single sphere and for the dimer (with different gaps) as a function of the wavelength. (c) Continuous lines: SERS enhancement (SERS EF in the figure) for a single sphere and for the dimer (with different gaps) as a function of the wavelength; the enhancement is calculated at the point where the nanoparticle crosses the axis Z. Dashed line: SERS enhancement for the dimer with g = 2 nm, averaged over the whole metallic surface. Reproduced with permission from ref. 4.

1.2.4 SERS Substrate Fabrication

Whether SERS can achieve a broader application really depends on the SERS activity and the reproducibility of the substrate.[56] The following milestones have been reached in SERS substrate preparation techniques since the initial observation of SERS on an electrochemically roughened Ag electrode: electrochemical oxidation and reduction cycles (EC-ORC) or vacuum deposition techniques can produce random and irregular substrates; wet chemical synthesis or laser ablation can produce nanoparticle sols with a wide size distribution; chemical synthesis can produce nanoparticles with controlled size and shape; and self-assembly, template, or other methods can produce large-area surface nanostructures with specified size, shape, and interparticle spacing. The requirements for ideal SERS substrate requirements are summarized in Table 1.1. The substrate should be uniform, which calls for a reasonably ordered arrangement of the nanoparticles on the substrate, such that the variation in enhancement throughout the whole surface may be less than 20%. The substrate has to be stable and reproducible. The enhancing effect might be maintained even after a lengthy shelf life. For various batches of substrates made using the same procedure, the enhancement variation should be less than 20%. The substrate has to be sufficiently clean to be used for the examination of materials other than strong adsorbates, such as weak adsorbates or even unidentified ones. In addition, the fabrication method should be scalable with low cost for a broader range of SERS applications.

Table 1.1 Desired features of SERS substrates, proposed by Natan[56] and Lin[57] et al. Reproduced with permission from ref. 48.

Feature	Suggested Benchmark	Notes
High average enhancement	$> 10^5$	Larger enhancements allow more sensitive and/or faster analysis.
Uniformity	Variations < 20%	Uniform and reproducible substrates make the work of the practitioner much easier, since one does not need to try several spots to find the most efficient one, and results are reproducible from substrate to substrate. Both these features are crucial if quantitative measurements are to be performed. Large areas are particularly useful with portable instruments, since they are normally not coupled to a microscope.
Reproducibility	Variations < 20%	
Large area	Some mm^2	
Stability		Substrates should preserve a good performance for a sufficient time (say a month) after fabrication. Moreover, they should not be degraded by the solvents (or other agents) they get in touch with under working conditions.
Ease of fabrication/low cost of production		Low-cost and scalable fabrication methods for substrates are crucial for a widespread diffusion of the SERS technique.
Cleanliness of the surface		The surface of the substrate should not have residual contaminants from the fabrication process.

Currently, it remains challenging to produce SERS substrates that can concurrently satisfy all of the aforementioned parameters. Certain trade-offs must be made based on the individual application goal. For instance, a homogeneous and repeatable substrate is crucial for quantitative analysis, but the need for trace analysis is a maximal enhancement. Due to the complexity of the examined biosystems, a clean and substantially improved substrate is often needed for bio-related detection in order to allow for a realistic assignment of the observed spectral bands.

The methods to prepare highly ordered SERS substrates include the nanoparticle assembly method, the Langmuir–Blodgett (LB) method, the template method, and nanolithography and nanoimprint methods. In the following part, the preparation method and the advantages and disadvantages will be analyzed for different methods.

Chemical assembly method is used to modify the solid substrate such as Si, glass indium tin oxide (ITO) with a bifunctional molecule. One part of the molecule creates a compact layer with the solid substrate, while the other part interacts chemically or electrostatically with the nanoparticles to create an ordered layer of nanoparticles. For different substrates, different bifunctional molecules should be chosen. The size, concentration, surface

charge, and type of bifunctional molecules are the main factors affecting the surface coverage and uniformity of the formed layer. Capping agents are often used throughout the synthesis process to stop nanoparticles from aggregating and provide a homogeneous substrate. The presence of the capping agent will, however, cause a significant amount of nanoparticle repulsion and impede the development of a compact assembly layer. As a consequence, there will not be strong electromagnetic coupling between nanoparticles, and the SERS activity will be minimal.[58] To solve this issue, it has been suggested to develop nanoparticles further using chemical or electrochemical processes in order to decrease interparticle spacing and boost SERS activity.[59] The method's benefit is that it allows for fine-tuning of the substrate's optical characteristics via interparticle spacing management. The signal is fairly homogeneous across the entire surface, despite the fact that the arrangement of nanoparticles on the surface during the assembly process is still somewhat random. This is because the laser spot covers a range of several microns containing several hundred nanoparticles, and the resulting signal is an average of the signals from these nanoparticles. The most alluring benefit is that a substrate with a wide area (up to several square centimeters) and very homogenous SERS signal may be created in a typical laboratory without the use of sophisticated equipment.

Compared with chemical assembly method, LB method has better control over the uniformity of substrate packing. On solid substrates, the LB method first applied in producing a thick layer of amphiphilic molecules.[60] If an amphiphilic molecule is dissolved in a volatile solvent that is immiscible with water and dispersed in the solution on the surface of the water phase, a monolayer of the molecule will form at the interface after the solvent has evaporated. By adjusting the movable barrier within the LB trough,

one may change the density of the monolayer film. The film may then be applied to the substrate using the dipping and pulling technique. In a manner similar to this, nanoparticles must first be modified with hydrophobic molecules before being dispersed in a highly volatile, water-incompatible solvent like chloroform or hexane. Due to the solution's dispersion into the water phase, a layer of randomly distributed nanoparticles will endure at the interface after the solvent has evaporated. As a result of the layer being squeezed by moving the barrier, an ordered layer of nanoparticles will form on the surface.[61] During compression, the interparticle distance will decrease, leading to strong electromagnetic coupling between nanoparticles and a significant shift in the LSPR band. The change is adequately supported by the apparent color shift that happens during compression. When under intense pressure, the nanoparticle layer even displays a metallic luster. Film structures produced by various nanoparticle types are quite varied. For instance, spherical and cubic nanoparticles may easily form a highly ordered close-packed film, but nanorods or nanowires tend to align perpendicular to the compression direction and produce a less ordered structure than spherical nanoparticles in a confined area. Due to its liquid crystal-like structure, the nanorod film is the ideal model to connect the laser polarization with the LSPR and the SERS signal. The nanoparticle film may then be applied on glass or a silicon wafer to generate a substrate with a surface area of up to 20 cm^2. Currently, the LB method has been successfully used to make SERS films, which include nanorods, nanowires, and spherical, cubic, cuboctahedral, and octahedral Ag nanoparticles as shown in **Figure 1.5**. When utilizing arsenite as a SERS substrate, a detection limit of 1 ppb has been achieved for the detection of arsenate and arsenite in solution.[62] It's also important to note that, similar to the CTAB-modified

methodology described above, the LB method calls for the modification of the nanoparticles with certain substances that might possibly interfere with the SERS measurement. However, the LB technique is the one that can provide the most homogenous substrate based on the nanoparticle assembly strategy.

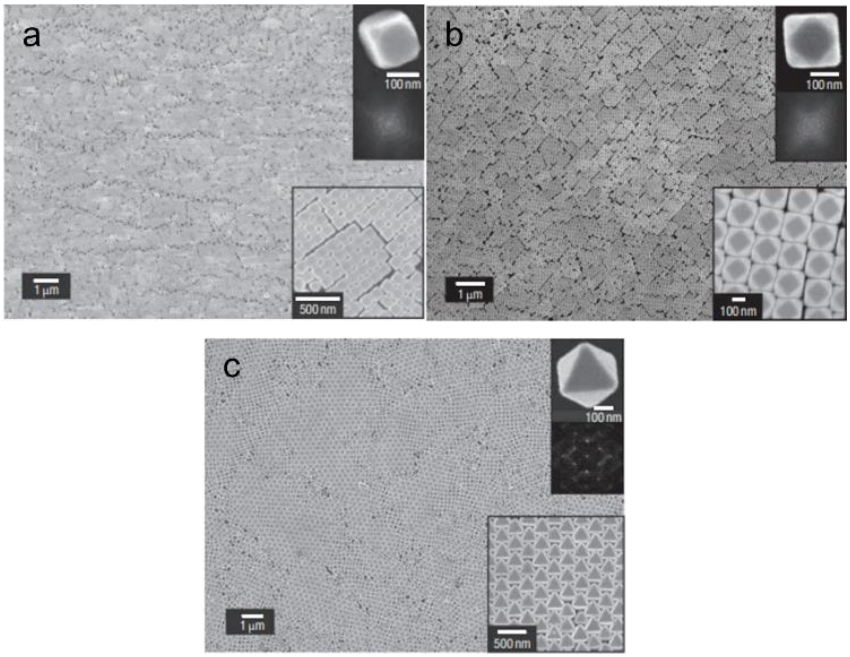

Figure 1.5 SEM images of close-packed superlattice NC monolayers made of truncated cubes (a), cuboctahedrons (b), octahedra (c). Reproduced with permission of ref. 63.

Another type of ordered SERS substrate that has been shown to very promising is fabricated on the basis of the nanosphere lithography method.[22, 64] A monolayer or a multilayer of the highly ordered nanosphere film will develop on the substrate by regulating the assembly conditions when polystyrene or silica spheres of the correct size are assembled on a clean substrate. After that, a metal layer of the specified thickness is formed on the template using vacuum deposition or electrochemical deposition. As a result, three kinds of structured SERS substrates may be produced. As shown in **Figure 1.6**, A metallic surface is created by physical vapor deposition on the nanosphere template, while surface-confined nanoparticles with a triangular footprint are produced

after the nanospheres are removed from the substrate by sonicating the whole sample. Depending on the thickness of the deposited film, electrochemical deposition followed by removal of the nanosphere produces a thin nanostructured film with a regular hexagonal array of uniform metal nanoislands, nanobowls, and nanovoids. The advantage of the nanosphere lithography method for creating the SERS substrate is that the LSPR position can be adjusted to match the excitation wavelength and to produce an optimized SERS enhancement because the size of the nanospheres and the thickness of the deposited metal can be used to control the shape, size, and spacing of the nanostructures.[65] The substrates produced by the first and third method will have a strong SERS enhancement. The second method's SERS activity is somewhat low because of the wide particle spacing, but the exceptional LSPR tenability yields a superior LSPR sensing chip. Although it is very common to create an ordered substrate with an area of 10-100 um^2, the success rate of this procedure mainly relies on the experimenter's expertise and how precisely the circumstances can be controlled. When the sphere is smaller than 200 nm, it is very difficult to produce an ordered surface free of any point or line flaws. It is nevertheless simple to locate an organized region for quantitative investigation with excellent repeatability and stability with the aid of a microscope.

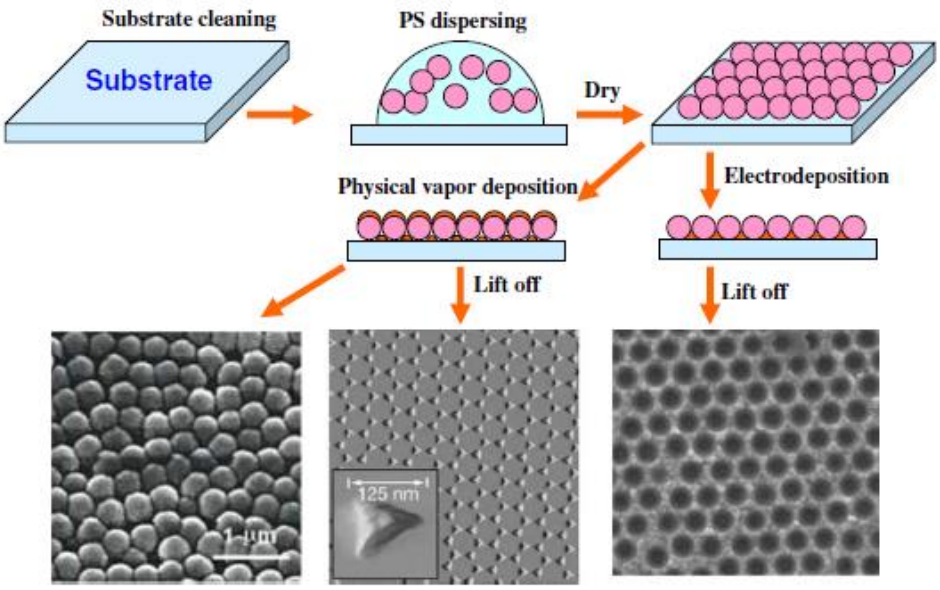

Figure 1.6 Template methods using nanosphere lithography to fabricate ordered nanostructured SERS-active substrates. Reproduced with permission from ref. 66.

1.3 Tip-Enhanced Raman Spectroscopy

After several decades of development, SERS that overcomes the weak signal issue has been demonstrated with single-molecule level chemical sensitivity and has been used for a variety of purposes, including the detection of biomolecules and the study of chemical reaction mechanism.[32] However, like with other optical microscopies, the ideal spatial resolution of SERS is limited by the optical diffraction limit at about half of the excitation wavelength, which in the visible wavelength range is greater than 200 nm. Furthermore, the nonuniform SERS amplification factors and their generally unpredictable spatial distributions[67] in most SERS substrates make chemical imaging difficult. As an important variation of SERS, tip-enhanced Raman spectroscopy (TERS), has emerged as a promising technique for in situ chemical analysis on the nanoscale. In TERS, enhancement arises from a metallic scanning probe microscopy (SPM) tip rather than from the substrate.

1.3.1 TERS Mechanisms

To overcome the shortcomings of substrates and spatial resolution in SERS, many researchers have attempted to extend the technology of SERS. The spatial resolution of Raman depends on the wavelength of incident light and the numerical aperture (NA) of the objective. The highest resolution is approximately half of the incident light wavelength, about 200 nm in the range of visible light, which is too low for nanoscience. Therefore, conventional Raman microscopy can only obtain the average chemical information on a sample rather than the nano composition and distribution of the specimen. To overcome the diffraction limit and increase the spatial resolution, Synge proposed the primary idea of scanning near-field optical microscopy (SNOM) by using a scanning aperture smaller than the wavelength of the illuminating light in 1928.[68] In 1984, inspired by the invention of scanning tunneling microscopy (STM), Pohl first achieved scanning near-field optical microscopy (SNOM) with a resolution of $\lambda/20$ using a very narrow aperture fiber tip.[69] The aperture scanning probes are expensive and time-consuming for fabrication and the signal is usually weak.

The theoretical concept of TERS was first proposed in 1985 by Wessel, who demonstrated an optical probe with nanometer resolution based on spatial confinement of an electromagnetic field by surface plasmons of a metal particle.[70] The metal particle would enhance Raman scattering at the sample surface, and microscopy could be accomplished by raster scanning the particle across the surface. The experimental realization of such a technique was achieved with the first TERS measurements conducted in 2000 by a few researchers independently and 50 nm spatial resolution had been achieved.[71-74] By bringing the metal tip to the sample, the restriction to coinage

metal surfaces or the need for surface modification of SERS-active substrates is avoided. TERS has the potential to be a completely substrate general technique, an obvious advantage for the study of various catalytic surfaces. Combined spectral and topographical imaging capabilities provide both structural and chemical information about the composition of a surface.

TERS systems can be classified into three types according to the different feedback mechanisms used to keep the tip in contact with the surface: contact/tapping mode atomic force microscope (AFM), shear force and scanning tunnelling microscope (STM), shown schematically in **Figure 1.7**, respectively. Because the AFM system is more adaptable in terms of use on both non-conductive and conductive materials, various home-made and commercial TERS systems have adopted the AFM-based TERS configuration. A feedback loop is used in AFM to maintain a consistent force of contact between the cantilever and the sample. Any cantilever deflection induced by differences in contact force is measured when the AFM probe scans across a sample surface using a semiconductor laser reflected from the back of an AFM cantilever onto a quadruple photo-detector, as shown in **Figure 1.7a**. The silver or gold-coated AFM tips can usually provide a TERS resolution of 20 nm.[75, 76] However, after a few hours, oxidation of silver in ambient air causes the tips to lose their ability to enhance. Although contact-mode AFM has been the most extensively used mode so far, multiple groups have discovered considerable Raman signal amplification using tapping-style AFM TERS.[77-79] In shear force AFM mode, shown in **Figure 1.7b**, a metal tip is mounted on to the prong of a quartz tuning fork. TERS measurements are conducted by positioning the tip at the center of the laser focus, and accurately controlling the tip-sample distance using shear-force as

the feedback.[80, 81] In case of STM-TERS, the tip-sample distance is controlled via a feedback loop using the tunnelling current between the tip and sample, as shown in **Figure 1.7c**. STM-TERS can be used to measure conductive and semiconductive samples on conductive substrates.

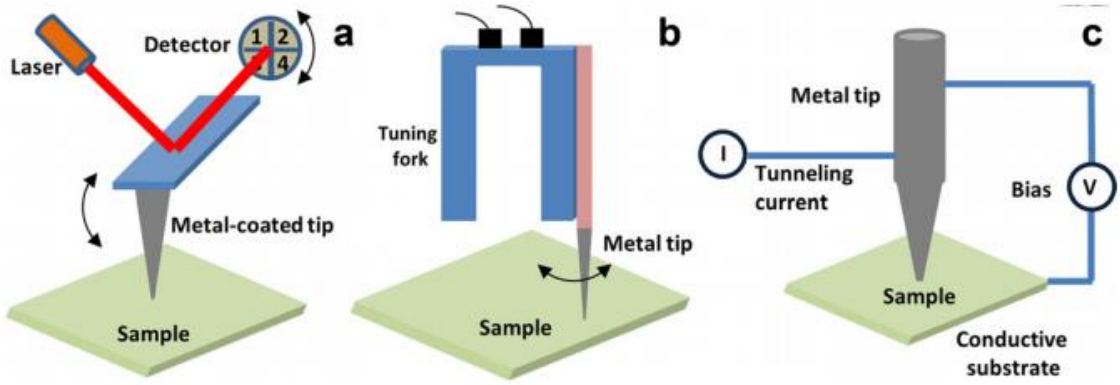

Figure 1.7 Schematic diagrams of SPM feedback mechanisms used in TERS. (a) AFM feedback mechanism. (b) Shear-force feedback mechanism. (c) STM feedback mechanism. Reproduced with permission from ref.82.

The combination of Raman spectroscope and an SPM tip provides nanometer spatial resolution and a significant improvement to the diffraction-limited spatial resolution of SERS which is $\lambda/2$. When a gold or silver SPM tip is irradiated with visible light, excitation of the LSPR results in an enhanced electromagnetic field which is locally confined around the tip apex. This enhanced electromagnetic field increases Raman scattering from molecules located in the near-field region of the tip by 3 to 6 orders of magnitude.[83] Under laser illumination, though a larger area was excited because of the laser spot size, only the area around the gap could be enhanced that Raman signals mostly come from the range of the gap between the tip and substrate, high spatial resolution can be achieved.

Similar to SERS, the enhancement mechanism of TERS includes the electric field enhancement and the chemical enhancement. Noble metals (such as Au/Ag) are usually used as SPM tips and can give a good optical response and large electric field enhancement in the visible light region.[84]

A particularly sharp metal tip in TERS could result in a highly concentrated surface charge density and be a source of localized electric field enhancements. In SPM, the distance between the tip and the substrate is typically regulated to one or a few nanometers using a feedback loop, which may create massive electric field coupling between the metal substrate and tip. This will result in a hot spot, and the enhanced region will be tightly contained under the tip apex.[85] The spatial resolution of TERS can reach a few nanometers,[86, 87] even down to the sub-molecule level.[88]

One of the important concepts in TERS is the enhancement factor. In the calculation, considering that the enhancement mostly originates from the electric field enhancement in TERS, the electric field enhancement can be written as

$$g = {E_{tip}}/{E_0}$$

where E_{tip} and E_0 are the enhanced electric field under the tip and the incident electric field intensity, respectively. The light intensity is proportional to the square of the electromagnetic field, and the enhancement depends on both the incident laser and Raman scattering light intensity; thus, the TERS enhancement factor is

$$EF_{TERS} = g_{laser}^2 \times g_{Raman}^2 \approx g^4$$

The electric field enhancement is frequency dependent; the wavelengths of the illuminating laser and the Raman scattering light are slightly different. If the Raman shift

is not very large, it can be assumed that the electric field enhancement from the laser and Raman scattering is almost the same. Thus, EF_{TERS} can be approximated as g^4.

By combining the sensitivity and rich chemical information of SERS with the excellent spatial resolution of scanning probe microscopy, TERS has the potential to be a very powerful tool for surface analysis.

1.3.2 TERS Substrate

The substrate in TERS typically uses a flat mica, glass slide, or silicon wafer.[79, 86, 89] The substrate for gap-mode TERS, in which the tip and substrate are both made of metal, is not often a gold or silver film or single crystal. To obtain higher enhancement signals, many research groups typically use gold or silver films made by depositing a 100-200 nm gold or silver film on a freshly cleaved mica or silicon wafer using thermal evaporation in a high vacuum. This is done because gold and silver single crystals are very expensive and challenging to work with in an air atmosphere.[90-93] The island distribution on the rough film is comparable to the arrays of metal points as compared to a single-crystal substrate. In comparison to flat single-crystal substrates, the connection between the probe tip and the roughness of the film as a nano island or SERS substrate may provide a stronger electric field enhancement and a higher Raman enhancement factor. However, a single crystal substrate is often required for a molecular pattern or submolecule TERS measurement.[94, 95] The second problem relates to the molecules' ability to adhere to the substrate. Distinct experimental settings need different sample preparation procedures. In certain circumstances, a monolayer of self-assembled molecules may be produced through chemisorption by submerging the substrate directly in molecule solutions.[96, 97] The samples are sometimes dispersed and physically adsorbed onto the surfaces using the

dying or spin coating process.[86] The aforementioned techniques may be used to measure the spectrum without any major issues. SPM can seldom be used to determine a molecule's topology, however. The molecular beam epitaxial (MBE) technique may be used in a UHV environment to evaporate the molecules onto a spotless single-crystal substrate. This method ensures that only the target molecules are on the substrate since no additional contaminants are present.[98-101] In this situation, measurements of the topography and spectrum may be made concurrently.

1.3.3 Development in TERS Probes

TERS measurements depend heavily on the SPM tip. Typically, a metal or metal-coated tip is used to produce a hot spot in TERS. Along with the enhancement factor and spatial resolution of TERS, the tip's material composition, diameter, and shape also affect the image quality of the SPM. Producing reproducible high-quality tips that are both appropriate for high-quality SPM imaging and in resonance with the excitation light to provide a greater enhancement factor is one of the major issues that TERS still faces today.[102-106] In TERS, two crucial aspects should be taken into account in order to get stronger signals and a higher signal-to-noise ratio. One is that a tip should be in resonance with the frequency of the incident light, which may be achieved by altering the tip's material and the form and size of the tip apex. [106-108] By modifying the shape and size of the tip apex, it is possible to control the frequency of SPR produced by the tip, and it is also possible to control the EM enhancement in the nanogap between the tip and substrate. The coupling efficiency of the incoming light to the tip surface plasmons should also be improved. There are also several examples of dropcast or spin coat films and chemisorbed monolayers that may be imaged using SPM. [109] Along with the radius

and shape of the tip, durability is another issue. Target molecules or environmental pollutants in an air atmosphere are very likely to contaminate the tips. Since the molecules are always in motion at room temperature or higher owing to the heating activity at the tip apex, contaminants like amorphous carbon will develop even in vacuum.[110-112]

A metal-coated commercial AFM cantilever is often utilized in the AFM-TERS system. The thermal evaporation technique is used in a high vacuum to evaporate the high-purity metal (silver or gold) onto the probe surface. The diameter of the metal-coated tip apex, which serves as the source of electric-field enhancement, is generally 20–50 nm, whereas the thickness of the coated metal film is typically several tens of nanometers.[103, 113]

Figure 1.8 shows a typical silver-coated AFM tip. Silver tips often display stronger enhancement in the UV–vis region than do gold tips, but chemical stability must also be taken into account since silver is prone to oxidation in air. The oxidation may change the tip's resonance, which would reduce the enhancement.[110] It is thus advisable to use the silver tips right away after the deposition, or several nanometers of silicon dioxide or gold may be put onto fresh tips to stop oxidation.[114]

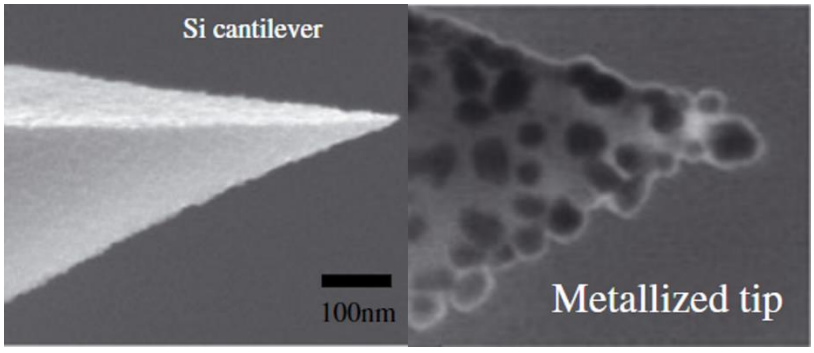

Figure 1.8 Scanning electron microscopy image of silicon tip, and met-allized tip. Reproduced with permission from ref.114.

Another typical technique for creating TERS probes is to assemble metal nanoparticles onto the tip of an AFM probe. Chemically produced nanoparticles may be applied to probe tips by mechanical attachment[115], dielectrophoresis (DEP) force attachment[116], or even direct electrochemical metal depositions[117], which are often formed of noble metals like Au or Ag (**Figure 1.9a**). In order to create probes with trimer antennas, Novotny et al. selected gold nanoparticles of various sizes (e.g., 80, 40, and 20 nm) as shown in **Figure 1.9b**.[115] The inherent quantum efficiency of the probe with trimer antennas may reach more than 80% in comparison to the TERS tips with a single nanoparticle at the apex, and the enhancement-confinement ratio is also enhanced. A technique for building close-packed colloidal Ag nanocubes (AgNCs) on blunt AFM probes using the Langmuir-Blodgett method was described by Tao et al. in 2016 (**Figure 1.9c**). [118]A spatial resolution of less than 50 nm was obtained, which is comparable with prior TERS studies that used large radius probes. Additionally, the probe is attractive for single-molecule detections due to the ability of AgNCs at the probe apex to produce plasmonic cavities with Raman enhancements reaching 10^9.

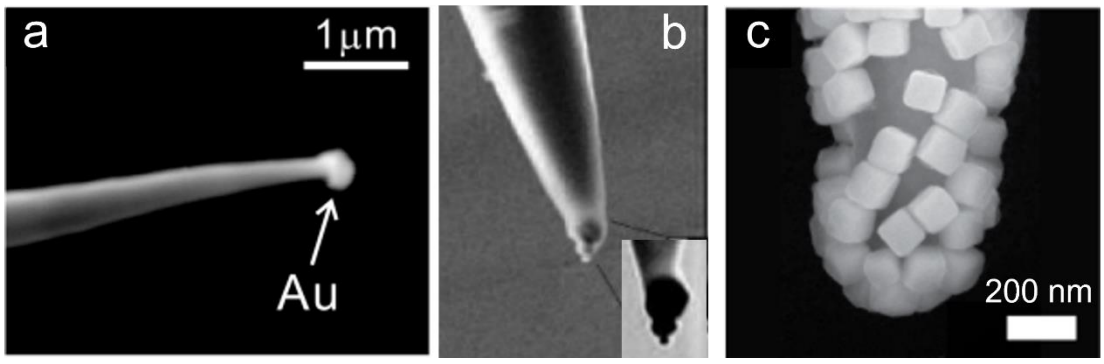

Figure 1.9 Scanning electron microscopy (SEM) images of conventional TERS probes are prepared with assembling nanoparticles. (a) is reprinted with permission from ref. 117; (b) is reproduced with permission from ref. 115; (c) is reproduced with permission from ref. 118.

For STM- and SFM-TERS systems, electrochemically etched Au/Ag tips are usually used. The focused ion beam (FIB) and mechanical cutting technologies, among others, have been developed in the last ten years to produce tips for TERS, but they are either excessively costly or complicated, or they have extremely poor repeatability. The electrochemical etching process may produce excellent TERS tips. For TERS measurements in various configurations, silver wire or gold wire are often etched as the tips due to the resonance effect with varying excitation wavelengths. The gold tips in the etching tests are typically created by electrochemically etching gold wire with ethanol.[119, 120] The gold tips may be produced with good reproducibility and are typically cone-shaped with a radius of curvature between 10 and 30 nm.[120] Similar techniques may be used to create the silver tips.[113, 121] By partly crystallizing the wire by flame annealing, the plasmonic loss may be further minimized. Due to the fact that the metal conductivity and tip morphology have an impact on the TERS enhancement of an etched probe, careful control of the electric bias is necessary, including potentiostatic control with current cut-offs and visual feedbacks to avoid over-etching. [107, 119, 122]Typical SEM images of etched silver and gold tips are shown in **Figure 1.10**.

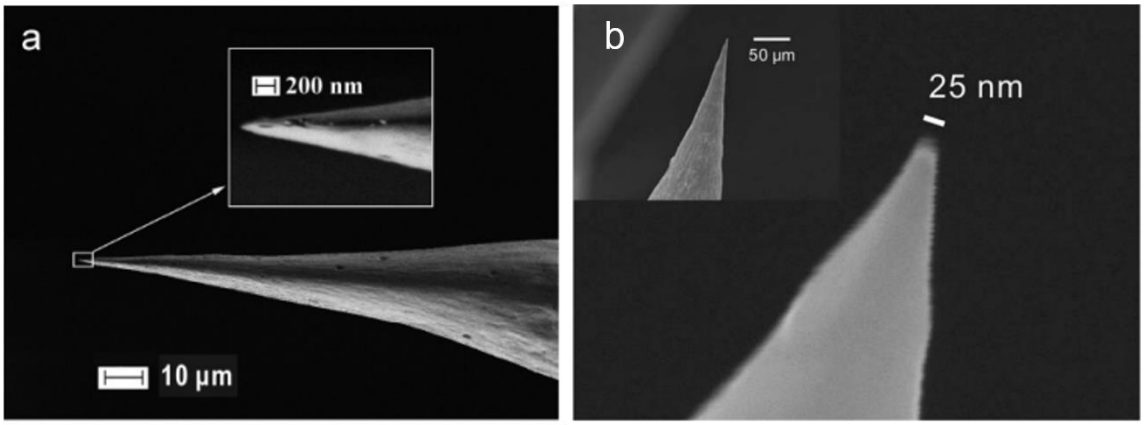

Figure 1.10 SEM images of a typical etched gold probe (a) and silver probe (b). (a) is reprinted with permission from ref. 120; (b) is reprinted with permission from ref. 121.

1.3.4 Silver Nanowires-Based Probes

Compared with some conventional TERS probe preparation methods, like coating thin metal on a tapered tip or etching metal tip into the tapped profile, AgNWs have crystalized smooth surfaces, the subwavelength apex of the tip, high electrical conductivity, and good mechanical performance, which make AgNWs a good candidate to serve as SPM-TERS probes tip. To date, AFM cantilever, sharp tip tungsten STM probe, and gold-coated tapered optical fiber have been combined with AgNWs to perform TERS experiments taking advantage of both ready designs for SPM feedback with commercial probes and the promising performance of AgNWs as probe tip.

To fabricate a TERS probe with good performance, two key aspects that should be taken into consideration are the attachment of AgNW to SPM probes and the apex of the AgNW tip. The attachment includes the method of putting an AgNW on an SPM probe, the adhesion between AgNW and the sidewall of the SPM probe, and the protruding length of the AgNW beyond the SPM probe, which are all crucial in probe fabrication. Besides fabrication, the apex of the AgNW tip would influence the spatial resolution of both the SPM and TERS imaging, the probe's electromagnetic field enhancement factor, and the probe's reproducibility.

The first AgNW SPM-TERS probe was made by using an alternating current electrophoresis (AC-DEP) method by the Z. Shen group in 2009.[123] A schematic is shown in **Figure 1.11**, a copper ring served as the ethanol drop holder and one of the electrodes while a tapered sharp tip tungsten tip acted as another electrode, 1 MHz and 10V AC voltage were applied, and the current in the loop of W tip-AgNWs solution-copper ring would drive AgNWs to place with lower electrical potential, i.e., the apex of

W tip or copper ring. They found the best condition for attaching one AgNWs on the W tip was a solution concentration of ~10^9 NWs per liter and ~1s reaction time, leading to a more than 50% success rate. It is worth noting that this AC-DEP method can be applied to many other metal tips or metal-coated tips, with conductivity beings the only requirement.

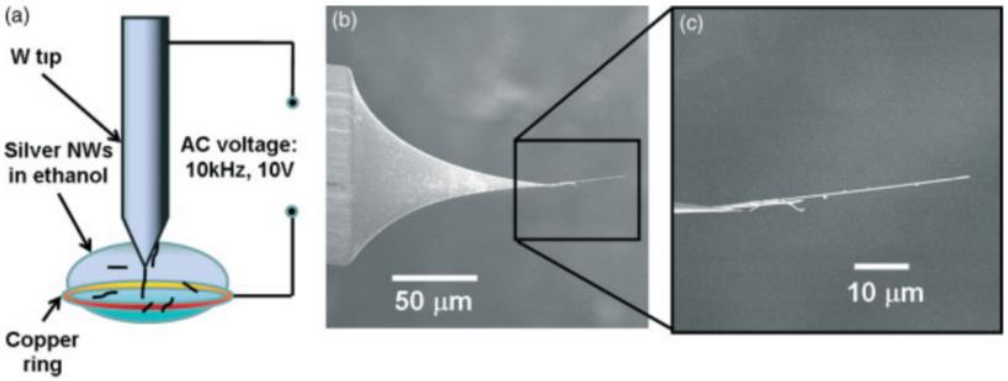

Figure 1.11 (a) Schematic illustration of the AC-DEP setup. (b) SEM images of W tip with attached AgNW. (c) Zoomed-in SEM image with more detail information. Reproduced with permission from ref. 123.

The AC-DEP method was welled applied in the last decade. Based on the same concept H. Uji-i group published many works [124-126]with altered conditions, e.g., different AC voltage and frequency, different materials of the ring electrode or different AgNW solution concentration. It worth noting that one of their studies[126], it was demonstrated that semiconductor AFM cantilevers also could serve as the electrode (higher voltage, 2-12V, required), which broke the restriction of the metal or metal-coated tip proposed in Z. Shen's work.[123]

Besides the AC-DEP method, H. Uji-i group reported another method for the AgNW attachment[127], taking advantage of the capillary force of instant glue drop to pick and fix a AgNW on a W tip. Super glue (Loctite SUPER GULE-3) which reacts with water when it is polymerized, was applied on the tip of an etched sharp tip tungsten probe and using a

3-D manipulator to control the tip to pick up AgNW spin-coated on a hydrophobized glass cover slide. The capillary force helps picking up the target AgNW, so that it can be attached to the W tip with glue. With the help of optical microscope, specific AgNW can be picked up and placed on SPM probes with controlled protruding length. **Figure 1.12** shows the procedure and results of this method.

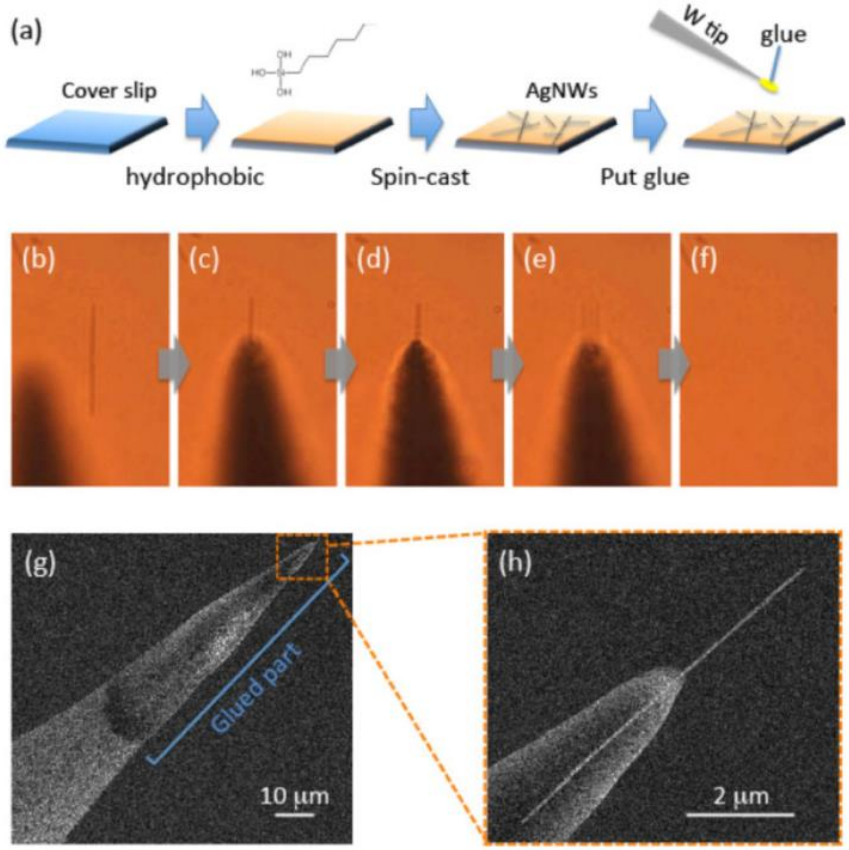

Figure 1.12 (a) Schematic of the process for attaching AgNW on Tungsten tip. (b-f) proof of the optical microscopy image of the attachment process. (g, h) SEM images of tungsten probe before and after attached the AgNW. Reproduced with permission from ref. 127.

As an alternative, J. Michler group proposed another method to attach the AgNW on AFM cantilever in 2011[128], the combined with an SEM-nano-manipulation attachment procedure. It was inspired by the work of attaching single-walled carbon nanotube (SWCNT) on AFM cantilever tip for high spatial resolution scanning probe microscopy

(SPM) that was accomplished by H. Dai in R. Smalley group in 1996.[129] Two x,y,z-piezo stages were used to control free-standing AgNWs mesh held by a razor blade and the AFM cantilever, both of two piezo stages have 50 μm range and sub-nanometer resolution. The compact design of operation setup was put into SEM chamber, therefore, under the observation by SEM, the AFM cantilever can be roughly aligned with a target AgNW, coarsely operated by a robot arm. With the help of two sub-nanometer resolution 3-D piezo stages, the apex of the AFM cantilever can be aligned at the top of a selected free-standing AgNWs, followed by pushing and gluing by focused electron beam induced deposition of an amorphous, carbonaceous blob. The procedure and results are shown in **Figure 1.13**. The focused ion beam (FIB, Lyra Tescan) has been used for modifying the apex and the protruding length of the attached AgNW. High-resolution and high-end performance SPM and TERS require apex with a small radius for spatial accuracy and large enhancement factor.

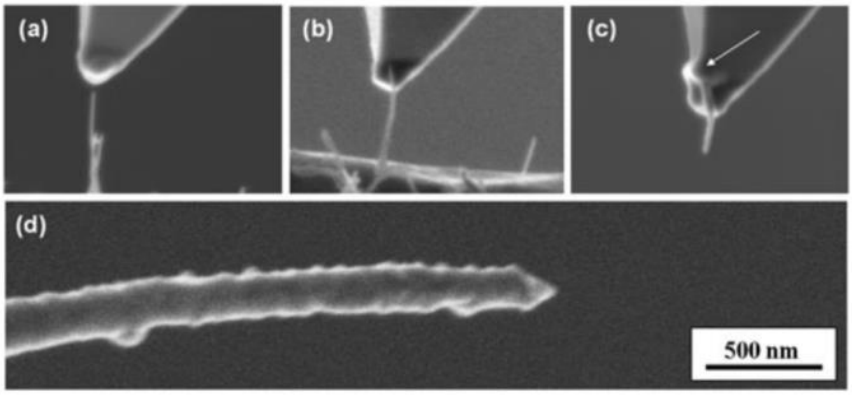

Figure 1.13 SEM images of silver nanowires on AFM cantilevers. (a), (b) and (c) illustrate the process of attachment (approach, welding, retraction).(d) shows a high-resolution image of the tip end. Reproduced with permission from ref.129.

With the established methods for probe fabrication using silver nanowires, studies in silver nanowires-based SPM probes have demonstrated high Raman signal enhancement and great spatial resolution in both STM and AFM TERS. M. Liu group and Dr. H. Uji-i

group have demonstrated the high-aspect-ratio and high resolution (HAR-HR) with AgNW-based AFM in 2016 and 2018, respectively.[126, 130] Deep trench sample has been used to benchmark the HAR performance and several nanometers spatial resolution has been achieved. The comparison between scanning over the same deep trench with AgNW-AFM probe (**Figure 1.14 a** and **d**) and conventional AFM cantilever (**Figure 1.14 b** and **e**) provide solid evidence to demonstrate the HAR performance of AgNW-AFM. Thanks to the ultra-sharp tip AgNW, a 6nm spatial resolution has been achieved in the single-walled CNTs scanning (**Figure 1.14 f** and **h**, the red cross line). Also, after 15 times dual scanning, the performance of this ultra-sharp AgNW-AFM probe shows no obvious decay, proving the high wear resistance of the probe.

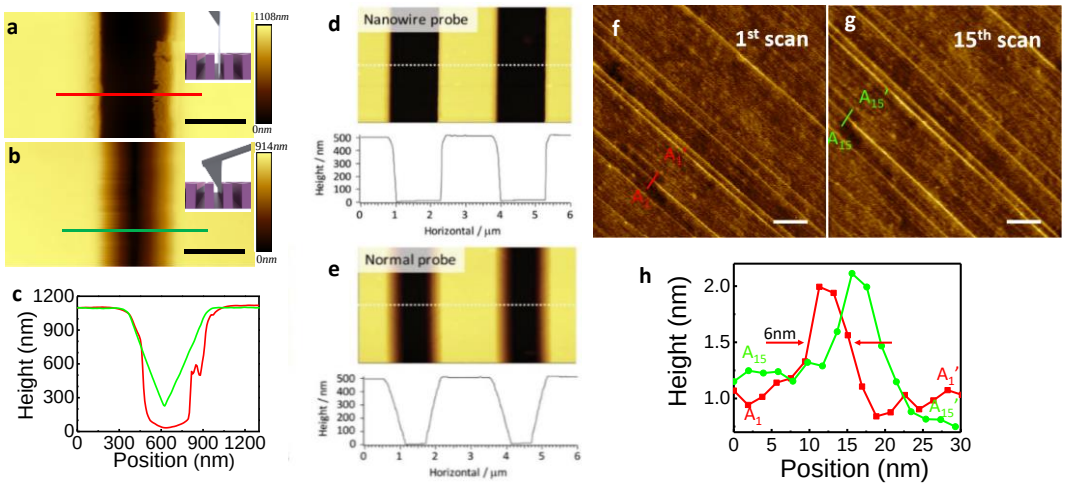

Figure 1.14 (a-e) High-Aspect-Ratio (HAR) benchmark for the AgNW-AFM probe using a deep trench sample. (f-h) High-Resolution (HR) and wear resistance benchmark for the AgNW-AFM probe using a single-walled CNTs sample. Reproduced with permission from ref. 126.

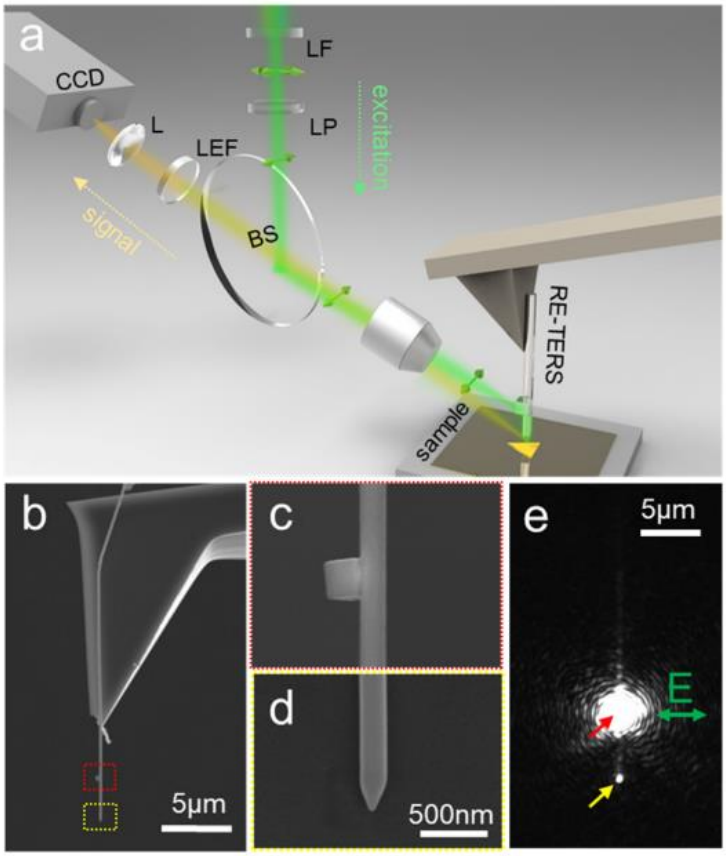

Figure 1.15 (a) Schematic illustration of the RE-TERS setup. The green excitation laser beam (532 nm) is sent through a laser line filter (LF), a linear polarizer (LP), and a beam splitter (BS) to an objective lens, which focuses it on an AgNC to excite SPPs on the AgNW waveguide. The SPPs propagate toward the tapered tip to excite TERS signals, which are collected through the same objective lens, filtered by a longpass edge filter (LEF), focused by a lens (L) and collected by a CCD spectrometer. (b) A SEM image of a RE-TERS probe. (c,d) Close-up SEM images of the AgNC−AgNW junction (c) and sharp AgNW tip (d). (e) An image obtained in bright-field optical microscopy showing the coupling between the 532 nm excitation laser beam (polarization along the green arrow) and the AgNC−AgNW junction coupler (red arrow). The yellow arrow marks the position of the AgNW tip. Reproduced with permission from ref. 131.

The silver nanowire probes are highly adjustable for manipulation during the fabrication process that in one of our previous work[131], silver nanowire was bundled with a silver nanocube that is around 2~3 μm away from the AgNW tip as shown in . The silver nanocube works as an antenna allowing remote excitation. This probe configuration is effective in decreasing background noise but is still relatively close to preserve the TM0 mode. In order to effectively excite the TM0 mode with an s-polarized laser beam that

has the electric field parallel to the sample surface and reduce direct excitation of the Raman background while increasing the TERS contrast (to 100), the azimuthal angle of the incident beam with respect to the AgNW axis was selected. Using a suitable-sized AgNC (500 nm) as the coupler, numerical simulations demonstrated that 4% of the incoming light could be transported to the tip apex. With the unique design of the RE-TERS probe, a 10 nm spatial resolution was demonstrated on a single-walled carbon nanotube sample, and the strain distribution in a monolayer molybdenum disulfide (MoS_2) was mapped with AFM-TERS.

AgNW-based probes have also been demonstrated in STM-TERS measurements that shows strong enhancement and high spatial resolution. In the work of Yasuhiko Fujita et al., chemically synthesized silver nanowires were attached to tungsten tip apex with AC-DEP method and used as scanning probes.[124] As shown in **Figure 1.16**, the STM scanning test on graphite sample shows atomical resolution when multiple silver nanowires were attached to the tungsten tip indicating multiple AgNWs attachment would increase the stability of operation increasing the conductivity and mechanical strength. This multiple silver nanowire bundle probe was also tested in TERS over a benzenethiol-modified Au (111) surface and showed less polarization dependence compared with single AgNW. It also worth noting that in their work they noticed Raman scattering from PVP induced during the synthesis of AgNWs which can be a problem when TERS is tested in a complicated chemical environment.

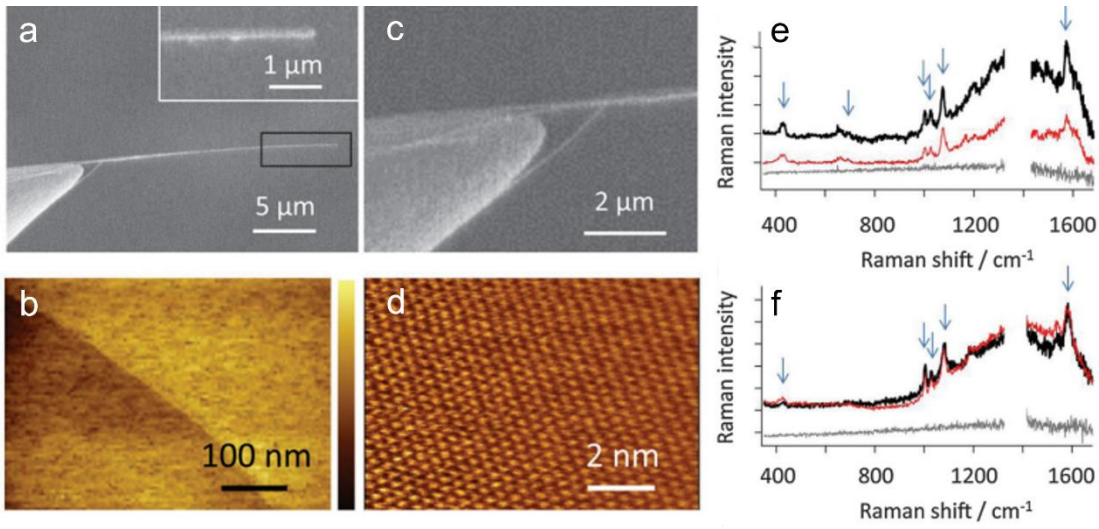

Figure 1.16 (a) SEM images of an AgNW-tip and zoom-in images of its end (inset). (b) An STM image of the graphite step edge (the colour bar: 0–2.5 nm). (c) The multiple AgNWs attachment on a W tip apex. (d) Atomicresolution image of a graphite lattice (constant height mode, tunnelling current: 2 nA, bias voltage: 0.1 V). (e) TERS spectra excited at p-polarization (black line) and s-polarization (red line) taken with a single NW and (f) a bundle of two NWs at the tip end. The weakest spectra plotted with grey lines in (e) and (f) represent Raman spectra of benzenethiol on Au(111) without the AgNW-tips. Arrows represent Raman peaks which are assigned to benzenethiol. Reproduced with permission from ref. 124.

In addition to the undesirable Raman signals, the PVP attached to silver nanowires could also lead to poor conductivity that affecting the scanning in STM. As indicated in Qiushi Liu et al.'s work[132], to improve the conductivity, efforts are needed for PVP removal. Purification with ethanol alone was effective to remove free PVP added to the synthesis, however even after 6 times of ethanol wash, there was still a thin layer (~1.6 nm) of PVP bound to the surface of silver nanowires which has poor conductivity and low current-distance sensitivity which result in poor STM imaging quality on a gold substrate. The PVP layer can be effectively removed with $NaBH_4$ solution demonstrated in **Figure 1.17b**. After the removal of PVP, conductivity of silver nanowire probe was significantly improved, and the high current-distance sensitivity led to increased quality of STM imaging. In the same work, the authors compared the performance of silver nanowires

with rounded and ultra-sharp tips in TERS measurements on graphite sample and the latter clearly showed higher Raman enhancement which confirmed a tip radius dependence of TERS measurements.

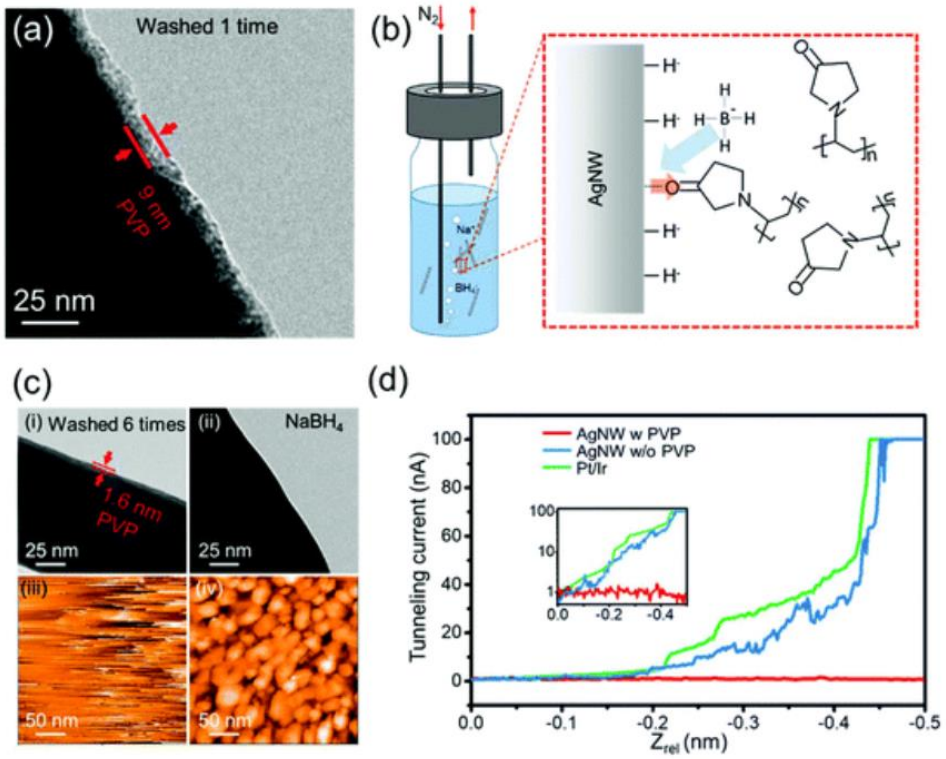

Figure 1.17 Removal of surfactant molecules from AgNW surfaces and its impacts on STM imaging. (a) TEM confirms that the as-prepared AgNWs are coated by a thin layer (~9 nm) of PVP molecules (b) Schematic illustration of the surfactant removal process. (c) Comparison of AgNWs prepared by the conventional cleaning method (6 times of washing with ethanol, inset i) and the $NaBH_4$ cleaning method (inset ii). The conventional method leaves ~1.6 nm of PVP residues that result in a poor STM image quality as shown in (iii). AgNWs treated by $NaBH_4$ cleaning have PVP-free surface and can serve as STM probes for topographical imaging (iv) (STM conditions: −1 V probe bias, −1 nA tunneling current). (d) Comparison of tunneling current variations as a function of the probe movement toward the substrate (probe bias: −1 V). Reproduced with permission from ref. 132.

Same PVP removal method was used in another work from the same group in 2019, where Liu and Yan designed a novel fiber-in-fiber-out STM-TERS configuration. By mounting AgNW onto a tapered optical fiber, they demonstrated that the SPP TM0 mode could be selectively excited from linearly-polarized incident light.[133] As shown in **Figure**

1.18a and **b**, the center of the axially symmetric TM0 mode and the Gaussian-like LP01 mode in the fiber are not aligned when the AgNW is attached to the sidewall of the fiber. As shown in **Figure 1.18c**, the effective mode index rapidly decreases and ultimately equals the mode index of the TM0 mode in coupling zone 1 as the light moves through the OF mode toward the tip, resulting in the efficient excitation of that mode. Additionally, the comparatively poor coupling efficiency in zone 2 precludes the conversion of SPPs via the atomic triggered fast adiabatic transit process from the TM0 mode to the HE1 mode. 131 As shown by the polarization analysis in **Figure 1.18 c**, all of these components work together to guarantee that around 70% of the incoming light is coupled from the fiber to the TM0 mode. Furthermore, it eliminates any potential disturbance during the LZ transition thanks to the uniform AgNW diameter and the atomically clean AgNW surface. High coupling efficiency is experimentally shown as a result. Additionally, the AgNW waveguide to optical fiber back coupling is effective, enabling the development of a fiber-in-fiber-out STM-based NSOM TERS with a 1 nm spatial resolution (**Figure 1.18 e, f**).

In our latest works, we have proved that chemically synthesized silver nanowires are promising 1D waveguide to be used as scanning probes for both AFM and STM-based TERS measurement. While with remote excitation at silver nanowire and silver nanocube junction, our AFM-TERS shows 10 nm spatial resolution, the fiber-in-fiber-out STM-TERS gave 1 nm resolution scanning over CNT samples. In addition, it has been demonstrated that silver nanowires tip radius has profound influence in the spatial resolution and Raman enhancement which is further demonstrated in the work shown in Chapter 3.

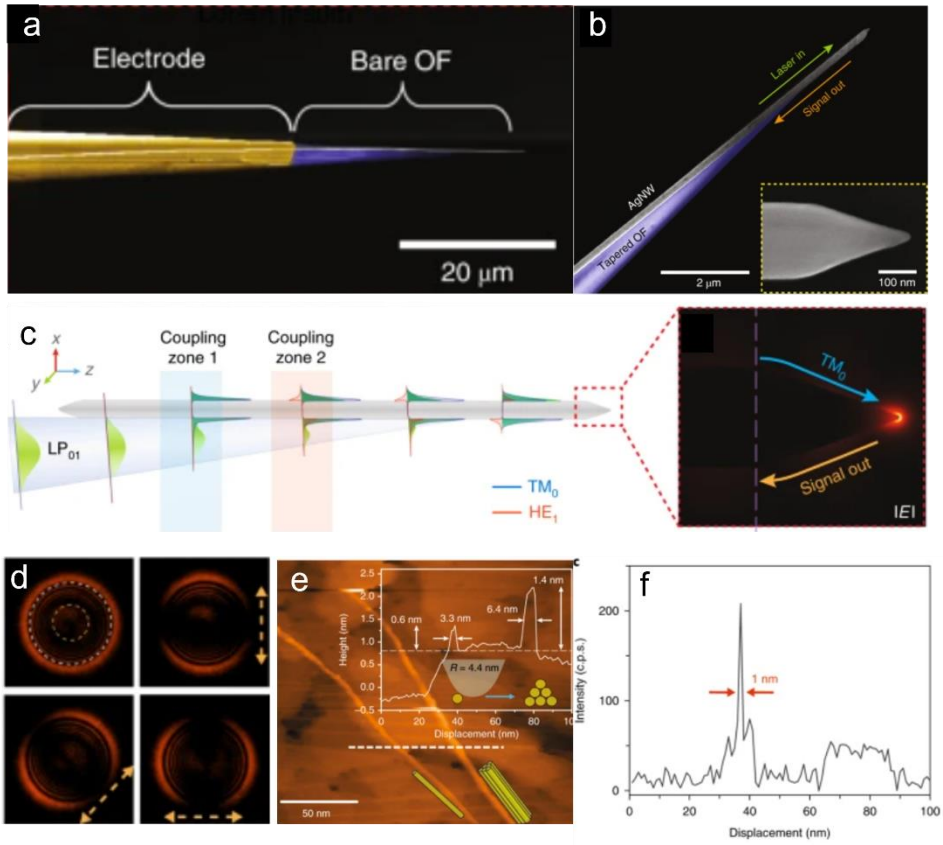

Figure 1.18 The lens-free TERS configuration of nanowire-assisted selective-coupling probes (a,b) images of a TERS probe for STM scanning. (c) Schematic illustration of the LZ coupling over the visible wavelength range. (d) Polarization analysis of the k-space verifies the TM0 mode generation. (e,f) The lens-free TERS measurement on a SW-CNT sample. Reprinted with permission from ref. 133.

1.4 References

1. Smith, G. D.; Clark, R. J. H., *Raman microscopy in archaeological science*, *J Archaeol Sci*, **2004**, 31, (8), 1137-1160.

2. Eberhardt, K.; Stiebing, C.; Matthaus, C.; Schmitt, M.; Popp, J., *Advantages and limitations of Raman spectroscopy for molecular diagnostics: an update*, *Expert Rev Mol Diagn*, **2015**, 15, (6), 773-787.

3. Richard, L. McCreery. *Raman Spectroscopy for Chemical Analysis*, *Meas Sci Technol*, **2001**, 12, (5), 653.

4. Le Ru, Eric; Etchegoin, Pablo, *Principles of Surface-Enhanced Raman Spectroscopy: and related plasmonic effects*. Elsevier: 2008.

5. Fleischmann, M.; Hendra, P. J.; Mcquillan, A. J., *Raman-Spectra of Pyridine Adsorbed at a Silver Electrode*, *Chemical Physics Letters*, **1974**, 26, (2), 163-166.

6. Jeanmaire, David L.; Van Duyne, Richard P., *Surface raman spectroelectrochemistry: Part I. Heterocyclic, aromatic, and aliphatic amines adsorbed on the anodized silver electrode*, *Journal of Electroanalytical Chemistry and Interfacial Electrochemistry*, **1977**, 84, (1), 1-20.

7. Albrecht, M Grant; Creighton, J Alan. *Anomalously intense Raman spectra of pyridine at a silver electrode*, *J Am Chem Soc*, **1977**, 99, (15), 5215-5217.

8. Nie, Shuming; Emory, Steven R. *Probing single molecules and single nanoparticles by surface-enhanced Raman scattering*, *science*, **1997**, 275, (5303), 1102-1106.

9. Kneipp, Katrin; Wang, Yang; Kneipp, Harald; Perelman, Lev T; Itzkan, Irving; Dasari, Ramachandra R; Feld, Michael S. *Single molecule detection using surface-enhanced Raman scattering (SERS)*, *Phys Rev Lett*, **1997**, 78, (9), 1667.

10. Cialla, Dana; Pollok, Sibyll; Steinbrücker, Carolin; Weber, Karina; Popp, Jürgen. *SERS-based detection of biomolecules*, *Nanophotonics*, **2014**, 3, (6), 383-411.

11. Ling, Xing Yi; Yan, Ruoxue; Lo, Sylvia; Hoang, Dat Tien; Liu, Chong; Fardy, Melissa A; Khan, Sher Bahadar; Asiri, Abdullah M; Bawaked, Salem M; Yang, Peidong. *Alumina-coated Ag nanocrystal monolayers as surfaceenhanced Raman spectroscopy platforms for the direct spectroscopic detection of water splitting reaction intermediates*, *Nano Res*, **2014**, 7, (1), 132-143.

12. Ding, S. Y.; You, E. M.; Tian, Z. Q.; Moskovits, M., *Electromagnetic theories of surface-enhanced Raman spectroscopy*, *Chem Soc Rev*, **2017**, 46, (13), 4042-4076.

13. Aroca, Ricardo, *Surface-enhanced vibrational spectroscopy*. John Wiley & Sons: 2006.

14. Lombardi, J. R.; Birke, R. L., *A Unified View of Surface-Enhanced Raman Scattering*, *Accounts Chem Res*, **2009**, 42, (6), 734-742.

15. Otto, A., *The 'chemical' (electronic) contribution to surface-enhanced Raman scattering*, *J Raman Spectrosc*, **2005**, 36, (6-7), 497-509.

16. Otto, Andreas. *Charge transfer in first layer enhanced Raman scattering and surface resistance*, *Quarterly Physics Review*, **2017**, 3, (3).

17. Jensen, Lasse; Aikens, Christine M; Schatz, George C. *Electronic structure methods for studying surface-enhanced Raman scattering*, *Chem Soc Rev*, **2008**, 37, (5), 1061-1073.

18. Long, Derek Albert; Long, DA, *The Raman effect: a unified treatment of the theory of Raman scattering by molecules*. Wiley Chichester: 2002; Vol. 8.

19. McFarland, Adam D; Young, Matthew A; Dieringer, Jon A; Van Duyne, Richard P. *Wavelength-scanned surface-enhanced Raman excitation spectroscopy*, *The Journal of Physical Chemistry B*, **2005**, 109, (22), 11279-11285.

20. Van Duyne, Richard P. *Laser excitation of Raman scattering from adsorbed molecules on electrode surfaces*, *Chemical and biochemical applications of lasers*, **2012**, 4, 101-185.

21. Biagioni, P.; Huang, J. S.; Hecht, B., *Nanoantennas for visible and infrared radiation*, *Rep Prog Phys*, **2012**, 75, (2).

22. Willets, Katherine A; Van Duyne, Richard P. *Localized surface plasmon resonance spectroscopy and sensing*, *Annual review of physical chemistry*, **2007**, 58, (1), 267-297.

23. West, P. R.; Ishii, S.; Naik, G. V.; Emani, N. K.; Shalaev, V. M.; Boltasseva, A., *Searching for better plasmonic materials*, *Laser Photonics Rev*, **2010**, 4, (6), 795-808.

24. Michieli, N.; Pilot, R.; Russo, V.; Scian, C.; Todescato, F.; Signorini, R.; Agnoli, S.; Cesca, T.; Bozio, R.; Mattei, G., *Oxidation effects on the SERS response of silver nanoprism arrays*, *Rsc Adv*, **2017**, 7, (1), 369-378.

25. Mcmahon, M.; Lopez, R.; Meyer, H. M.; Feldman, L. C.; Haglund, R. F., *Rapid tarnishing of silver nanoparticles in ambient laboratory air*, *Appl Phys B-Lasers O*, **2005**, 80, (7), 915-921.

26. Burge, D. K.; Bennett, J. M.; Peck, R. L.; Bennett, H. E., *Growth of Surface Films on Silver*, *Surface Science*, **1969**, 16, 303-&.

27. Bennett, H. E.; Peck, R. L.; Burge, D. K.; Bennett, J. M., *Formation and Growth of Tarnish on Evaporated Silver Films*, *J Appl Phys*, **1969**, 40, (8), 3351-&.

28. Chan, G. H.; Zhao, J.; Hicks, E. M.; Schatz, G. C.; Van Duyne, R. P., *Plasmonic properties of copper nanoparticles fabricated by nanosphere lithography*, *Nano Lett*, **2007**, 7, (7), 1947-1952.

29. Muniz-Miranda, M.; Gellini, C.; Giorgetti, E., *Surface-Enhanced Raman Scattering from Copper Nanoparticles Obtained by Laser Ablation*, *J Phys Chem C*, **2011**, 115, (12), 5021-5027.

30. Markin, A. V.; Markina, N. E.; Popp, J.; Cialla-May, D., *Copper nanostructures for chemical analysis using surface-enhanced Raman spectroscopy*, *Trac-Trend Anal Chem*, **2018**, 108, 247-259.

31. Taguchi, A.; Hayazawa, N.; Furusawa, K.; Ishitobi, H.; Kawata, S., *Deep-UV tip-enhanced Raman scattering*, *J Raman Spectrosc*, **2009**, 40, (9), 1324-1330.

32. Lay, Chee Leng; Koh, Charlynn Sher Lin; Wang, Jing; Lee, Yih Hong; Jiang, Ruibin; Yang, Yijie; Yang, Zhe; Phang, In Yee; Ling, Xing Yi. *Aluminum nanostructures with strong visible-range SERS activity for versatile micropatterning of molecular security labels*, *Nanoscale*, **2018**, 10, (2), 575-581.

33. Tian, Shu; Neumann, Oara; McClain, Michael J; Yang, Xiao; Zhou, Linan; Zhang, Chao; Nordlander, Peter; Halas, Naomi J. *Aluminum nanocrystals: a sustainable substrate for quantitative SERS-based DNA detection*, *Nano Lett*, **2017**, 17, (8), 5071-5077.

34. Knight, Mark W; King, Nicholas S; Liu, Lifei; Everitt, Henry O; Nordlander, Peter; Halas, Naomi J. *Aluminum for plasmonics*, *Acs Nano*, **2014**, 8, (1), 834-840.

35. Naik, Gururaj V; Shalaev, Vladimir M; Boltasseva, Alexandra. *Alternative plasmonic materials: beyond gold and silver*, *Adv Mater*, **2013**, 25, (24), 3264-3294.

36. Lombardi, John R; Birke, Ronald L. *Theory of surface-enhanced Raman scattering in semiconductors*, *The Journal of Physical Chemistry C*, **2014**, 118, (20), 11120-11130.

37. Demirel, Gokhan; Usta, Hakan; Yilmaz, Mehmet; Celik, Merve; Alidagi, Husniye Ardic; Buyukserin, Fatih. *Surface-enhanced Raman spectroscopy (SERS): an adventure from plasmonic metals to organic semiconductors as SERS platforms*, *J Mater Chem C*, **2018**, 6, (20), 5314-5335.

38. Ji, Wei; Zhao, Bing; Ozaki, Yukihiro. *Semiconductor materials in analytical applications of surface -enhanced Raman scattering*, *J Raman Spectrosc*, **2016**, 47, (1), 51-58.

39. Mahmoudi, Morteza; Lohse, Samuel E; Murphy, Catherine J; Fathizadeh, Arman; Montazeri, Abbas; Suslick, Kenneth S. *Variation of protein corona composition of gold nanoparticles following plasmonic heating*, *Nano Lett*, **2014**, 14, (1), 6-12.

40. Alessandri, Ivano; Lombardi, John R. *Enhanced Raman scattering with dielectrics*, *Chem Rev*, **2016**, 116, (24), 14921-14981.

41. Naik, Gururaj V; Schroeder, Jeremy L; Ni, Xingjie; Kildishev, Alexander V; Sands, Timothy D; Boltasseva, Alexandra. *Titanium nitride as a plasmonic material for visible and near-infrared wavelengths [erratum]*, *Optical Materials Express*, **2013**, 3, (10), 1658-1659.

42. Patsalas, Panos; Kalfagiannis, Nikolaos; Kassavetis, Spyros. *Optical properties and plasmonic performance of titanium nitride*, *Materials*, **2015**, 8, (6), 3128-3154.

43. Juneja, Soniya; Shishodia, Manmohan Singh. *Surface plasmon amplification in refractory transition metal nitrides based nanoparticle dimers*, *Optics Communications*, **2019**, 433, 89-96.

44. Boltasseva, Alexandra. *Empowering plasmonics and metamaterials technology with new material platforms*, *Mrs Bull*, **2014**, 39, (5), 461-468.

45. Guler, Urcan; Suslov, Sergey; Kildishev, Alexander V; Boltasseva, Alexandra; Shalaev, Vladimir M. *Colloidal plasmonic titanium nitride nanoparticles: properties and applications*, *Nanophotonics*, **2015**, 4, (3), 269-276.

46. Kerker, Milton, *The scattering of light and other electromagnetic radiation*. Elsevier: 2016.

47. Bontempi, Nicolò; Vassalini, Irene; Alessandri, Ivano. *All‐dielectric core/shell resonators: From plasmon‐free SERS to multimodal analysis*, *J Raman Spectrosc*, **2018**, 49, (6), 943-953.

48. Pilot, Roberto; Signorini, Raffaella; Durante, Christian; Orian, Laura; Bhamidipati, Manjari; Fabris, Laura. *A review on surface-enhanced Raman scattering*, *Biosensors*, **2019**, 9, (2), 57.

49. Wustholz, Kristin L; Henry, Anne-Isabelle; McMahon, Jeffrey M; Freeman, R Griffith; Valley, Nicholas; Piotti, Marcelo E; Natan, Michael J; Schatz, George C; Van Duyne, Richard P. *Structure− activity relationships in gold nanoparticle dimers and trimers for surface-enhanced Raman spectroscopy*, *J Am Chem Soc*, **2010**, 132, (31), 10903-10910.

50. Huang, Yu; Zhou, Qin; Hou, Mengjing; Ma, Lingwei; Zhang, Zhengjun. *Nanogap effects on near-and far-field plasmonic behaviors of metallic nanoparticle dimers*, *Phys Chem Chem Phys*, **2015**, 17, (43), 29293-29298.

51. McMahon, Jeffrey M; Gray, Stephen K; Schatz, George C. *Fundamental behavior of electric field enhancements in the gaps between closely spaced nanostructures*, *Phys Rev B*, **2011**, 83, (11), 115428.

52. McMahon, Jeffrey M; Li, Shuzhou; Ausman, Logan K; Schatz, George C. *Modeling the effect of small gaps in surface-enhanced Raman spectroscopy, The Journal of Physical Chemistry C*, **2012**, 116, (2), 1627-1637.

53. Mahmoud, MA; El-Sayed, MA. *Aggregation of gold nanoframes reduces, rather than enhances, SERS efficiency due to the trade-off of the inter-and intraparticle plasmonic fields, Nano Lett*, **2009**, 9, (8), 3025-3031.

54. Pilot, R; Zoppi, A; Trigari, S; Deepak, FL; Giorgetti, E; Bozio, R. *Wavelength dispersion of the local field intensity in silver–gold nanocages, Phys Chem Chem Phys*, **2015**, 17, (11), 7355-7365.

55. Hajisalem, Ghazal; Nezami, Mohammedreza S; Gordon, Reuven. *Probing the quantum tunneling limit of plasmonic enhancement by third harmonic generation, Nano Lett*, **2014**, 14, (11), 6651-6654.

56. Natan, Michael J. *Concluding remarks surface enhanced Raman scattering, Faraday Discussions*, **2006**, 132, 321-328.

57. Lin, Xiu-Mei; Cui, Yan; Xu, Yan-Hui; Ren, Bin; Tian, Zhong-Qun. *Surface-enhanced Raman spectroscopy: substrate-related issues, Anal Bioanal Chem*, **2009**, 394, (7), 1729-1745.

58. Grabar, Katherine C; Smith, Patrick C; Musick, Michael D; Davis, Jennifer A; Walter, Daniel G; Jackson, Michael A; Guthrie, Andrea P; Natan, Michael J. *Kinetic control of interparticle spacing in Au colloid-based surfaces: rational nanometer-scale architecture, J Am Chem Soc*, **1996**, 118, (5), 1148-1153.

59. Brown, Kenneth R; Natan, Michael J. *Hydroxylamine seeding of colloidal Au nanoparticles in solution and on surfaces, Langmuir*, **1998**, 14, (4), 726-728.

60. Roberts, GG; Films, Langmuir–Blodgett. *Plenum, New York*, **1990**, 990.

61. Tao, Andrea R; Huang, Jiaxing; Yang, Peidong. *Langmuir− Blodgettry of nanocrystals and nanowires, Accounts Chem Res*, **2008**, 41, (12), 1662-1673.

62. Mulvihill, Martin; Tao, Andrea; Benjauthrit, Kanokraj; Arnold, John; Yang, Peidong. *Surface-enhanced Raman spectroscopy for trace arsenic detection in contaminated water, Angewandte Chemie International Edition*, **2008**, 47, (34), 6456-6460.

63. Tao, Andrea; Sinsermsuksakul, Prasert; Yang, Peidong. *Tunable plasmonic lattices of silver nanocrystals, Nat Nanotechnol*, **2007**, 2, (7), 435-440.

64. Mahajan, Sumeet; Abdelsalam, Mamdouh; Suguwara, Yoshiro; Cintra, Suzanne; Russell, Andrea; Baumberg, Jeremy; Bartlett, Philip. *Tuning plasmons on nano-structured substrates for NIR-SERS, Phys Chem Chem Phys*, **2007**, 9, (1), 104-109.

65. Haynes, Christy L; Van Duyne, Richard P. *Plasmon-sampled surface-enhanced Raman excitation spectroscopy, The Journal of Physical Chemistry B*, **2003**, 107, (30), 7426-7433.

66. Wu, De-Yin; Li, Jian-Feng; Ren, Bin; Tian, Zhong-Qun. *Electrochemical surface-enhanced Raman spectroscopy of nanostructures, Chem Soc Rev*, **2008**, 37, (5), 1025-1041.

67. Myers, Anne B. *Resonance Raman intensity analysis of excited-state dynamics, Accounts Chem Res*, **1997**, 30, (12), 519-527.

68. Synge, E. H., *XXXVIII. A suggested method for extending microscopic resolution into the ultra-microscopic region, The London, Edinburgh, and Dublin Philosophical Magazine and Journal of Science*, **1928**, 6, (35), 356-362.

69. Pohl, D. W.; Denk, W.; Lanz, M., *Optical stethoscopy: Image recording with resolution λ/20, Appl Phys Lett*, **1984**, 44, (7), 651-653.

70. Wessel, John. *Surface-enhanced optical microscopy, JOSA B*, **1985**, 2, (9), 1538-1541.

71. Anderson, Mark S. *Locally enhanced Raman spectroscopy with an atomic force microscope, Appl Phys Lett*, **2000**, 76, (21), 3130-3132.

72. Hayazawa, Norihiko; Inouye, Yasushi; Sekkat, Zouheir; Kawata, Satoshi. *Metallized tip amplification of near-field Raman scattering, Optics Communications*, **2000**, 183, (1-4), 333-336.

73. Pettinger, Bruno; Picardi, Gennaro; Schuster, Rolf; Ertl, Gerhard. *Surface Enhanced Raman Spectroscopy: Towards Single Molecule Spectroscopy, Electrochemistry*, **2000**, 68, (12), 942-949.

74. Stöckle, Raoul M; Suh, Yung Doug; Deckert, Volker; Zenobi, Renato. *Nanoscale chemical analysis by tip-enhanced Raman spectroscopy, Chemical Physics Letters*, **2000**, 318, (1-3), 131-136.

75. Su, Weitao; Roy, Debdulal. *Visualizing graphene edges using tip-enhanced Raman spectroscopy, Journal of Vacuum Science & Technology B, Nanotechnology and Microelectronics: Materials, Processing, Measurement, and Phenomena*, **2013**, 31, (4), 041808.

76. Johnson, Timothy W.; Lapin, Zachary J.; Beams, Ryan; Lindquist, Nathan C.; Rodrigo, Sergio G.; Novotny, Lukas; Oh, Sang-Hyun. *Highly Reproducible Near-Field Optical Imaging with Sub-20-nm Resolution Based on Template-Stripped Gold Pyramids, Acs Nano*, **2012**, 6, (10), 9168-9174.

77. Yu, Jun; Saito, Yuika; Ichimura, Taro; Kawata, Satoshi; Verma, Prabhat. *Far-field free tapping-mode tip-enhanced Raman microscopy*, *Appl Phys Lett*, **2013**, 102, (12), 123110.

78. Neugebauer, Ute; Rösch, Petra; Schmitt, Michael; Popp, Jürgen; Julien, Carine; Rasmussen, Akiko; Budich, Christian; Deckert, Volker. *On the way to nanometer-sized information of the bacterial surface by tip-enhanced Raman spectroscopy*, *Chemphyschem: a European journal of chemical physics and physical chemistry*, **2006**, 7, (7), 1428-1430.

79. Bailo, Elena; Deckert, Volker. *Tip-enhanced Raman spectroscopy of single RNA strands: towards a novel direct-sequencing method*, *Angewandte Chemie International Edition*, **2008**, 47, (9), 1658-1661.

80. Ghislandi, Marcos; Hoffmann, Günter G; Tkalya, Evgeniy; Xue, Lijing; With, Gijsbertus De. *Tip-enhanced Raman spectroscopy and mapping of graphene sheets*, *Appl Spectrosc Rev*, **2012**, 47, (5), 371-381.

81. Rickman, RH; Dunstan, PR. *Enhancement of lattice defect signatures in graphene and ultrathin graphite using tip-enhanced Raman spectroscopy*, *J Raman Spectrosc*, **2014**, 45, (1), 15-21.

82. Kumar, Naresh; Mignuzzi, Sandro; Su, Weitao; Roy, Debdulal. *Tip-enhanced Raman spectroscopy: principles and applications*, *EPJ Techniques and Instrumentation*, **2015**, 2, (1), 9.

83. Kneipp, Katrin; Moskovits, Martin; Kneipp, Harald, *Surface-enhanced Raman scattering: physics and applications*. Springer Science & Business Media: 2006; Vol. 103.

84. Sharma, Bhavya; Frontiera, Renee R; Henry, Anne-Isabelle; Ringe, Emilie; Van Duyne, Richard P. *SERS: Materials, applications, and the future*, *Materials today*, **2012**, 15, (1-2), 16-25.

85. Pettinger, Bruno. *Single-molecule surface-and tip-enhanced Raman spectroscopy*, *Molecular Physics*, **2010**, 108, (16), 2039-2059.

86. Yano, Taka-aki; Verma, Prabhat; Saito, Yuika; Ichimura, Taro; Kawata, Satoshi. *Pressure-assisted tip-enhanced Raman imaging at a resolution of a few nanometres*, *Nature Photonics*, **2009**, 3, (8), 473-477.

87. Chen, Chi; Hayazawa, Norihiko; Kawata, Satoshi. *A 1.7 nm resolution chemical analysis of carbon nanotubes by tip-enhanced Raman imaging in the ambient*, *Nat Commun*, **2014**, 5, (1), 1-5.

88. Zhang, Renhe; Zhang, Yao; Dong, ZC; Jiang, S; Zhang, C; Chen, LG; Zhang, L; Liao, Y; Aizpurua, J; Luo, Y ea. *Chemical mapping of a single molecule by plasmon-enhanced Raman scattering*, *Nature*, **2013**, 498, (7452), 82-86.

89. Kharintsev, SS; Hoffmann, GG; Dorozhkin, PS; Loos, J. *Atomic force and shear force based tip-enhanced Raman spectroscopy and imaging*, *Nanotechnology*, **2007**, 18, (31), 315502.

90. Zhang, Renhe; Zhang, Y; Dong, ZC; Jiang, S; Zhang, C; Chen, LG; Zhang, L; Liao, Y; Aizpurua, J; Luo, Y ea. *Chemical mapping of a single molecule by plasmon-enhanced Raman scattering*, *Nature*, **2013**, 498, (7452), 82.

91. Fang, Yurui; Zhang, Zhenglong; Sun, Mengtao. *High vacuum tip-enhanced Raman spectroscope based on a scanning tunneling microscope*, *Rev Sci Instrum*, **2016**, 87, (3), 033104.

92. Sun, Mengtao; Zhang, Zhenglong; Chen, Li; Sheng, Shaoxiang; Xu, Hongxing. *Plasmonic gradient effects on high vacuum tip-enhanced Raman spectroscopy*, *Advanced Optical Materials*, **2014**, 2, (1), 74-80.

93. Sun, Mengtao; Fang, Yurui; Zhang, Zhenyu; Xu, Hongxing. *Activated vibrational modes and Fermi resonance in tip-enhanced Raman spectroscopy*, *Phys Rev E*, **2013**, 87, (2), 020401.

94. Zhang, Weihua; Cui, Xudong; Yeo, Boon-Siang; Schmid, Thomas; Hafner, Christian; Zenobi, Renato. *Nanoscale roughness on metal surfaces can increase tip-enhanced Raman scattering by an order of magnitude*, *Nano Lett*, **2007**, 7, (5), 1401-1405.

95. Sun, Mengtao; Fang, Yurui; Yang, Zhilin; Xu, Hongxing. *Chemical and electromagnetic mechanisms of tip-enhanced Raman scattering*, *Phys Chem Chem Phys*, **2009**, 11, (41), 9412-9419.

96. Ren, Bin; Picardi, Gennaro; Pettinger, Bruno; Schuster, Rolf; Ertl, Gerhard. *Tip-enhanced Raman spectroscopy of benzenethiol adsorbed on Au and Pt single-crystal surfaces*, *Angewandte Chemie International Edition*, **2005**, 44, (1), 139-142.

97. Love, J Christopher; Estroff, Lara A; Kriebel, Jennah K; Nuzzo, Ralph G; Whitesides, George M. *Self-assembled monolayers of thiolates on metals as a form of nanotechnology*, *Chem Rev*, **2005**, 105, (4), 1103-1170.

98. Steidtner, Jens; Pettinger, Bruno. *Tip-enhanced Raman spectroscopy and microscopy on single dye molecules with 15 nm resolution*, *Phys Rev Lett*, **2008**, 100, (23), 236101.

99. Sun, Mengtao; Zhang, Zhenglong; Zheng, Hairong; Xu, Hongxing. *In-situ plasmon-driven chemical reactions revealed by high vacuum tip-enhanced Raman spectroscopy*, *Scientific reports*, **2012**, 2, (1), 1-4.

100. Klingsporn, Jordan M; Jiang, Nan; Pozzi, Eric A; Sonntag, Matthew D; Chulhai, Dhabih; Seideman, Tamar; Jensen, Lasse; Hersam, Mark C; Duyne, Richard P Van. *Intramolecular insight into adsorbate–substrate interactions via low-temperature, ultrahigh-vacuum tip-enhanced Raman spectroscopy*, *J Am Chem Soc*, **2014**, 136, (10), 3881-3887.

101. Domke, Katrin F; Pettinger, Bruno. *Studying surface chemistry beyond the diffraction limit: 10 years of TERS*, *Chemphyschem*, **2010**, 11, (7), 1365-1373.

102. Kharintsev, SS; Hoffmann, GG; Fishman, AI; Salakhov, M Kh. *Plasmonic optical antenna design for performing tip-enhanced Raman spectroscopy and microscopy*, *Journal of Physics D: Applied Physics*, **2013**, 46, (14), 145501.

103. Zhang, Mingqian; Wang, Rui; Zhu, Zhendong; Wang, Jia; Tian, Qian. *Experimental research on the spectral response of tips for tip-enhanced Raman spectroscopy*, *Journal of Optics*, **2013**, 15, (5), 055006.

104. Asghari-Khiavi, Mehdi; Wood, Bayden R; Hojati-Talemi, Pejman; Downes, Andrew; McNaughton, Don; Mechler, Adam. *Exploring the origin of tip-enhanced Raman scattering; preparation of efficient TERS probes with high yield*, *J Raman Spectrosc*, **2012**, 43, (2), 173-180.

105. Yeo, Boon-Siang; Stadler, Johannes; Schmid, Thomas; Zenobi, Renato; Zhang, Weihua. *Tip-enhanced Raman Spectroscopy–Its status, challenges and future directions*, *Chemical Physics Letters*, **2009**, 472, (1-3), 1-13.

106. Pettinger, Bruno; Domke, Katrin F; Zhang, Dai; Picardi, Gennaro; Schuster, Rolf. *Tip-enhanced Raman scattering: influence of the tip-surface geometry on optical resonance and enhancement*, *Surface Science*, **2009**, 603, (10-12), 1335-1341.

107. Kharintsev, SS; Rogov, AM; Kazarian, SG. *Nanopatterning and tuning of optical taper antenna apex for tip-enhanced Raman scattering performance*, *Rev Sci Instrum*, **2013**, 84, (9), 093106.

108. Stadler, Johannes; Schmid, Thomas; Zenobi, Renato. *Developments in and practical guidelines for tip-enhanced Raman spectroscopy*, *Nanoscale*, **2012**, 4, (6), 1856-1870.

109. Langelüddecke, Lucas; Singh, Prabha; Deckert, Volker. *Exploring the nanoscale: fifteen years of tip-enhanced Raman spectroscopy*, *Appl Spectrosc*, **2015**, 69, (12), 1357-1371.

110. Downes, Andrew; Salter, Donald; Elfick, Alistair. *Heating effects in tip-enhanced optical microscopy*, *Opt Express*, **2006**, 14, (12), 5216-5222.

111. Domke, Katrin F; Zhang, Dai; Pettinger, Bruno. *Enhanced Raman spectroscopy: single molecules or carbon?*, *The Journal of Physical Chemistry C*, **2007**, 111, (24), 8611-8616.

112. Malkovskiy, AV; Malkovsky, VI; Kisliuk, AM; Barrios, CA; Foster, MD; Sokolov, AP. *Tip-induced heating in apertureless near-field optics*, *Journal of Raman Spectroscopy: An International Journal for Original Work in all Aspects of Raman Spectroscopy, Including Higher Order Processes, and also Brillouin and Rayleigh Scattering*, **2009**, 40, (10), 1349-1354.

113. Schmid, T.; Opilik, L.; Blum, C.; Zenobi, R., *Nanoscale Chemical Imaging Using Tip-Enhanced Raman Spectroscopy: A Critical Review*, *Angew Chem Int Edit*, **2013**, 52, (23), 5940-5954.

114. Hayazawa, Norihiko; Yano, Taka-aki; Kawata, Satoshi. *Highly reproducible tip-enhanced Raman scattering using an oxidized and metallized silicon cantilever tip as a tool for everyone*, *J Raman Spectrosc*, **2012**, 43, (9), 1177-1182.

115. Höppener, Christiane; Lapin, Zachary J; Bharadwaj, Palash; Novotny, Lukas. *Self-similar gold-nanoparticle antennas for a cascaded enhancement of the optical field*, *Phys Rev Lett*, **2012**, 109, (1), 017402.

116. Leiterer, Christian; Deckert-Gaudig, Tanja; Singh, Prabha; Wirth, Janina; Deckert, Volker; Fritzsche, Wolfgang. *Dielectrophoretic positioning of single nanoparticles on atomic force microscope tips for tip-enhanced Raman spectroscopy*, *Electrophoresis*, **2015**, 36, (9-10), 1142-1148.

117. Ma, X; Grüßer, M; Schuster, R. *Plasmonic nanospheres with a handle—Local electrochemical deposition of Au or Ag at the apex of optically inactive W-or C-tips*, *Appl Phys Lett*, **2015**, 106, (24), 241103.

118. Dill, Tyler J; Rozin, Matthew J; Palani, Stephen; Tao, Andrea R. *Colloidal nanoantennas for hyperspectral chemical mapping*, *Acs Nano*, **2016**, 10, (8), 7523-7531.

119. Ren, Bin; Picardi, Gennaro; Pettinger, Bruno. *Preparation of gold tips suitable for tip-enhanced Raman spectroscopy and light emission by electrochemical etching*, *Rev Sci Instrum*, **2004**, 75, (4), 837-841.

120. Xu, Gengzhao; Liu, Zhenghui; Xu, Ke; Zhang, Yi; Zhong, Haijian; Fan, Yingmin; Huang, Zengli. *Constant current etching of gold tips suitable for tip-enhanced Raman spectroscopy*, *Rev Sci Instrum*, **2012**, 83, (10), 103708.

121. Zhang, Weihua; Yeo, Boon Siang; Schmid, Thomas; Zenobi, Renato. *Single molecule tip-enhanced Raman spectroscopy with silver tips*, *The Journal of Physical Chemistry C*, **2007**, 111, (4), 1733-1738.

122. Wang, Xi; Liu, Zheng; Zhuang, Mu-De; Zhang, Hai-Ming; Wang, Xiang; Xie, Zhao-Xiong; Wu, De-Yin; Ren, Bin; Tian, Zhong-Qun. *Tip-enhanced Raman spectroscopy for investigating adsorbed species on a single-crystal surface using electrochemically prepared Au tips*, *Appl Phys Lett*, **2007**, 91, (10), 101105.

123. You, Yumeng; Purnawirman, NA; Hu, Hailong; Kasim, Johnson; Yang, Huanping; Du, Chaoling; Yu, Ting; Shen, Zexiang. *Tip‐enhanced Raman spectroscopy using single‐crystalline Ag nanowire as tip*, *J Raman Spectrosc*, **2010**, 41, (10), 1156-1162.

124. Fujita, Yasuhiko; Chiba, Rie; Lu, Gang; Horimoto, Noriko N; Kajimoto, Shinji; Fukumura, Hiroshi; Uji-i, Hiroshi. *A silver nanowire-based tip suitable for STM tip-enhanced Raman scattering*, *Chem Commun*, **2014**, 50, (69), 9839-9841.

125. Lu, Gang; De Keersmaecker, Herlinde; Su, Liang; Kenens, Bart; Rocha, Susana; Fron, Eduard; Chen, Chang; Van Dorpe, Pol; Mizuno, Hideaki; Hofkens, Johan. *Live‐Cell SERS Endoscopy Using Plasmonic Nanowire Waveguides*, *Adv Mater*, **2014**, 26, (30), 5124-5128.

126. Walke, Peter; Fujita, Yasuhiko; Peeters, Wannes; Toyouchi, Shuichi; Frederickx, Wout; De Feyter, Steven; Uji-i, Hiroshi. *Silver nanowires for highly reproducible cantilever based AFM-TERS microscopy: towards a universal TERS probe*, *Nanoscale*, **2018**, 10, (16), 7556-7565.

127. Fujita, Yasuhiko; Walke, Peter; De Feyter, Steven; Uji-i, Hiroshi. *Remote excitation-tip-enhanced Raman scattering microscopy using silver nanowire*, *Japanese Journal of Applied Physics*, **2016**, 55, (8S1), 08NB03.

128. Brodard, Pierre; Bechelany, Mikhael; Philippe, Laetitia; Michler, Johann. *Synthesis and attachment of silver nanowires on atomic force microscopy cantilevers for tip‐enhanced Raman spectroscopy*, *J Raman Spectrosc*, **2012**, 43, (6), 745-749.

129. Dai, Hongjie; Hafner, Jason H; Rinzler, Andrew G; Colbert, Daniel T; Smalley, Richard E. *Nanotubes as nanoprobes in scanning probe microscopy*, *Nature*, **1996**, 384, (6605), 147.

130. Ma, Xuezhi; Zhu, Yangzhi; Kim, Sanggon; Liu, Qiushi; Byrley, Peter; Wei, Yang; Zhang, Jin; Jiang, Kaili; Fan, Shoushan; Yan, Ruoxue. *Sharp-tip silver nanowires mounted on cantilevers for high-aspect-ratio high-resolution imaging*, *Nano Lett*, **2016**, 16, (11), 6896-6902.

131. Ma, Xuezhi; Zhu, Yangzhi; Yu, Ning; Kim, Sanggon; Liu, Qiushi; Apontti, Leonard; Xu, Da; Yan, Ruoxue; Liu, Ming. *Toward High-Contrast Atomic Force Microscopy-Tip-Enhanced Raman Spectroscopy Imaging: Nanoantenna-Mediated Remote-Excitation on Sharp-Tip Silver Nanowire Probes*, *Nano Lett*, **2018**, 19, (1), 100-107.

132. Liu, Qiushi; Kim, Sanggon; Ma, Xuezhi; Yu, Ning; Zhu, Yangzhi; Deng, Siyu; Yan, Ruoxue; Zhao, Huijuan; Liu, Ming. *Ultra-sharp and surfactant-free silver nanowire for scanning tunneling microscopy and tip-enhanced Raman spectroscopy*, *Nanoscale*, **2019**, 11, (16), 7790-7797.

133. Kim, Sanggon; Yu, Ning; Ma, Xuezhi; Zhu, Yangzhi; Liu, Qiushi; Liu, Ming; Yan, Ruoxue. *High external-efficiency nanofocusing for lens-free near-field optical nanoscopy*, *Nature Photonics*, **2019**.

Chapter 2. Size-Tunable Monodispersed Silver Nanocubes for Surface-Enhanced Raman Spectroscopy

2.1 Introduction

Noble metal nanocrystals have been extensively studied for their unique physical and chemical properties different from bulk materials.[1-4] Among the noble metals, low-cost silver nanocrystals gain special attention for their performance in multiple fields such as catalysis, electronics and biosensing.[3, 5, 6] In literature, silver nanoparticles have been synthesized with different shapes such as sphere, cube, octahedron, nanorod and nanowires and the nanostructures are found to have great potential in the field of catalysis, plasmonic sensing, substrate for surface-enhanced Raman scattering (SERS). [7-10] Among these applications, silver nanocrystals are extensively studied and used in SERS to resolve the weak Raman signal issue due to the low inelastic scattering. Silver nanoparticles exhibit localized surface plasmonic resonance (LSPR) absorption depending on many factors including the size and shape of the particles and interparticle distance.[11, 12] Polyhedral such as cubes with well-defined facets and corners are predicted to have distinct scattering signatures and the scattering efficiencies are orders of magnitude higher than their spherical counterparts.[13] In multiple research, silver nanocubes have been used as SERS substrate in the form of monomer, dimer and monolayer.[14-17] While the assembly monolayer of silver nanocubes would provide strongest Raman signal enhancement, no research has been conducted on the size effect of silver nanocubes over a broad range in the form of assembled close-pack monolayers. To address this, monodispersed silver nanocubes need to be synthesized for high quality assembling of the monolayer substrate.

The synthesis of silver nanocubes have been extensively studied and many methods have been developed.[18-25] However, it is still challenging to synthesize monodispersed silver nanocubes with high yield to cubes with controllable lengths over a broad range. Qiang Zhang et al. shared a method with which the authors were able to prepare AgNCs with edge length range of 30-200 nm, but this method was seed-mediated that single-crystal silver seeds need to be prepared separately before growth of AgNCs.[26]

In this work, we report a one-pot synthesis method for monodispersed silver nanocube with tunable size in a broad range from 60 to 180 nm and investigate the size effect of silver nanocubes when monolayer close-packed silver nanocubes are used as SERS substrate.

2.2 Silver Nanocube Synthesis

2.2.1 Chemicals and Materials

Silver nitrate (>99.7%), 1,5-pentanediol (1,5-PD) were purchased from Fisher Chemical. Polyvinylpyrrolidone (PVP, Mw~55000) and copper (II) chloride dihydrate (>99.0%) were purchased from Sigma-Aldrich. All chemicals were used as received.

2.2.2 Synthesis of Silver Nanocubes (AgNCs)

The synthesis of silver nanocubes are based on the work of Andrea Tao *et al.*[23] with modifications. In a typical synthesis, precursor solutions were prepared by dissolving 0.20 g silver nitrate in 10 ml 1,5-PD with addition of 40 ul $CuCl_2$ in 1,5-PD (30 mM) by sonication in ice-water. PVP/1,5-PD solution was prepared by dissolving 0.20 g of PVP in 10 ml 1,5-PD. The precursors were stored in refrigerator before use. In AgNC synthesis, 20 ml 1,5-PD was added to a 100 ml round-bottom flask (RBF) and preheated to synthesis temperature in oil bath for 10 mins under stirring. 500 ul of cold $AgNO_3$

solution was fast injected to the RBF followed by dropwise injection of 500 ul of PVP solution. In every minute after the initial injection, 500 ul $AgNO_3$ and 500 ul PVP solutions were added to the RBF using syringe pump. After a certain reaction time, the feeds were stopped, and the reaction solution was refluxed. The length of reaction and reflux time depend on the size of AgNC needed. After reflux, the reaction solution was quickly removed from the silicon oil bath and cooled down in ice-water. After cooling down, the AgNCs produced were separated from the reaction solution and washed with ethanol to remove excess PVP with centrifuge, after which the AgNCs were redispersed in ethanol and stored in refrigerator.

In polyol-mediated silver nanocube synthesis described above, 1,5-pentanediol which has hydroxyl groups act as both solvent and reducing agent. The capping agent, PVP, was used to build the cubic shape. Finally, the molar ratio of the repeating units of PVP to silver ions determines the morphology of the product that high molar ratio is used for nanocubes and low molar ratio is used for nanowires. A small amount of $CuCl_2$ was added that the formation precipitation of the low solubility of AgCl salt prevents the rapid reduction of metal ions. Besides of the chemicals added to the RBF, we also found that reactions conditions such as reaction temperatures, stirring speed, reaction time and feeding rate could also play an important role in achieving high yield of AgNCs with small variation in size distribution.

2.2.3 Silver Nanocubes and Synthesis Conditions

The synthesis of silver nanocubes is sensitive to a number of factors such as temperature, precursor concentration, precursor feed rate, stirring speed which are important to nucleation, growth rate that directly relate to the final yield to cubes, cube size, and size

distributions. The reaction temperature in our synthesis is the set temperature of the silicon oil bath. As the reaction temperature can greatly affect the seeding and growth speed, it is important to study how the reaction temperature could affect the final yield of silver nanocubes and size distribution. AgNC synthesis were carried out at a temperature from 188 to 192 °C while keeping other reaction conditions such as preheating time, reaction time, the feeding rate of $AgNO_3$ and PVP solutions fixed. The yield of silver nanocubes as well as size distributions has been analyzed from the SEM images obtained with the ethanol purified samples as shown in **Figure 2.1**. The yield of nanocube is defined as the ratio of nanocubes counts to the total nanparticle counts by randomly counting around 400 particles and size distribution is analyzed by measuring the edge length of over 100 nanocubes. Average size and standard deviation are calculated and the ratio of standard deviation to average size is used as an indicator for size distribution. Clearly, the temperature can affect the yield of cubes that with the same amount precursor feed into the reaction system the cube size also varies depending on the amount of Ag precursors grow into cubes. From the results of AgNC prepared at different temperatures, while lower temperatures around 190 °C show yield to AgNCs around 90%, high temperature would decrease the AgNCs yield. This can be attributed to the seeding stage that when temperature is high, different kinds of seeds were formed and the undesirable seeds quickly grow into rods, polyhedrons, and irregular particles. Therefore, in silver nanocubes synthesis, the temperature needs to be well controlled with minimal temperature fluctuations as a few degrees difference in synthesis temperature can lead to significant lower yield to nanocubes.

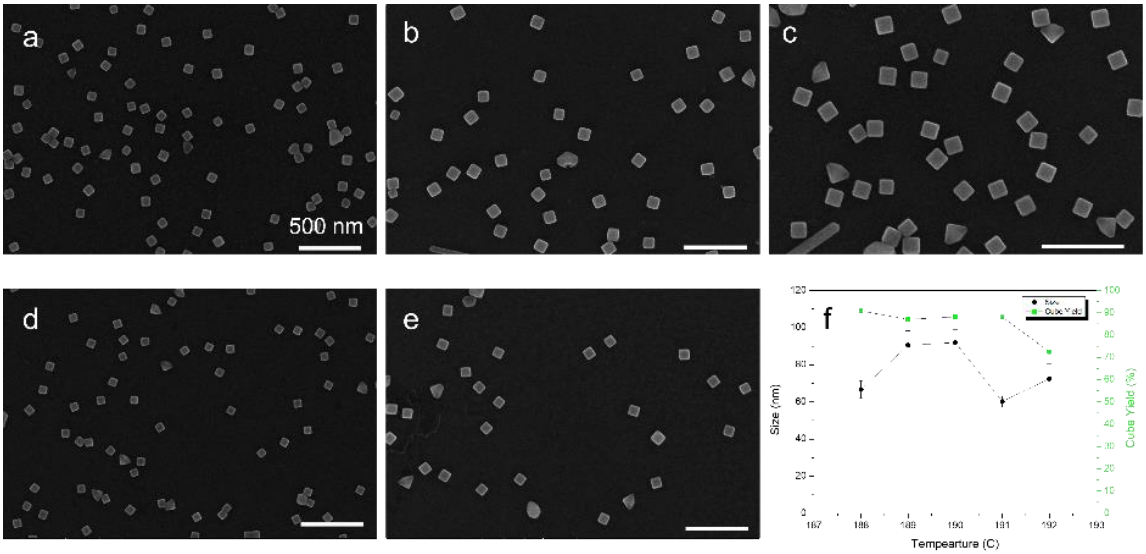

Figure 2.1 Effects of reaction temperature on silver nanowire synthesis. (a~e) show SEM images of silver nanocube synthesized at 188, 189, 190, 191, 192 °C, respectively. F shows the yield of silver nanocubes in each batch of synthesis and the according size distribution. Fixed reaction parameters include preheating time (10 mins), reactants feeding rate (500 ul/min), reaction time (12 mins) and stirring speed (270 rpm).

In our synthesis, $AgNO_3$ and PVP dissolved in 1,5-PD were fed into the RBF using two syringe pumps from which the feeding rate could be easily tuned and well maintained. The amount of reactant injected to the reaction solution could greatly affect the number of seeds produced in the solution as well the growth rate in the later stage which could give us significant different outcomes in terms of cube yield and size distribution. While keeping reaction temperature at 190 °C and reaction time at 12 mins, we varied the amount of $AgNO_3$ and PVP solutions fed into the RBF by tuning the pump feed rate from 400 to 600 ul/min of the same precursor concentrations. The feed rate of precursors is directly relevant to the concentration of $AgNO_3$ in the reaction solution that affect the nucleation to Ag seeds and the growth rate. By analyzing the yield and size distribution, the synthesis conducted with rate of 500 ul/min shows 88.2% yield to silver nanocubes and small size distribution 92.04 ± 6.93 (7.53%).

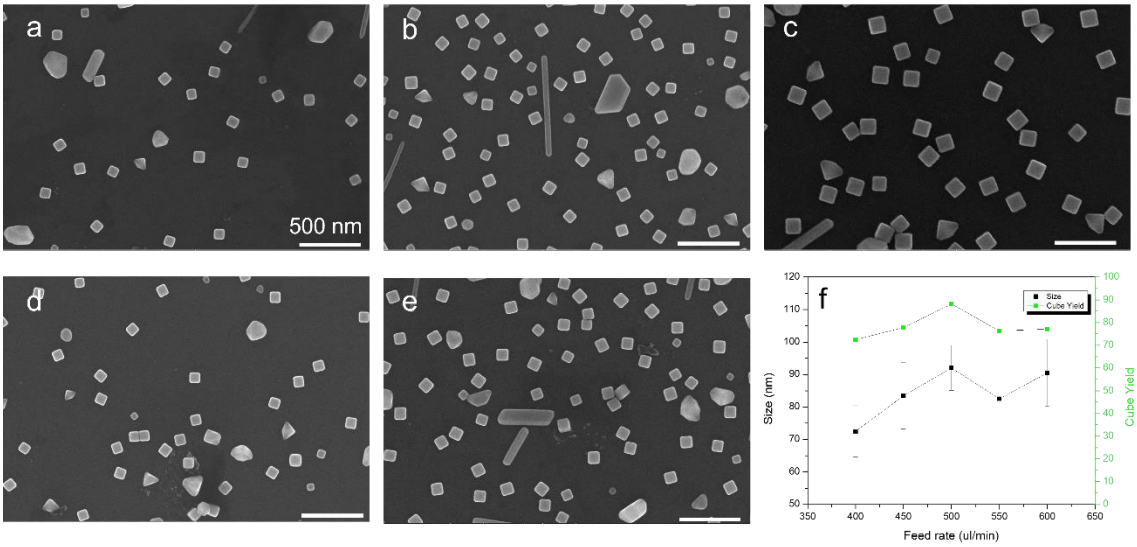

Figure 2.2 Effects of reactants feeding rate on silver nanowire synthesis. (a~e) SEM images of silver nanocube synthesized with a feeding rate of 400, 450, 500, 550, 600 ul, respectively; (f) shows the yield of silver nanocubes in each batch of synthesis and the according size distribution. Reaction temperature (190 °C), reaction time (12 mins) and stirring speed (270 rpm).

From the study of reaction temperature and feed rate above, although with 190 °C reaction time and 500 ul/min feeding rate we can prepare AgNC with good yield, the silver nanocubes we synthesized are not uniform in size which can be easily told from the SEM images in **Figure 2.1** and **Figure 2.2** with the existence of silver nanocubes that are much smaller than the averaging cubes. These smaller silver nanocubes might be produced from multiple stages of seeding which lead to a variation in size from 7 % to 13 % in all the above synthesis that vigorous stirring with 270 rpm in the reaction solution might be too high for monodispersed AgNC synthesis. Therefore, lower stirring speeds were tested at 190 rpm and 230 rpm. Decreasing stirring speed to 230 rpm could improve the uniformity of AgNC size that after 12 mins of reaction, the silver nanocubes produced has smaller variation in size (5.5 %) while further decreasing stirring speed to 190 rpm lead to low yield of AgNC with a large portion of wires and irregular-shaped particles as shown in Figure 2.3. With 190 rpm, the batch of synthesis produced 69.2%

silver nanocubes with a size distribution of 85.3 ± 7.0 nm (8.2%) while with stirring speed of 230 rpm, the yield of AgNCs was 91.0% with a size distribution of 86.4 ± 4.7 nm (5.5%). The results suggest that a lower stirring speed than 270 rpm can reduce the secondary nucleation but if the stirring speed is too low, insufficient stirring might cause large concentration gradient which also results in larger size distribution and lower AgNC yield.

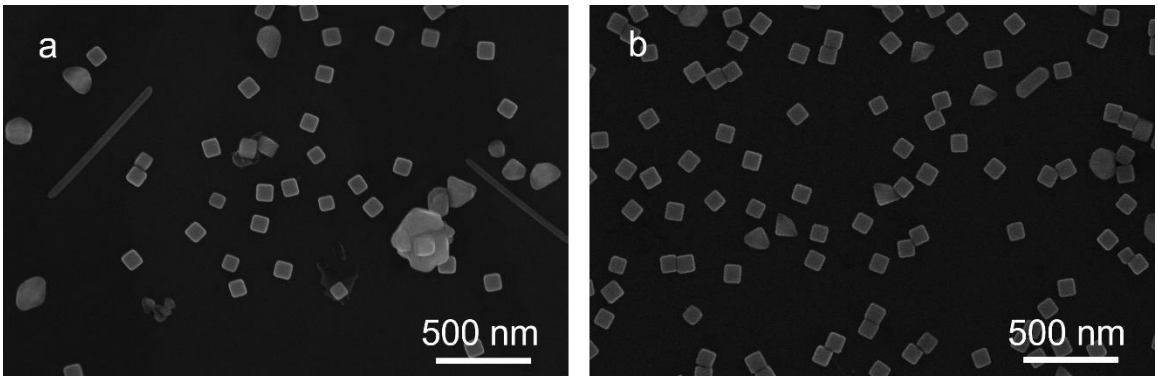

Figure 2.3 Effects of stirring speed on silver nanowire synthesis. (a, b) show SEM images of silver nanocube synthesized with a stirring speed of 190 rpm and 230 rpm, respectively. Fixed reaction parameters include preheating time (10 mins), reaction temperature (190 °C), reaction time (12 mins) and feeding rate (500 ul/min).

As decreasing the stirring speed to 230 rpm helps achieving a uniform size in AgNC synthesis, we then moved a step further to put our effort in tunable size over a broad range monodispersed silver nanocubes synthesis. While it is easier to synthesize small AgNCs, larger cubes cannot be synthesized by simply increasing the amount of $AgNO_3$ addition with longer reaction time. As indicated in Adrea Tao *et al.'s* work[27], at the early stage of silver nanocube synthesis, the {100} planes were stabilized by PVP which lead to the formation of cubes. As the cubes grow larger, the {111} corners are stabilized which leads to the formation of cuboctahedrons and then octahedrons. The shape control of the silver nanocrystals may not be dictated by the capping polymer, but more likely by a kinetically limited equilibrium. Therefore, the challenge in prepare large cubes is to

avoid the truncation at corners of cubes which produces cuboctahedron, and this needs well balance the kinetics and thermodynamics in the synthesis. If only increasing the $AgNO_3$ amount, cuboctahedron forms as shown in **Figure 2.4** with the edge length of 154 nm.

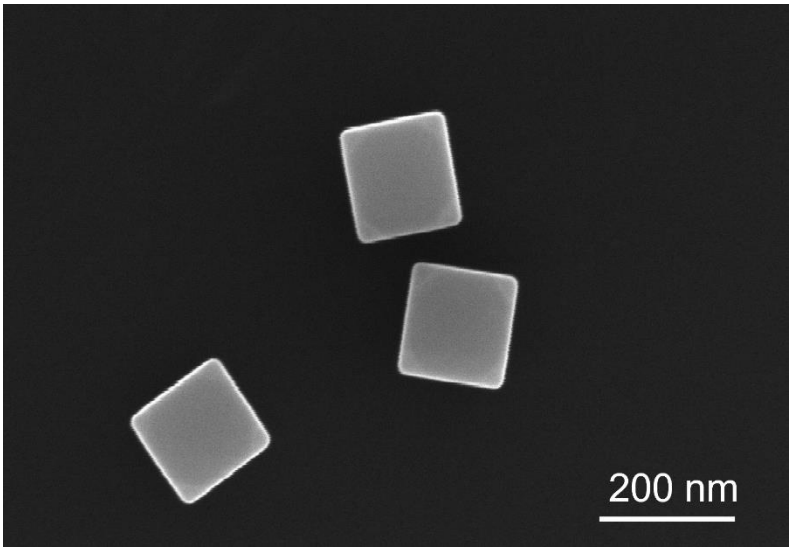

Figure 2.4 SEM image of truncated silver nanocubes. Synthesized with a stirring speed of 230 rpm, reaction temperature (190 °C), reaction time (18 mins) and precursors feeding rate (500 ul/min).

To avoid the cube truncation, we added a reflux step after stopping the feed of $AgNO_3$ and PVP precursors. By stopping the feed, the concentration of free Ag^+ decreases that slow down the growth rate. Therefore, the more thermodynamically stable PVP-passivated {100} can be preferably preserved maintaining a cubic morphology. As shown in **Figure 2.5**, after stopping the injection, silver nanocubes still grow during the reflux period consuming the unreacted Ag^+ that immediately after the feeds were stopped, the average size of cubes was 65.6 ± 3.9 nm (5.9%), and with reflux time of 2 mins, 4 mins, 6mins, the average size of AgNCs increase to 87.2 ± 4.7 nm (5.4%), 109.8 ± 4.9 nm (4.4%) and 125.0 ± 4.9 nm (3.9%), respectively. Further increase the reflux time to 8 and 10 mins the average sizes were measured to be 128.7 ± 4.9 nm (3.8%), 126.4± 3.8 nm

(3.0%) which show no obvious change from 6 mins reflux time indicating the depletion of Ag^+. The small variation in size might be caused by human measurements error. Furthermore, with including a reflux step, we found the size distribution showed a decreasing trend in general which favors the preparation of monodispersed AgNCs. The decrease in size distribution can be attributed to ostwald ripening that consumes the smaller AgNCs formed from secondary nucleation.

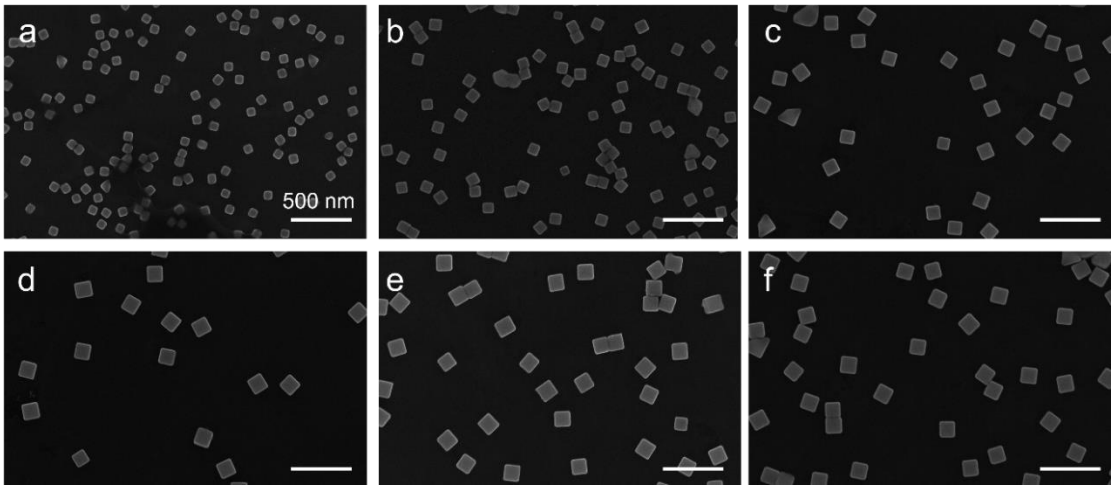

Figure 2.5 Effect of reflux time after stopping precursor feeds. (a~f) SEM images of AgNCs with reflux time of 0, 2, 4, 6, 8, 10 mins, respectively. Synthesis conducted at 190 °C, feed 10 mins, 230 rpm stirring.

After carefully control the reaction time from 8 mins to 16 mins and reflux time from 2 mins to 10 mins, we are able to synthesize silver nanocubes with size over a broad range (60 ~180 nm) with high uniformity (<5 % size variation) as shown in **Figure 2.6** that even with size greater than 150 nm, there is no obvious truncation to the corners of silver nanocubes. UV-Vis spectrums were measured for AgNCs with different sizes (**Figure 2.7**). With the increase of cube size from 61 nm to 180 nm, an obvious redshift in dipolar LSP mode from 489 nm to 861 nm was observed. The position of the dipolar LSP mode and quadrupolar mode can serve as a reference of cube size during synthesis in achieving desired size.[28]

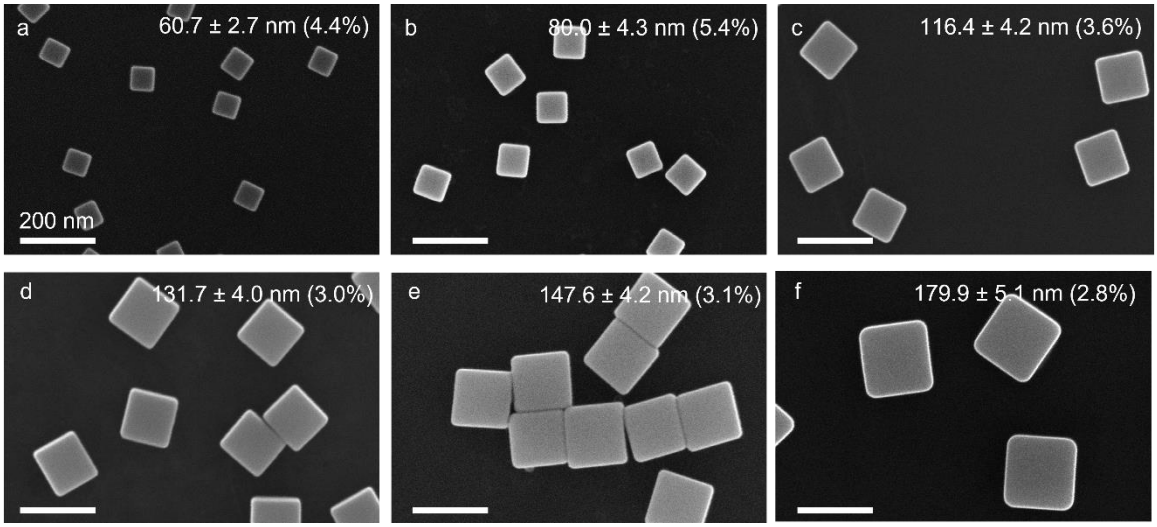

Figure 2.6 Tunable size of silver nanocubes varying reaction and reflux time.

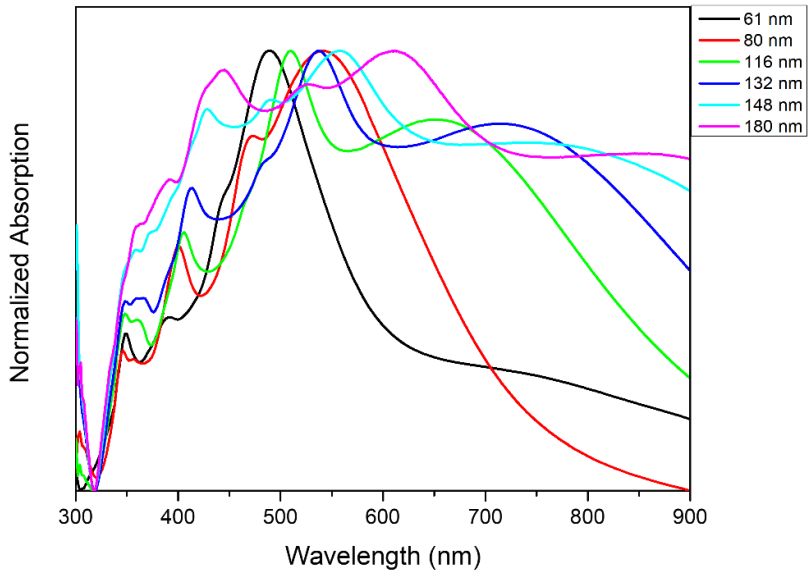

Figure 2.7 Normalized UV-Vis spectra of silver nanocubes with size ranging from 60 nm to 180 nm.

2.3 Tunable Size of AgNC for SERS Substrate

2.3.1 Simulation on Size Dependency

With carefully control the reaction conditions, we can now prepare silver nanocubes over a broad range of 60-180 nms with small size distribution and we then want to take a step

further to see what size of AgNC would provide greater signal enhancement when they are used for SERS substrate. Instead of taking the action and trying blindly with AgNCs of all sizes, we conducted a series of numerical simulations to obtain the electromagnetic field distributions as a guide to at least find out a general trend with COMSOL Multiphysics.

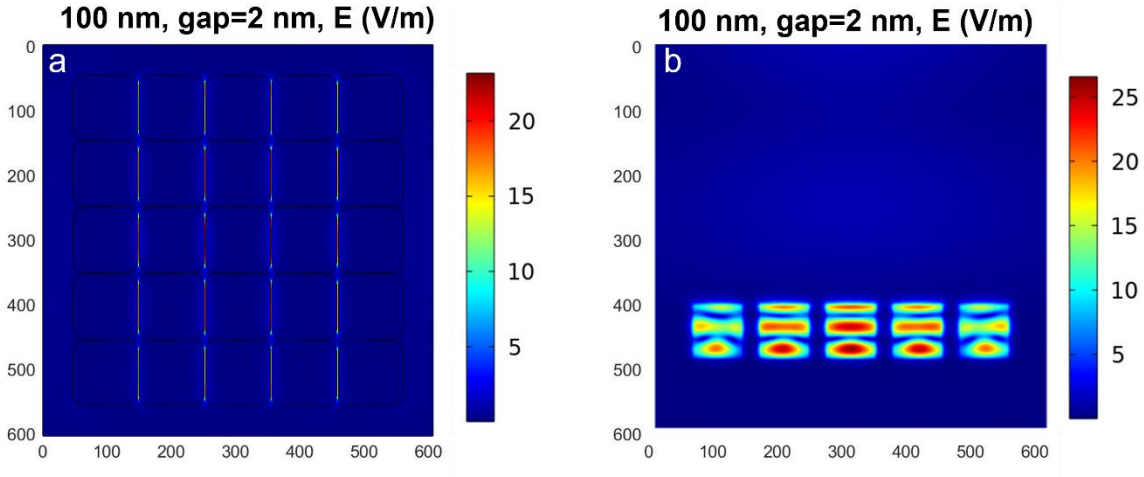

Figure 2.8 Electrical field distribution with 100 nm AgNCs substrate from COMSOL simulation at XY plane (a) and YZ plane. Simulation conducted with 1 V/m excitation electrical field at x-polarization, gap distance of 2 nm between cubes.

As demonstrated by **Figure 2.8**, on the close-packed 100 nm AgNC substrate with gap distance of 2 nm, strong electromagnetic field was observed in the gaps. While the excitation electric field was set to 1 V/m, the electric field in the gaps can reach as large as 26.6 V/m, indicating strong enhancement. Simulations were conducted for AgNCs with varied size (80-180 nm) under the same conditions. As discussed in chapter 1, the enhancement factor is roughly proportional to $|E|^4$, therefore, for each size total $|E|^4$ integrated from the surfaces of AgNCs was calculated and summarized in **Table 2.1**. Based on the simulation results, under perfect conditions, SERS substrate fabricated with AgNCs of around 120 nm size should give the best performance in terms of Raman signal enhancement assuming the matter of interest can get into the gaps between

nanocubes. In the case that materials could not diffuse into the gaps utilizing the top surface only, AgNCs with size around 90 nm might be better candidates for SERS substrate fabrication.

Table 2.1 Summary of E^4 calculation results based on COMSOL simulation from all surfaces of AgNCs and top surface only for AgNCs substrate with cube size from 80 to 180 nm.

AgNC Size nm	Overall E^4 V^4/m^2	Top surface E^4 V^4/m^2
80	1.35E-10	1.07E-13
90	1.06E-09	1.55E-11
100	4.76E-11	5.08E-13
110	3.21E-11	8.39E-15
120	1.94E-09	1.03E-11
130	5.61E-11	6.44E-13
140	4.39E-11	5.65E-14
150	3.88E-10	8.77E-13
160	1.70E-10	1.73E-12
170	5.80E-11	1.91E-13
180	1.25E-10	1.18E-13

2.3.2 LB Assembling of Silver Nanocube Substrate

After silver nanocubes are synthesized, they need to be properly purified before being used for preparing substrate for SERS as the synthesis product includes silver nanoparticles of different morphologies, such as rods, nanowires, triangular plates etc., which would preventing the close pack of nanocubes. These undesirable nanoparticles are removed with filtration. When conducting filtration, filter papers from large to small pore size are used and special attention needs to be paid to the amount of PVP used in diluting the silver nanocube suspensions for filtration, and carefully mix the silver nanocubes with

PVP/H_2O solution to avoid aggregation. After the filtration is complete the resulting solution are concentrated by centrifugation and redispersed and stored in ethanol.

The preparation of the nanocrystal solution for suspension on the water subphase is crucial for successfully film assembly. The nanocrystal solution is a mixture of ethanol and chloroform of round 2:5 ratio. The ethanol suspends the particles better, while the chloroform helps the deposition of nanoparticles to water surface. Usually a solution of 1:5 parts ethanol: chloroform is very slowly added to a concentrated solution of nanoparticles (5-10 mg in 1 ml ethanol). The concentrated solution of particles can be achieved by settling the purified AgNCs overnight or a few days for small size cubes, followed by removal of the settled solution from the bottom of a centrifuge tube with a pipet. The solution with nanoparticles should be added dropwise to the surface of the water on a freshly cleaned Langmuir-Blodgett trough. Care should be taken that nanoparticle do not end up in the subphase through rapid addition of large drops. The remaining solvent from the nanoparticle solution should be allowed to evaporate over the course of 20 minutes to 1.5 hours. During this time the particles should form an even layer over the surface of the water. Close-packed monolayer should form by gently compressing the surface particles. Silicon wafer substrate is then slowly pulled out of the subphase so that the film is transferred to the substrate. With the method described above, LB monolayer substrates were prepared with AgNCs of size around 100 nm, 125 nm and 140 nm as shown in **Figure 2.9**. The SEM images shows closely packed AgNCs monolayer on Si wafer substrates for SERS. The Si wafer substrates were uniformly coated with silver nanocubes at a scale of centimeters suitable for SERS measurements.

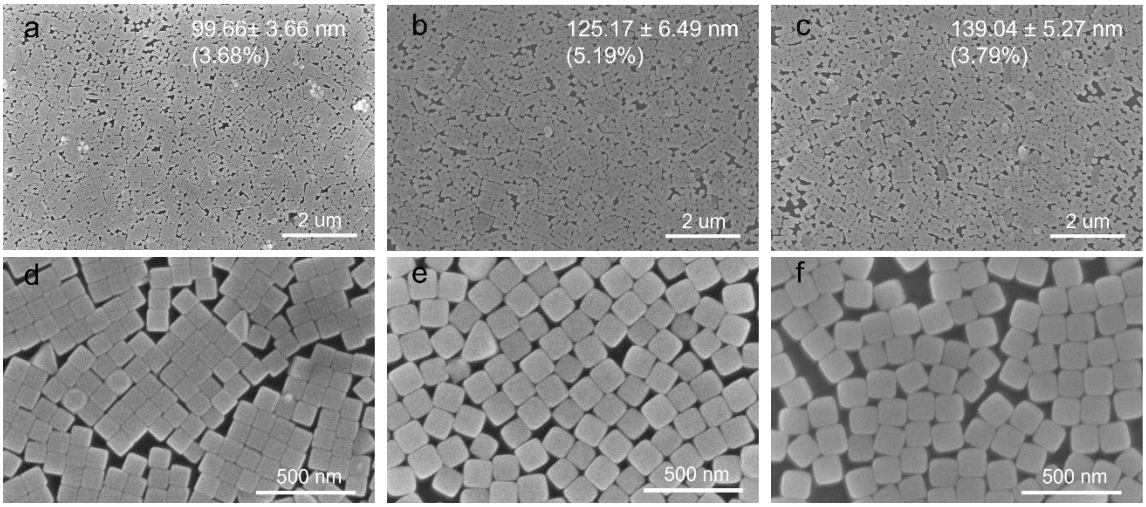

Figure 2.9 Zoom out and zoom in SEM images of LB assembled silver nanocube monolayer with size of 100 nm (a, d), 125 nm (b, e) and 140 nm (c, f).

2.3.3 Substrate PVP Removal and SERS Measurements

During the AgNC synthesis and LB assembling for SERS substrate, surfactant PVP was added to control the crystal growth and prevent aggregation. While it is beneficial to have PVP during synthesis and substrate preparation, the PVP chemically bound to the AgNCs could be a problem for several reasons. Excess PVP in the ethanol/chloroform solution can occupy the space around nanoparticles and affect the packing density leaving pinholes on the substrate. The strongly absorbed PVP on nanoparticles could also block the accessible spots for chemicals of interest. In addition, the existence of PVP may show strong Raman signal during Raman tests and creating complicated Raman spectrums for chemical identifications. Therefore, it is desirable to remove the PVP after preparing the SERS substrate without significantly affecting the morphology and packing of AgNCs. The way we applied for PVP removal is to soak the substrate in 25 mM $NaBH_4$ ethanol solution as $NaBH_4$ solution has been demonstrated effective in removing PVP from silver and other noble metal nanoparticles. After the substrate is made, it is then immersed in $NaBH_4$ solution under gentle stirring (150 rpm) which promotes diffusion while not lift

AgNCs off from Si wafer. After 5 minutes, the substrate was then taken out of the solution and rinsed with water and ethanol and quickly dried in N_2 flow. The PVP residue was then measured with Raman spectroscopy. As shown in **Figure 2.10a**, an obvious drop in PVP signal was observed. The same process was repeated 3 more times and for each time freshly made $NaBH_4$ solution was used. The Raman measurements show that after the second trial, the Raman signal of PVP does not further decrease suggesting removal PVP trapped in the gaps among AgNCs and between AgNCs and Si wafer is hardly accessible under diffusion limit. Based on the peak intensity at 1580 cm^{-1}, the Raman signal from PVP decreased by roughly 80% as shown in **Figure 2.10b**.

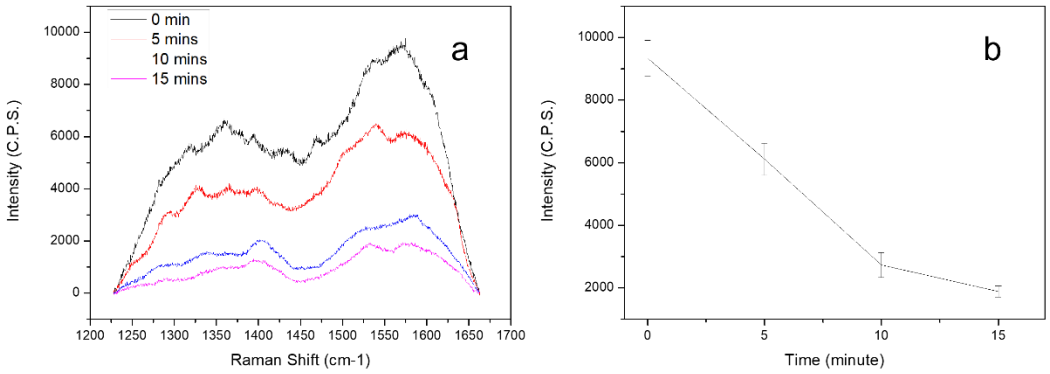

Figure 2.10 PVP removal from LB assembled substrates with $NaBH_4$ aqueous solutions. (a) Raman measurements of LB assembled AgNC substrate soaked with 25 mM $NaBH_4$ ethanolsolution with a period of 0, 5, 10 and 15 minutes, respectively. Raman spectrums were collected with 60 mW 532 nm laser, D0 filter; (b) averaged Raman intensity at Raman shift at around 1580 cm^{-1}.

To illustrate the dependency of SERS enhancement on the size of AgNCs used for substrate assembling, we used 4-Aminothiophenol (4-ATP) as a probing chemical to be tested in SERS. After the SERS substrates are purified with $NaBH_4$ solution, a majority of PVP molecules are removed from the surface of AgNCs. The purified substrates were then soaked in 20 mM 4-ATP ethanol solution for 12 hours allowing ligand exchange

between PVP and 4-ATP molecules. After the completion of ligand exchange, the substrates were rinsed with ethanol and quickly dried with N_2 gun which leaves a monolayer of 4-ATP molecules absorbed on the surface of AgNCs. The SERS measurements were carried out in backscattering geometry using a commercial Raman spectrometer (Horiba Labram HR800), equipped with a motorized objective lens holder, 1800 grooves per mm grating, and a long-working-distance 50× objective lens with a numerical aperture (NA) of 0.5. SERS substrates were tested under 532 nm incident light (Laser Quantum Ventus) with 60 mW power and D1 filter. For each substrate, spectrums collected from 10 randomly chosen spots are shown in **Figure 2.11** where significant signal enhancement was observed from all LB assembled AgNCs monolayer substrates. The signal at a Raman shift of 1579 cm^{-1}, originated from CC stretching vibration, was used for enhancement factor (EF) calculations following the equation below.

$$EF = \frac{I_{SERS} \times N_{vol}}{I_{NRS} \times N_{surf}}$$

In the above equation, I_{SERS} is Raman intensity in count per second (C.P.S.) collected from 4-ATP absorbed on SERS substrates; I_{NRS} is the Raman intensity from 4-ATP ethanol solution shown in **Figure 2.12**; N_{surf} is the number of 4-ATP molecules absorbed on the surfaces of AgNCs under focused laser beam; N_{vol} is the number of 4-ATP molecules in the ethanol solution under focused laser.

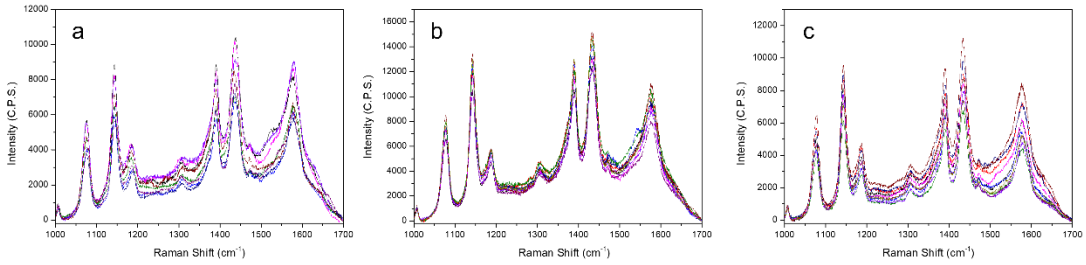

Figure 2.11 4-ATP spectrums collected from LB assembled AgNC substrates with average cube size of 100 nm (a), 125 nm (b) and 140 nm (c). 532 nm laser, 60 mW power, D1 filter.

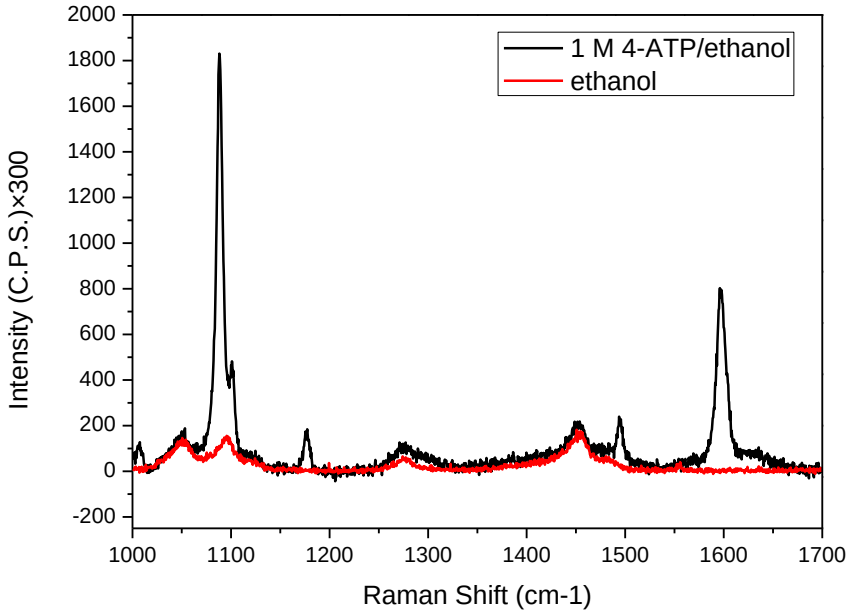

Figure 2.12 Normal Raman spectrum of pure ethanol and 1 M 4-ATP/ethanol solution. Spectrums collected with 60 mW 532 nm laser, D1 filter.

Based on the 4-ATP spectrums collected from 4-ATP/ethanol solution and SERS substrates assembled from AgNCs of 100 nm, 125 nm and 140 nm, the enhancement factors were calculated to be 6.49×10^5, 8.46×10^5, and 6.00×10^5, respectively, suggesting the medium-sized AgNCs works better when used to create close-packed monolayer substrates for SERS. The experimental results match the trend from COMSOL simulation results but are not as significant.

In summary, within this work we demonstrated that by carefully control the reaction conditions, such as temperature, concentration of precursors, feeding rate, reaction time and feeding rate, monodispersed silver nanocubes could be synthesized with a broad size range of 60-200 nm. Allowing the synthesis solution to reflux for just a few minutes after stopping the precursor feeds, free Ag^{+} in the solution continues to be reduced, but the low concentration slowed down the growth rate which allows growth in more thermodynamically stable PVP passivated Ag (111) facets preventing the truncation at corners making large cube synthesis possible. SERS substrates were fabricated using LB assembly method from AgNCs with size of 100, 125, 140 nm, and the SERS measurement of 4-ATP absorbed on the corresponding substrates suggest the medium size AgNCs perform better as SERS substrate in terms of Raman signal enhancement.

2.4 References

1. Lewis, L. N., *Chemical Catalysis by Colloids and Clusters*, *Chem Rev*, **1993**, 93, (8), 2693-2730.

2. Daniel, M. C.; Astruc, D., *Gold nanoparticles: Assembly, supramolecular chemistry, quantum-size-related properties, and applications toward biology, catalysis, and nanotechnology*, *Chem Rev*, **2004**, 104, (1), 293-346.

3. Anker, J. N.; Hall, W. P.; Lyandres, O.; Shah, N. C.; Zhao, J.; Van Duyne, R. P., *Biosensing with plasmonic nanosensors*, *Nat Mater*, **2008**, 7, (6), 442-453.

4. Xia, Y. N.; Xiong, Y. J.; Lim, B.; Skrabalak, S. E., *Shape-Controlled Synthesis of Metal Nanocrystals: Simple Chemistry Meets Complex Physics?*, *Angew Chem Int Edit*, **2009**, 48, (1), 60-103.

5. Peng, H. I.; Strohsahl, C. M.; Leach, K. E.; Krauss, T. D.; Miller, B. L., *Label-Free DNA Detection on Nanostructured Ag Surfaces*, *Acs Nano*, **2009**, 3, (8), 2265-2273.

6. He, J. H.; Ichinose, I.; Kunitake, T.; Nakao, A.; Shiraishi, Y.; Toshima, N., *Facile fabrication of Ag-Pd bimetallic nanoparticles in ultrathin TiO2-gel films: Nanoparticle morphology and catalytic activity*, *J Am Chem Soc*, **2003**, 125, (36), 11034-11040.

7. Zhang, X. F.; Liu, Z. G.; Shen, W.; Gurunathan, S., *Silver Nanoparticles: Synthesis, Characterization, Properties, Applications, and Therapeutic Approaches*, *Int J Mol Sci*, **2016**, 17, (9).

8. Wei, L. Y.; Lu, J. R.; Xu, H. Z.; Patel, A.; Chen, Z. S.; Chen, G. F., *Silver nanoparticles: synthesis, properties, and therapeutic applications*, *Drug Discov Today*, **2015**, 20, (5), 595-601.

9. Sun, Y. G., *Silver nanowires - unique templates for functional nanostructures*, *Nanoscale*, **2010**, 2, (9), 1626-1642.

10. Jana, N. R.; Gearheart, L.; Murphy, C. J., *Wet chemical synthesis of silver nanorods and nanowires of controllable aspect ratio*, *Chem Commun*, **2001**, (7), 617-618.

11. Kelly, K. L.; Coronado, E.; Zhao, L. L.; Schatz, G. C., *The optical properties of metal nanoparticles: The influence of size, shape, and dielectric environment*, *J Phys Chem B*, **2003**, 107, (3), 668-677.

12. Quinten, M., *The color of finely dispersed nanoparticles*, *Appl Phys B-Lasers O*, **2001**, 73, (4), 317-326.

13. Sosa, I. O.; Noguez, C.; Barrera, R. G., *Optical properties of metal nanoparticles with arbitrary shapes*, *J Phys Chem B*, **2003**, 107, (26), 6269-6275.

14. Li, L. M.; Chin, W. S., *Rapid Fabrication of a Flexible and Transparent Ag Nanocubes@PDMS Film as a SERS Substrate with High Performance, Acs Appl Mater Inter*, **2020**, 12, (33), 37538-37548.

15. Zhou, Z. A.; Bai, X. H.; Li, P. S.; Wang, C. Z.; Guo, M.; Zhang, Y.; Ding, P. R.; Chen, S. W.; Wu, Y. Y.; Wang, Q., *Silver nanocubes monolayers as a SERS substrate for quantitative analysis, Chinese Chem Lett*, **2021**, 32, (4), 1497-1501.

16. Cheng, S. C.; Wen, T. C., *Robust SERS substrates with massive nanogaps derived from silver nanocubes self-assembled on massed silver mirror via 1,2-ethanedithiol monolayer as linkage and ultra-thin spacer*, *Mater Chem Phys*, **2014**, 143, (3), 1331-1337.

17. Fang, C.; Brodoceanu, D.; Kraus, T.; Voelcker, N. H., *Templated silver nanocube arrays for single-molecule SERS detection, Rsc Adv*, **2013**, 3, (13), 4288-4293.

18. Yu, D. B.; Yam, V. W. W., *Controlled synthesis of monodisperse silver nanocubes in water*, *J Am Chem Soc*, **2004**, 126, (41), 13200-13201.

19. Chen, H.; Wang, Y.; Dong, S., *An effective hydrothermal route for the synthesis of multiple PDDA-protected noble-metal nanostructures, Inorg Chem*, **2007**, 46, (25), 10587-10593.

20. Fan, F. R.; Liu, D. Y.; Wu, Y. F.; Duan, S.; Xie, Z. X.; Jiang, Z. Y.; Tian, Z. Q., *Epitaxial growth of heterogeneous metal nanocrystals: From gold nano-octahedra to palladium and silver nanocubes*, *J Am Chem Soc*, **2008**, 130, (22), 6949-+.

21. Zhang, Q.; Huang, C. Z.; Ling, J.; Li, Y. F., *Silver Nanocubes Formed on ATP-Mediated Nafion Film and a Visual Method for Formaldehyde, J Phys Chem B*, **2008**, 112, (51), 16990-16994.

22. Kundu, S.; Maheshwari, V.; Niu, S.; Saraf, R. F., *Polyelectrolyte mediated scalable synthesis of highly stable silver nanocubes in less than a minute using microwave irradiation*, *Nanotechnology*, **2008**, 19, (6).

23. Tao, A.; Sinsermsuksakul, P.; Yang, P. D., *Polyhedral silver nanocrystals with distinct scattering signatures*, *Angew Chem Int Edit*, **2006**, 45, (28), 4597-4601.

24. Zhu, J. J.; Kan, C. X.; Zhu, X. G. G.; Wan, J. G.; Han, M.; Zhao, Y.; Wang, B. L.; Wang, G. H., *Synthesis of perfect silver nanocubes by a simple polyol process*, *J Mater Res*, **2007**, 22, (6), 1479-1485.

25. Im, S. H.; Lee, Y. T.; Wiley, B.; Xia, Y. N., *Large-scale synthesis of silver nanocubes: The role of HCl in promoting cube perfection and monodispersity*, *Angew Chem Int Edit*, **2005**, 44, (14), 2154-2157.

26. Zhang, Q. A.; Li, W. Y.; Moran, C.; Zeng, J.; Chen, J. Y.; Wen, L. P.; Xia, Y. N., *Seed-Mediated Synthesis of Ag Nanocubes with Controllable Edge Lengths in the Range*

of 30-200 nm and Comparison of Their Optical Properties, *J Am Chem Soc*, **2010**, 132, (32), 11372-11378.

27. Tao, Andrea; Sinsermsuksakul, Prasert; Yang, Peidong. *Polyhedral Silver Nanocrystals with Distinct Scattering Signatures, Angewandte Chemie International Edition*, **2006**, 45, (28), 4597-4601.

28. Hung, L.; Lee, S. Y.; McGovern, O.; Rabin, O.; Mayergoyz, I., *Calculation and measurement of radiation corrections for plasmon resonances in nanoparticles, Phys Rev B*, **2013**, 88, (7).

Chapter 3. Engineering Tip Morphology of Silver Nanowire for Super Spatial Resolution Scanning Probes

3.1 Introduction

In an era of nanoscales, it is of fundamental importance for researchers to characterize the physical and chemical properties of the sample surface with a nondestructive yet precise method for most of the research in nanotechnology and material science. The development of electron microscopy (SEM and TEM) and scanning probe microscopy (SPM, such as AFM and STM) allows topographical characterization, however, obtaining chemical information at the nanoscale is still challenging. Although vibrational spectroscopy such as Raman spectroscopy has the potential to gather chemical information of every single molecule on sample surface, the spatial resolution is normally no less than few hundred nanometers due to diffraction limitation which hinders the further usage in chemical information characterization at the nanoscale level.

Tip-enhanced Raman spectroscopy (TERS) that integrates Raman spectroscopy with SPM techniques has been demonstrated to break the diffraction limit and simultaneously obtain topographic and chemical information with nanometer spatial resolutions *via* utilizing SPM probes with sharp metal tips.[1-3] In TERS, the sharpness of the metal tips notably determines the spatial resolution of topographic and chemical information and the intensity of the Raman signal. While there are studies using probes prepared by coating thin metal on a tapered tip or etching metal tip into the tapped profile, those probe fabrication methods are either expensive or time consuming.[4-9] Efforts have also been placed on TERS probes prepared by attaching silver nanowires (AgNWs) to commercial SPM probes for scanning, which significantly lowered the cost and increased the efficiency of probe fabrication.[6, 10-13]

As a deep subwavelength plasmonic waveguide, AgNWs, which can be chemically synthesized on large scale with high crystallinity and atomically smooth surface, have drawn special attention because of low ohmic damping and scattering loss.[3] Different kinds of AgNW-based TERS probes have been reported with promising results. [10, 11, 14-17] Synthesis of AgNWs have been widely studied in literature due to the fact that AgNW growth is sensitive to various parameters, including temperature, reaction time, reaction additives, concentration of precursors.[18-26] So far, most researches in AgNWs synthesis have been focusing on increasing yield and controlling aspect ratio of the NW products with only a few research groups have extended the study into tip morphology of AgNWs. To push the spatial resolution of scanning to the limit, it is intuitive to use sharp tip AgNWs with small radius. While almost all syntheses from the literature showed (111) faceted or rounded tip shapes of AgNWs due to melting or oxidative etching during the synthesis process, our previous works apply sharp tip AgNWs in AFM, STM and TERS studies[6, 10-12, 27] showed improved spatial resolution and enhanced Raman signals. As the first research group emphasizes controlling the tip morphology of AgNWs, here we investigated the high yield ultra-sharp silver nanowire synthesis through selective etching and the effects of reaction parameters such as temperature, the concentration of reactants and reaction time. The capability of ultra-sharp AgNWs in AFM scanning and AFM-TERS is compared with AgNWs with faceted and rounded tips synthesized with the established method elsewhere from literature.[15]

3.2 Experimental Section

3.2.1 Chemicals and Materials

Silver nitrate (>99.7%), ammonium carbonate (>30%), ethylene glycol were purchased from Fisher Chemical. Polyvinylpyrrolidone (PVP, Mw~55000) and copper (II) chloride dihydrate (>99.0%) were purchased from Sigma-Aldrich. All chemicals were used as received.

3.2.2 Synthesis of Ultra-Sharp Silver Nanowires

In this work, silver nanowires were synthesized with the modified method described elsewhere.[21] In a typical synthesis, 0.160 g silver nitrate and 0.164 g PVP was dissolved in 10 ml ethylene glycol separately. 5 ml ethylene glycol in a 50 ml pear-sharp flask was preheated at 172 °C in an oil bath and 40 μl 5 mM $CuCl_2$ was added. After preheating 150 μl silver nitrate solution was quickly injected to the flask, followed by dropwise adding PVP and $AgNO_3$ solutions at a rate of 150 μl/min for 45 minutes. 1 ml ammonium carbonate ethylene glycol solution was then added to the reaction solution for further oxidative etching. Magnetic stirring of 260 rpm was maintain throughout the whole process. At the end of synthesis, the reaction solution was quickly cooled down in ice-water and then washed and centrifuged with ethanol for 6 times. After washing the AgNWs were dispersed in ethanol and stored in refrigerator.

3.2.3 AFM Probe Fabrication

A drop of diluted AgNWs ethanol solution was added to a piece of clean PDMS and spread the AgNWs on PDMS with airgun. Under optical microscope, a sharp-tip tungsten needle was controlled by 3D manipulator to pick up a AgNW from the PDMS and place it onto the commercial AFM probe. By moving the AgNW with the tungsten needle, the

protruding length can be carefully adjusted to be 1~2 μm. Commercial silicon AFM probes were purchased from Bruker.

3.3 Results and Discussion

3.3.1 High Yield Ultra-Sharp Silver Nanowires

Under different reaction conditions, AgNWs could be produced with great variation in length, diameter and tip morphology. With the traditional polyol-mediated method reported, AgNWs can be produced with pentagonal pyramid tips, while due to oxidative etching, many AgNWs show rounded morphology at the tips.[28] With our modified synthetic method described in the experimental section, the addition of $(NH_4)_2CO_3$ promoted the oxidative etching to the ends of AgNWs as the ends with Ag (111) facets bind less strongly with polyvinylpyrrolidone (PVP) making the silver atoms more vulnerable to oxidative etching. Figure 1 shows the structure and characterization of ultra-sharp AgNWs. Without the addition of ammonium carbonate, the AgNWs showed a high yield of pentagonal pyramid tips (**Figure 3.1**). In contrast, by promoting the oxidative etching with the addition of ammonium carbonate, AgNWs with sharpened yet smooth tips can be produced.

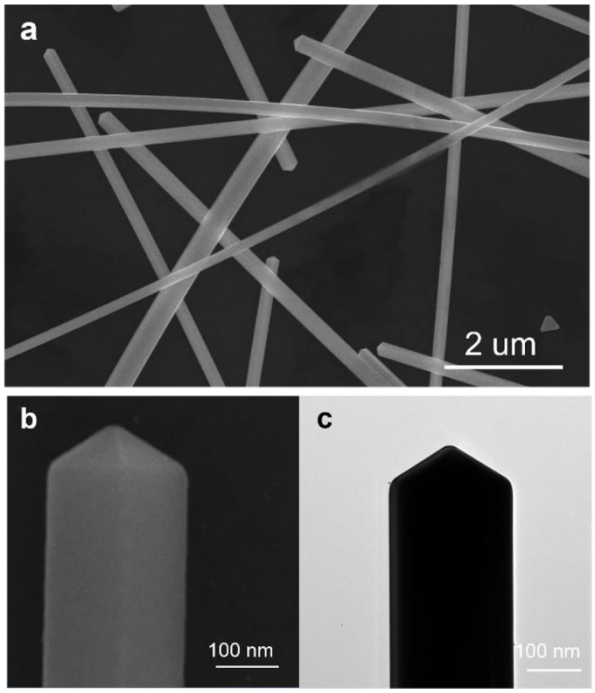

Figure 3.1 Structural and morphological characterization of Ag pentagonal pyramid tip nanowires prepared: (a) Zoom out SEM image; (b) Zoom in SEM image; (c) TEM image.

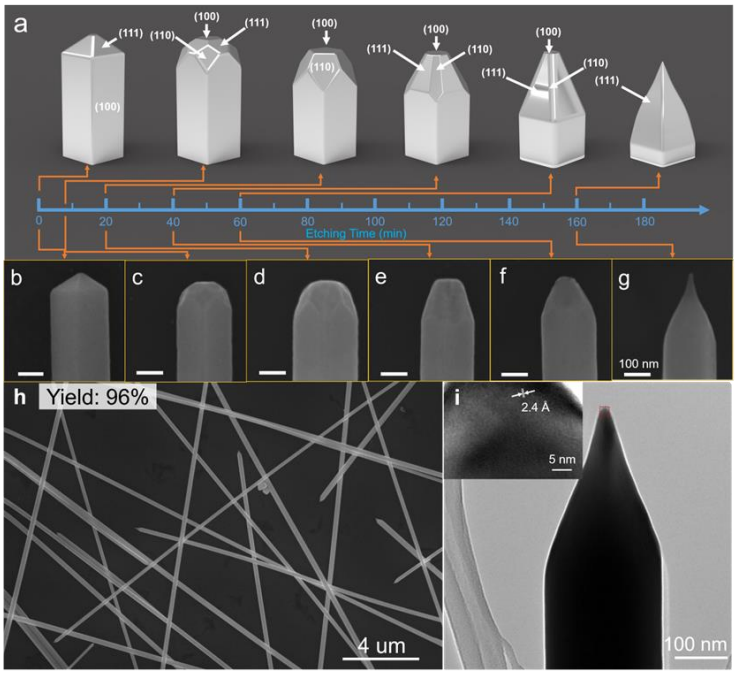

Figure 3.2 Ultra-sharp silver nanowires synthesis. (a) Illustration of tip evolution during oxidative etching and exposed facets at tips of silver nanowires; (b-g) SEM images of Ag nanowires at different etching time 0 min, 8 mins, 20 mins, 40 mins, 60 mins, 160 mins; (h) Zoom out SEM image show over 96% yield of ultra-sharp tip silver nanowires; (i) TEM image of ultra-sharp silver nanowire (inset shows HRTEM image at Ag nanowire tip of boxed area).

The evolution from pentagonal pyramid end AgNWs to ultra-sharp smooth AgNWs is a slow and gradual process. **Figure 3.2a** shows the proposed oxidative etching process to the pentagonal pyramid end silver nanowires with proof of SEM images of AgNWs at different etching time (**Figure 3.2b-g**). As face-centered cubic (FCC) metal nanocrystals, the surface free energy of silver nanowires decreases in the order of $\gamma_{(100)} > \gamma_{(110)} > \gamma_{(111)}$.[20] The evolution of ultra-sharp tip from faceted Ag {111} *via* oxidative etching promoted by $(NH_4)_2CO_3$ is firstly controlled by kinetics that the more reactive sites are quickly etched, and then with increasing the reaction time, thermodynamically stable {111} facets become dominant at the tips. Before the introduction of ammonia carbonate, the AgNWs showed Ag {111} faceted pentagonal pyramid end morphology. The addition of ammonia carbonate immediate promoted the oxidative etching that within 8 minutes of oxidative etching, the NW tip notably became flat and the corners at the tip were significantly etched starting from the very tip of the AgNWs and grain boundaries, where the Ag atoms are more chemically reactive and hence were the first to be etched. The etching to the very tip leads to flatted tip with {100} exposure facet. With the excessive PVP in the reaction solution, the higher surface energy {100} facet was stabilized as PVP bind stronger with {100} facets, thus {110} facets were developed and continuously etched. As reaction time increases, the area of {110} facets increases. Surface energy of {110} is larger than {111} facets in fcc crystals, and thermodynamically, {111} facets are more stable. Therefore, the oxidative etching and redeposit of Ag atoms to the tip of silver nanowires gradually developed {111} facets at the cost of {110} facets. Eventually, ultra-sharp tipped AgNWs were produced with {111} facets dominant at the ends but curved surfaces. Therefore, it is of great importance to control the reaction time

in order to produce ultra-sharp silver nanowires. After oxidative etching for 160 minutes, ultra-sharp AgNWs were successfully prepared with a selectivity to sharp tip of around 96%. The silver nanowires we produced have an average diameter of 191 nm with average length over 70 μm. The tip angles are mostly between 40~50° and the average tip radius of the sharp tips is 7.87 nm. After tapering the ends via oxidative etching, the ends of the silver nanowires still have 5-fold symmetry structures, and the AgNW body maintained the pentagonal prism structure (**Figure 3.3**). From the HR-TEM at the sharp AgNW tip, the spacing of lattice fringes was measured to be 0.24 nm indicating Ag (111) plane. Instead of ideal crystalline planes, the ends showed curved surfaces which are in good agreement with the literature.[23] It is also worth mentioning that after 160 mins of oxidative etching, the average length of silver nanowires becomes only a little smaller as shown in **Figure 3.4**.

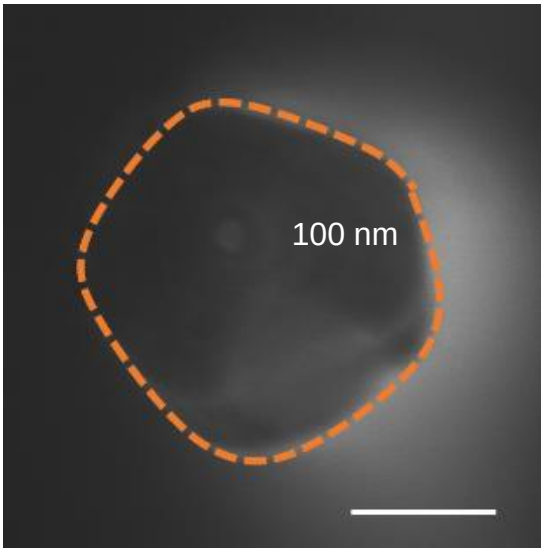

Figure 3.3 Cross-section SEM ultra-sharp tip silver nanowires.

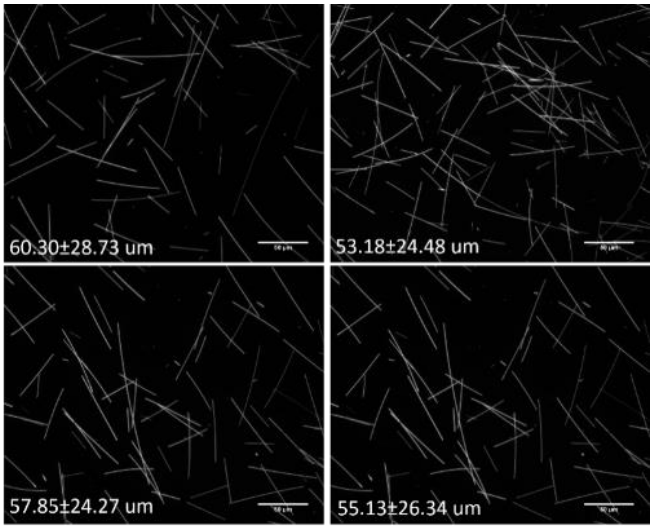

Figure 3.4 The effect of reflux time in on length of Ag nanowires. (a-d) Optical images of Ag nanowires at different reflux time 0 min, 40 mins, 100 mins, 160 mins.

The addition of ammonium carbonate has been proved to promote the oxidative etching to the tip of AgNWs that yield rounded or sharp tip.[17, 23] The presence of ammonium carbonate in the reaction solution promotes stripping off silver atoms from the tip of AgNWs where PVP binds less robust *via* forming Ag_2CO_3 and $[Ag(NH_3)_2]^+$.[12] In order to well control the oxidative etching to yield AgNWs with sharp yet smooth tips, the concentration of ammonium carbonate in the reaction solution is of crucial necessity to be optimized as the concentration of ammonium carbonate significantly affects the etching reaction rate. As shown in the SEM images of **Figure 3.5**, when 1 mL of $(NH_4)_2CO_3$ (42 mM) was added to the reaction solution to promote oxidative etching, the silver nanowires showed severe oxidative etching with asymmetric tips of the rough surface. Over 92% of the silver nanowire tips showed over-etching that even reducing the reaction time would not lead to smoother tips. In fact, within 5 mins of oxidative etching with $(NH_4)_2CO_3$, significant etching can be observed already, suggesting a fast oxidative etching rate. When 1 mL $(NH_4)_2CO_3$ (28 mM) ethylene glycol solution was added to the

reaction solution after 160 mins reaction AgNWs were produced with sharp and smooth tips with a small amount of AgNWs being over-etched to asymmetric tips. When the concentration of $(NH_4)_2CO_3$ was further decreased to 14 mM, after 160 minutes of reaction, the tip radius of silver nanowires was still about 26 nm on average due to the slower oxidative etching rate caused by a lower $(NH_4)_2CO_3$ concentration. Comparing the AgNW tip morphology after 5 minutes of oxidative etching, the tip of silver nanowires showed less etching when 1 mL 14 mM $(NH_4)_2CO_3$ was added. Extending the reaction time to 200 minutes allows more etching to the tip, which yield sharper tips, as shown in **Figure 3.5i** insert. Clearly, controlling the concentration of ammonium carbonate in the reaction solution to slow down the oxidative etching favors the production of smooth and ultra-sharp AgNWs through gradually etching with a longer reaction time.

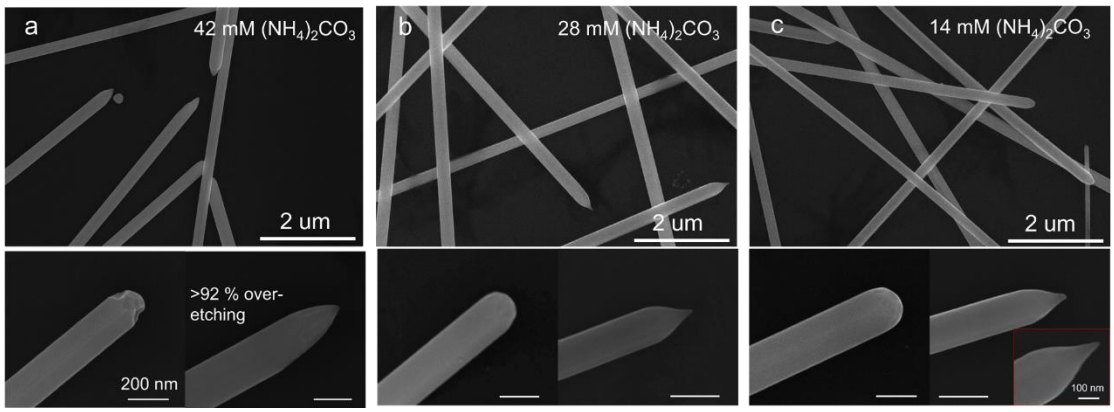

Figure 3.5 SEM images of Ag nanowires synthesized with 1 ml of (a) 42 mM $(NH_4)_2CO_3$ showed significant over-etching to tips, (b) 28 mM $(NH_4)_2CO_3$ yield smooth and sharp tips, (c) 14 mM $(NH_4)_2CO_3$ showed slow oxidative etching; lower left images show t_{etch}= 5 mins, lower right images show t_{etch}= 160 mins, insert image from t_{etch}= 200 mins.

In addition to the concentration of ammonium carbonate, in the production of ultra-sharp AgNWs, it is vital to control of reaction temperature as well. In this study, the effects of temperature on AgNW growth and tip morphology engineering were investigated at 170, 172, 177 and 182 °C and summarized in **Figure 3.7**. With the increase of synthesis

temperature, it is obvious that the average diameter of AgNWs increased. This is possible due to raising the reaction temperature promotes the growth of seeds at the initial seeding stage producing larger seeds. Therefore, with good control of the synthesis temperature, the diameter of silver nanowires can be deliberately controlled. More importantly, the reaction temperature was also found to affect the tip morphology of the products. The sharpest AgNWs were synthesized at 172°C. At 170 °C, the tip radius of AgNWs was large (~35 nm), indicating insufficient etching, while at 177 and 182°C, the SEM images showed significant over-etching to the tips. At 177 °C, a large portion of AgNWs was unevenly etched resulting sharp, but rough asymmetric morphology while at 182°C the over-etching to the AgNWs produced rounded tip silver nanowires. Clearly, increasing the reaction temperature favors the oxidative etching reactions that when the oxidative etching rate is much faster than the redeposition of Ag atoms to the tip of silver nanowires, the ends of silver nanowires become rough.

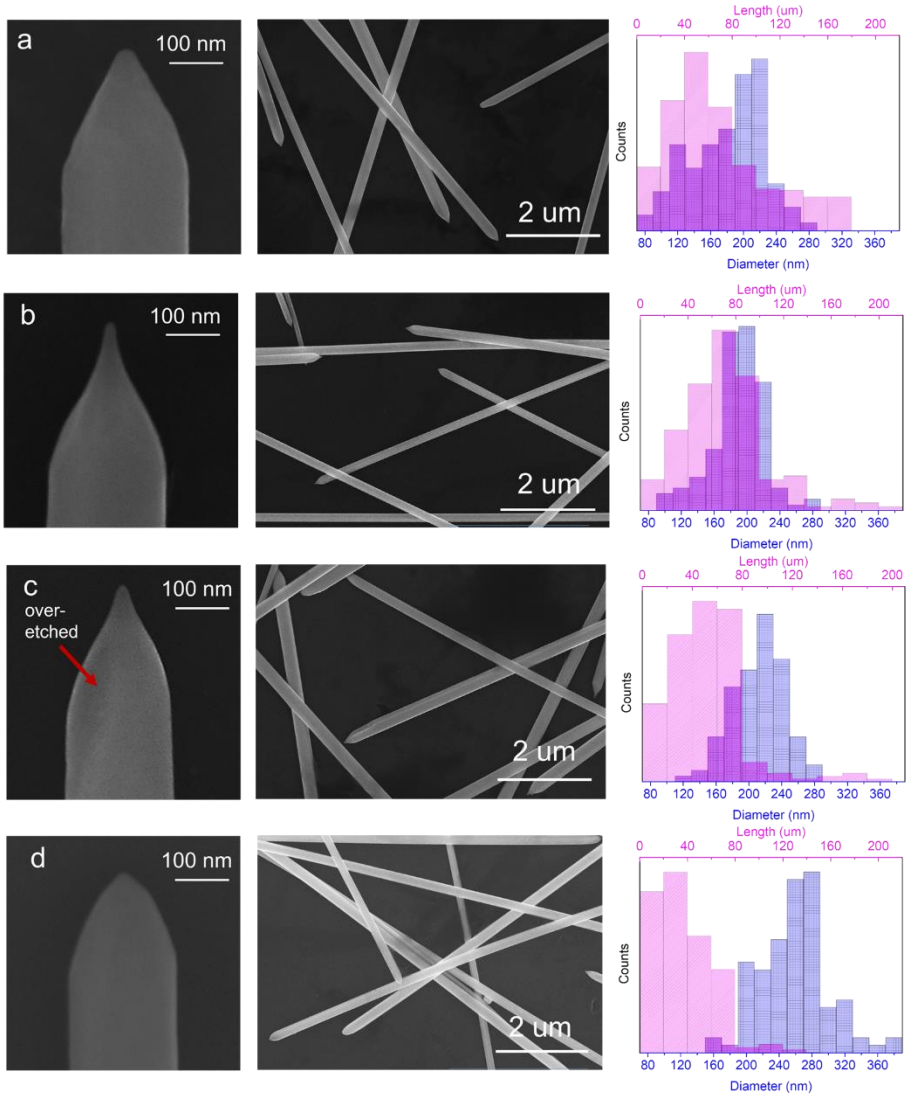

Figure 3.6 Effects of reaction temperature on tip shape, length and diameter of Ag nanowires. (a~d) Ag nanowires synthesized at 170, 172, 177 and 182 ℃, respectively. Higher temperature showed over-etching and low temperature showed insufficient etching. Ag nanowires etched with 1 ml 28 mM $(NH_4)_2CO_3$ for 160 mins.

In addition, the length of the silver nanowire products was also affected by temperature. From the optical images of silver nanowires (**Figure 3.7**), at 172 °C the average length of AgNWs was 73 μm while increasing or decreasing the reaction temperature led to shorter nanowires. The length variation is directly related to the seeding process. At different synthesis temperatures, with the same amount of $AgNO_3$ injected, higher temperature produces larger seeds which lead to fatter and shorter silver nanowires. In comparison, at

lower temperature, smaller seeds were formed, resulting in thinner AgNWs. Meanwhile, more irregular-shaped nanoparticles were produced at low temperatures.

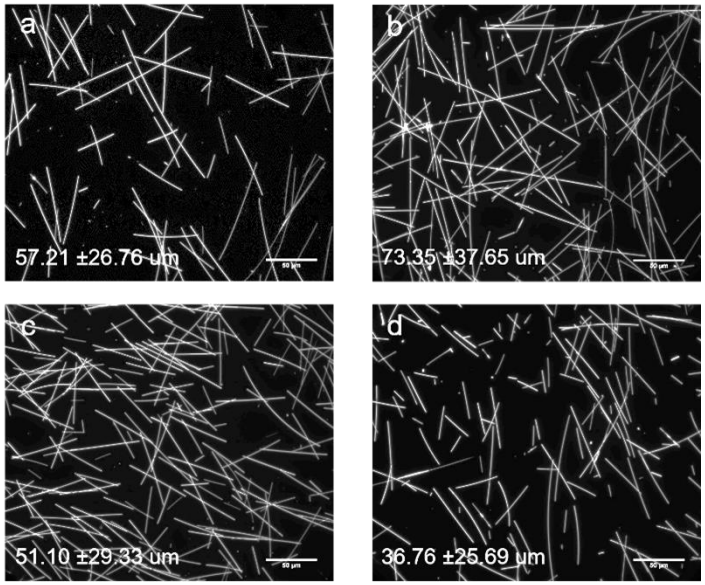

Figure 3.7 Effects of reaction temperature on length of Ag nanowires. (a~d) Ag nanowires synthesized at 170, 172, 177 and 182 °C, respectively. Ag nanowires etched with 1 ml of $(NH_4)_2CO_3$ (14 mM) refluxing 160 mins.

Besides the reaction temperature, reaction time and concentration of $(NH_4)_2CO_3$, $CuCl_2$ also plays an essential role in the synthesis of ultra-sharp silver nanowires. At the beginning of synthesis, $CuCl_2$ was added to the reaction solution for two purposes. Firstly, the presence of Cl^- in the reaction solution reacts with free Ag^+ forming AgCl, which serve as seeds for subsequent growth of multi-twinned particles.[27] The slow release of Ag^+ benefits the uniformity of AgNWs. Secondly, copper works as an oxygen scavenger that Cu (II) can be reduced to Cu (I) by ethylene glycol, which reacts with oxygen atoms absorbed on silver particles being oxidized back to Cu (II), so that the presence of $CuCl_2$ promotes the growth of AgNWs by removing oxygen atoms that blocking sites for silver deposition.[21] However, in the synthesis of ultra-sharp AgNW synthesis, it is desirable to promote oxidative etching, which would be inhibited with

Cu^{2+} addition. Therefore, in order to have long silver nanowires and promote oxidative etching, the amount of Cu^{2+} addition needs to be controlled. As shown in **Figure 3.8**, whiling we have fixed amount of Cl^- added, without the addition of Cu^{2+}, most of the product was irregular silver nanoparticles. The silver nanowires produced were short with an average length of 9.75 μm. When 20 uL Cu^{2+} (5 mM) were added, the average length of AgNWs increased to 36.62 μm and with 40 ul Cu^{2+} addition, the length increased to 60.30 μm. The result confirmed that the addition of Cu^{2+} is essential to synthesize long AgNWs.

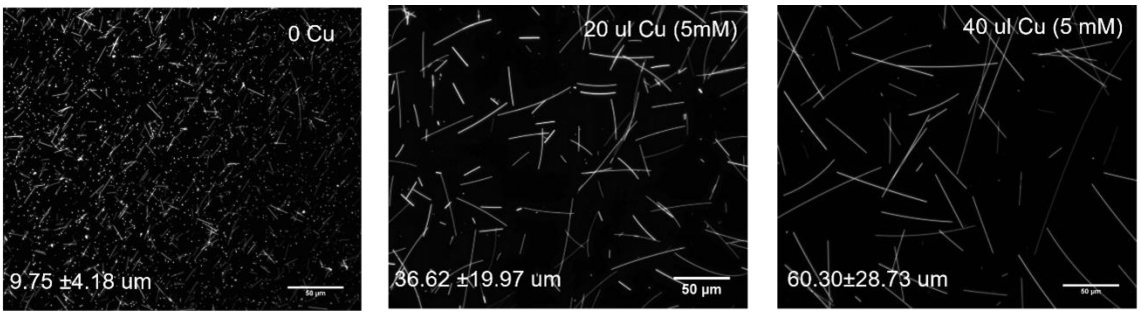

Figure 3.8 Effects of amount of Cu^{2+} addition while keeping Cl^- amount fixed. (a~c) 0, 20, 40 ul of 5 mM Cu^{2+}, respectively.

3.3.2 High-Resolution AFM Probes Based on Ultra-Sharp AgNWs

After fully understanding the AgNW growth and etching mechanism and successful production of ultra-sharp AgNWs, we fabricated AgNW-based AFM probes for high spatial resolution scanning. The spatial resolution of AFM highly depends on the sharpness of AFM probes. While the commercial sharp silicon AFM probes can scan with high spatial resolution, they are expensive and can only maintain high resolution for several scans. Ultra-sharp AgNWs can be synthesized with high yield and would be an ideal replacement for the high cost and easily wear-out silicon probes. Our previous work utilizing thin ultra-sharp AgNWs has demonstrated that silver nanowires can be mounted

onto commercial silicon AFM probes and scan with high resolution and good stability.[12] When scanning with AgNWs-based AFM probes, the morphology of silver nanowires plays a crucial role in the resulting spatial resolution of the three-dimensional (3D) topographic AFM scanning. As the tip radius increases, the spatial resolution becomes poorer as shown in **Figure 3.9** that AgNWs with ultra-sharp tip, pentagonal pyramid tip and rounded tip were mounted onto commercial AFM cantilever as scanning probes and tested in tapping mode AFM scanning over single wall carbon nanotubes on a glass substrate. The SWCNT sample is prepared with the catalytic chemical vapor deposition method. The AFM scanning images showed a significant difference in terms of spatial resolution for both height and phase scanning. When probe made of an ultra-sharp AgNW (tip radius of 7.2 nm) scans over a single walled carbon nanotube (SWCNT) with a diameter around 2 nm, the full width at half maximum (FWHM) of the marked line scan in **Figure 3.9d** was 8.50 nm. When pentagonal pyramid end (tip radius of 36.8 nm) and rounded end (tip radius of 135.4 nm) AgNWs were used, the FWHM of line scan across the same SWCNT were 20.25 nm and 35.21 nm, respectively. The FWHM measured in AFM scans are slightly greater than the mathematically calculated FWHM values based on the SEM-measured tip radius R and estimated CNT radius (1 nm) from the AFM height profile. The calculation is based on the assumption that AFM probes are closely in contact with the CNTs and substrates and there is no shape change of CNTs due to pression from probes. As demonstrated in **Figure 3.10a**, when the probe with a tip radius of R scans over CNT with a radius of r, the distance between probe tip and substrate (height h) is a function of x (Equation 1). The full width of the half maximum (FWHM) of the height profile is a function of R and r (Equation 2). Based on Equation 2,

FWHM was calculated for probe tip radius from 2 to 140 nm and CNT radius of 0.5 nm, 1 nm, 1.5 nm, respectively.

$$h = \sqrt{(R+r)^2 - x^2} + r - R \quad (1)$$

$$WFHM = 2\sqrt{2Rr + r^2} \quad (2)$$

The AFM scanning showed superior spatial resolution performance of the ultra-sharp silver nanowires. With the high yield synthesis of ultra-sharp AgNWs, the cost for high-resolution AFM probes can be decreased significantly.

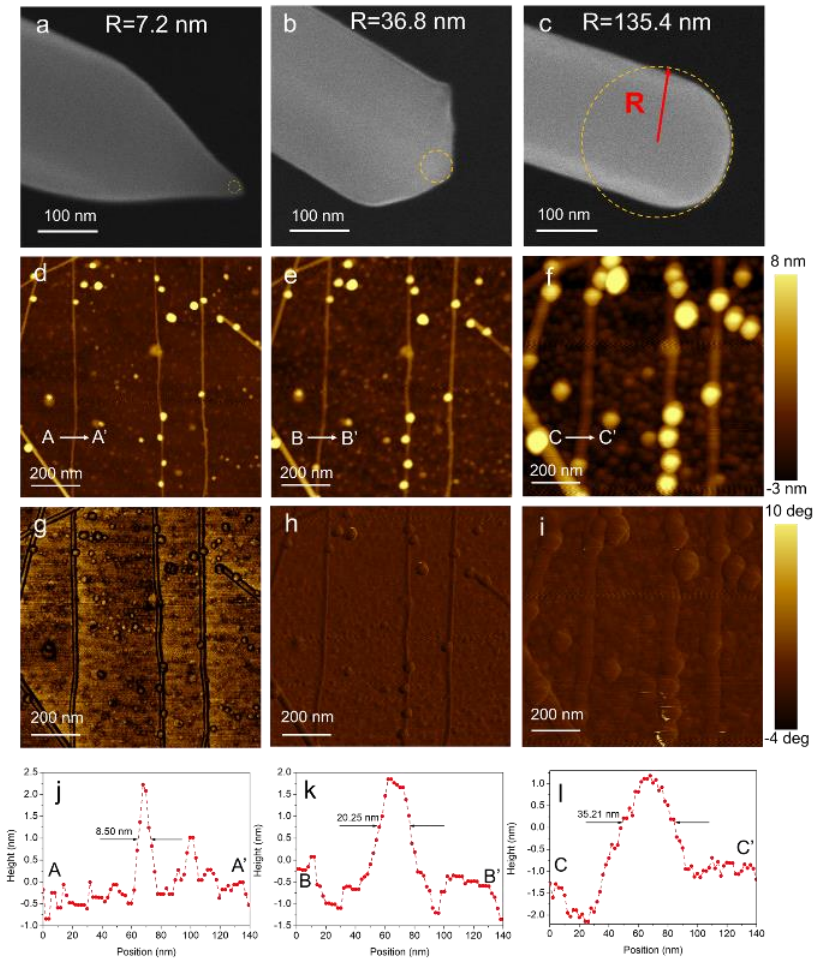

Figure 3.9 Tapping mode AFM topography images of SWCNT on quartz substrate using Ag nanowires of different tip radius. (a-c) SEM images of Ag nanowires used for AFM scanning. (d-f) AFM topography images of height scanning. (g-i) Phase image of AFM scanning; (j-l) height profile of the marked line in (d-f).

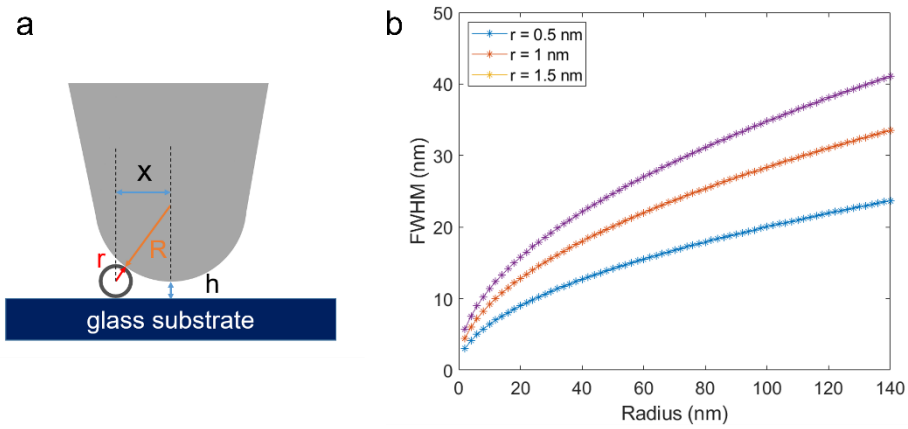

Figure 3.10 Calculation of AFM spatial resolution. (a) Model illustration for AFM scanning over CNT on glass substrate; (b) AFM spatial resolution dependence on tip radius of Ag nanowires from 2 nm to 140 nm assuming scanning over CNT of 0.5, 1 and 1.5 nm in radius.

3.3.3 Enhancement Factor Dependency on Tip Radius in AFM-TERS

The above-mentioned AgNW-based AFM probes with different tip radius were also used in tip-enhanced Raman tests. The Raman spectroscopy measurements were carried out in backscattering geometry using a commercial Raman spectrometer (Horiba Labram HR800), equipped with a motorized objective lens holder, 600 grooves per mm grating, and a long-working-distance 100× with a numerical aperture (NA) of 0.6. Incident light (Laser Quantum Ventus, 532 nm) was aligned to the AgNW tip apex with the objective lens mounted on the motorized holder and Raman signals were also collected with the same lens. TERS experiments were performed on a monolayer 4-Aminobenzenethiol (4-ATP) on a smooth Ag microplate prepared through the ligand exchange method. The atomic smooth surface of the microplate is effective in suppressing the surface-enhanced Raman scattering (SERS). The position of the sample was marked to ensure all tests were conducted at the same spot to avoid sample discrepancy effects. The Raman signals from the far field and near field TERS of different probes are shown in **Figure 3.10.** Under contact mode, all three probes showed enhancement to the Raman signals but with a

significant difference in terms of contrast and enhancement factors (EF). Contrast and EF were calculated based on Raman intensity at the far field (I_{FF}) and near field (I_{NF}) as well as the corresponding area using the equations below.

$$C_{TERS} = \frac{I_{NF} - I_{FF}}{I_{FF}} = \frac{I_{NF}}{I_{FF}} - 1 \quad (1)$$

$$EF_{TERS} = \frac{I_{NF} A_{FF}}{I_{FF} A_{NF}} \quad (2)$$

In calculations, the Raman intensity was from **Figure 3.11**at Raman shift of 1438 cm^{-1} which was attributed to C-C ring stretching and C-H bending movement. [1, 29, 30] The excitation areas were estimated based on the numerical simulations that described in our previous work[10], which yield radius of 3.1 nm, 3.9 nm and 7.3 nm for ultra-sharp, pentagonal pyramid, and rounded end AgNWs, respectively. In contrast, the laser spot of far-field was estimated to be $A_{FF} \approx \pi \times (540\ nm)^2/\sin(20°)$. The Raman contrast C_{TERS} for ultra-sharp AgNW-based probe were 37.2, which is much higher than the pyramid end ($C_{TERS} \approx 16.8$) and rounded end ($C_{TERS} \approx 6.7$) probes. The Raman enhancement factor of ultra-sharp AgNW-based AFM probe was calculated to be 3.39×10^6, while the EF of the pyramid and rounded AgNW-based probes were 9.99×10^5 and 3.58×10^5, respectively.

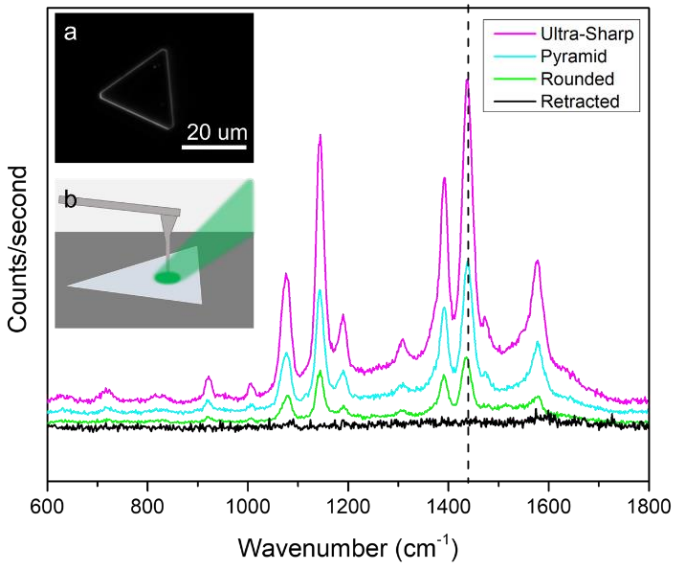

Figure 3.11 AFM contact mode tip enhanced Raman spectra of monolayer 4-Aminothiophenol on silver plate with AgNW-based AFM probes. 532 nm laser, 20 mW power, D2 filter, 600 grating. (a) Silver plate under microscope; (b) Illustration of AFM-TERS measurement.

To conclude, in this work, we introduced a novel method to engineer the tip morphology of silver nanowires. By controlling the reaction temperature, amount of oxidative etchant $(NH_4)_2CO_3$, and oxidative etching time, silver nanowires can be produced with over 96 % selectivity to ultra-sharp ends. The produced ultra-sharp AgNWs showed outstanding performance in tapping mode AFM scanning and contact mode AFM-TERS with excellent improvement in spatial resolution and enhancement factor compared with AgNWs with a pentagonal pyramid or rounded end AgNWs synthesized with existing polyol mediated synthesis methods. The promising results indicate the synthesis of ultra-sharp silver nanowires can significantly increase the yield and efficiency of sharp metal probe fabrication and lower the cost of high-resolution SPM probes.

3.4 References

1. Jiao, L. S.; Niu, L.; Shen, J.; You, T. Y.; Dong, S. J.; Ivaska, A., *Simple azo derivatization on 4-aminothiophenol/Au monolayer*, *Electrochem Commun*, **2005**, 7, (2), 219-222.

2. Stöckle, Raoul M; Suh, Yung Doug; Deckert, Volker; Zenobi, Renato. *Nanoscale chemical analysis by tip-enhanced Raman spectroscopy*, *Chemical Physics Letters*, **2000**, 318, (1-3), 131-136.

3. Kim, S.; Bailey, S.; Liu, M.; Yan, R. X., *Decoupling co-existing surface plasmon polariton (SPP) modes in a nanowire plasmonic waveguide for quantitative mode analysis*, *Nano Res*, **2017**, 10, (7), 2395-2404.

4. Eligal, L.; Culfaz, F.; McCaughan, V.; Cade, N. I.; Richards, D., *Etching gold tips suitable for tip-enhanced near-field optical microscopy*, *Rev Sci Instrum*, **2009**, 80, (3).

5. Lloyd, J. S.; Williams, A.; Rickman, R. H.; McCowen, A.; Dunstan, P. R., *Reproducible electrochemical etching of silver probes with a radius of curvature of 20 nm for tip-enhanced Raman applications*, *Applied Physics Letters*, **2011**, 99, (14).

6. Ma, X. Z.; Zhu, Y. Z.; Yu, N.; Kim, S.; Liu, Q. S.; Apontti, L.; Xu, D.; Yan, R. X.; Liu, M., *Toward High-Contrast Atomic Force Microscopy-Tip-Enhanced Raman Spectroscopy Imaging: Nanoantenna-Mediated Remote-Excitation on Sharp-Tip Silver Nanowire Probes*, *Nano Lett*, **2019**, 19, (1), 100-107.

7. Meng, L. Y.; Huang, T. X.; Wang, X.; Chen, S.; Yang, Z. L.; Ren, B., *Gold-coated AFM tips for tip-enhanced Raman spectroscopy: theoretical calculation and experimental demonstration*, *Opt Express*, **2015**, 23, (11), 13804-13813.

8. Taguchi, A.; Hayazawa, N.; Saito, Y.; Ishitobi, H.; Tarun, A.; Kawata, S., *Controlling the plasmon resonance wavelength in metal-coated probe using refractive index modification*, *Opt Express*, **2009**, 17, (8), 6509-6518.

9. Yang, L. K.; Huang, T. X.; Zeng, Z. C.; Li, M. H.; Wang, X.; Yang, F. Z.; Ren, B., *Rational fabrication of a gold-coated AFM TERS tip by pulsed electrodeposition*, *Nanoscale*, **2015**, 7, (43), 18225-18231.

10. Liu, Qiushi; Kim, Sanggon; Ma, Xuezhi; Yu, Ning; Zhu, Yangzhi; Deng, Siyu; Yan, Ruoxue; Zhao, Huijuan; Liu, Ming. *Ultra-sharp and surfactant-free silver nanowire for scanning tunneling microscopy and tip-enhanced Raman spectroscopy*, *Nanoscale*, **2019**, 11, (16), 7790-7797.

11. Kim, Sanggon; Yu, Ning; Ma, Xuezhi; Zhu, Yangzhi; Liu, Qiushi; Liu, Ming; Yan, Ruoxue. *High external-efficiency nanofocusing for lens-free near-field optical nanoscopy*, *Nature Photonics*, **2019**.

12. Ma, Xuezhi; Zhu, Yangzhi; Kim, Sanggon; Liu, Qiushi; Byrley, Peter; Wei, Yang; Zhang, Jin; Jiang, Kaili; Fan, Shoushan; Yan, Ruoxue. *Sharp-tip silver nanowires mounted on cantilevers for high-aspect-ratio high-resolution imaging*, *Nano Lett*, **2016**, 16, (11), 6896-6902.

13. Zhu, Yangzhi; Kim, Sanggon; Ma, Xuezhi; Byrley, Peter; Yu, Ning; Liu, Qiushi; Sun, Xiaoming; Xu, Da; Peng, Sangshan; Hartel, Martin C.; Zhang, Shiming; Jucaud, Vadim; Dokmeci, Mehmet R.; Khademhosseini, Ali; Yan, Ruoxue. *Ultrathin-shell epitaxial Ag@Au core-shell nanowires for high-performance and chemically-stable electronic, optical, and mechanical devices*, *Nano Research*, **2021**.

14. You, Yumeng; Purnawirman, NA; Hu, Hailong; Kasim, Johnson; Yang, Huanping; Du, Chaoling; Yu, Ting; Shen, Zexiang. *Tip‐enhanced Raman spectroscopy using single‐crystalline Ag nanowire as tip*, *J Raman Spectrosc*, **2010**, 41, (10), 1156-1162.

15. Fujita, Yasuhiko; Chiba, Rie; Lu, Gang; Horimoto, Noriko N; Kajimoto, Shinji; Fukumura, Hiroshi; Uji-i, Hiroshi. *A silver nanowire-based tip suitable for STM tip-enhanced Raman scattering*, *Chem Commun*, **2014**, 50, (69), 9839-9841.

16. Walke, Peter; Fujita, Yasuhiko; Peeters, Wannes; Toyouchi, Shuichi; Frederickx, Wout; De Feyter, Steven; Uji-i, Hiroshi. *Silver nanowires for highly reproducible cantilever based AFM-TERS microscopy: towards a universal TERS probe*, *Nanoscale*, **2018**, 10, (16), 7556-7565.

17. Ma, Xuezhi; Zhu, Yangzhi; Yu, Ning; Kim, Sanggon; Liu, Qiushi; Apontti, Leonard; Xu, Da; Yan, Ruoxue; Liu, Ming. *Toward High-Contrast Atomic Force Microscopy-Tip-Enhanced Raman Spectroscopy Imaging: Nanoantenna-Mediated Remote-Excitation on Sharp-Tip Silver Nanowire Probes*, *Nano Lett*, **2018**, 19, (1), 100-107.

18. Caswell, K. K.; Bender, C. M.; Murphy, C. J., *Seedless, surfactantless wet chemical synthesis of silver nanowires*, *Nano Lett*, **2003**, 3, (5), 667-669.

19. Chen, D. P.; Qiao, X. L.; Qiu, X. L.; Chen, J. G.; Jiang, R. Z., *Convenient synthesis of silver nanowires with adjustable diameters via a solvothermal method*, *J Colloid Interf Sci*, **2010**, 344, (2), 286-291.

20. Tao, Andrea; Sinsermsuksakul, Prasert; Yang, Peidong. *Polyhedral Silver Nanocrystals with Distinct Scattering Signatures*, *Angewandte Chemie International Edition*, **2006**, 45, (28), 4597-4601.

21. Korte, K. E.; Skrabalak, S. E.; Xia, Y. N., *Rapid synthesis of silver nanowires through a CuCl- or CuCl2-mediated polyol process*, *Journal of Materials Chemistry*, **2008**, 18, (4), 437-441.

22. Lin, J. Y.; Hsueh, Y. L.; Huang, J. J.; Wu, J. R., *Effect of silver nitrate concentration of silver nanowires synthesized using a polyol method and their application as transparent conductive films*, *Thin Solid Films*, **2015**, 584, 243-247.

23. Liu, S. H.; Sun, B. M.; Li, J. G.; Chen, J. L., *Silver nanowires with rounded ends: ammonium carbonate-mediated polyol synthesis, shape evolution and growth mechanism*, *Crystengcomm*, **2014**, 16, (2), 244-251.

24. Liu, Q. S.; Kim, S.; Ma, X. Z.; Yu, N.; Zhu, Y. Z.; Deng, S. Y.; Yan, R. X.; Zhao, H. J.; Liu, M., *Ultra-sharp and surfactant-free silver nanowire for scanning tunneling microscopy and tip-enhanced Raman spectroscopy*, *Nanoscale*, **2019**, 11, (16), 7790-7797.

25. Sun, Y. G.; Gates, B.; Mayers, B.; Xia, Y. N., *Crystalline silver nanowires by soft solution processing*, *Nano Lett*, **2002**, 2, (2), 165-168.

26. Sun, Y. G.; Xia, Y. N., *Large-scale synthesis of uniform silver nanowires through a soft, self-seeding, polyol process*, *Adv Mater*, **2002**, 14, (11), 833-837.

27. Ma, X. Z.; Liu, Q. S.; Yu, N.; Xu, D.; Kim, S.; Liu, Z. B.; Jiang, K. L.; Wong, B. M.; Yan, R. X.; Liu, M., *6 nm super-resolution optical transmission and scattering spectroscopic imaging of carbon nanotubes using a nanometer-scale white light source*, *Nat Commun*, **2021**, 12, (1).

28. Sun, Y. G.; Mayers, B.; Herricks, T.; Xia, Y. N., *Polyol synthesis of uniform silver nanowires: A plausible growth mechanism and the supporting evidence*, *Nano Lett*, **2003**, 3, (7), 955-960.

29. Madzharova, Fani; Heiner, Zsuzsanna; Kneipp, Janina. *Surface-Enhanced Hyper Raman Spectra of Aromatic Thiols on Gold and Silver Nanoparticles*, *The Journal of Physical Chemistry C*, **2020**, 124, (11), 6233-6241.

30. Osawa, M.; Matsuda, N.; Yoshii, K.; Uchida, I., *Charge-Transfer Resonance Raman Process in Surface-Enhanced Raman-Scattering from P-Aminothiophenol Adsorbed on Silver - Herzberg-Teller Contribution*, *J Phys Chem-Us*, **1994**, 98, (48), 12702-12707.

Chapter 4. Enriching Silver Nanowires With a Second Noble Metal

4.1 Introduction

The fact that tip enhanced Raman spectroscopy (TERS) technique exhibits highly localized chemical sensitivity, makes it ideal for studying chemical reactions, including processes at catalytic surfaces combining the high chemical sensitivity of SERS and high spatial resolution of scanning probe microscopy (SPM).[1, 2] Catalyst structures, adsorbates, and reaction intermediates can be observed in low quantities at hot spots where electromagnetic fields are the strongest, providing ample opportunities to elucidate reaction mechanisms.

Among metal nanowires, silver nanowires have highest electrical and thermal conductivity. Silver nanowires synthesized with polyol methods show high crystallinity, low impurity level and atomically flat surface led to low ohmic loss, strong plasmonic enhancement, high mechanical strength and flexibility making it an ideal candidate for plasmonic waveguide to be used in SERS and TERS measurement. [3-12]

While TERS has great potential in the field of catalysis and silver nanowires have been proved to be a great plasmonic waveguide, the application of silver nanowires in TERS is significantly limited by their short lifetime and demanding operating conditions due to poor chemical stability. In addition, with AgNW-based SPM probes, we can study silver catalyzed reactions, however, silver is limited in terms of catalytic application as it only shows activity toward oxidation reactions such as epoxidation, not reduction reactions. Therefore, the application of the AgNW-based probe will be largely broadened if a second metal such as Pd and Pt could be deposited at the tip of silver nanowires meanwhile a more stable noble metal can significantly improve the chemical stability of

silver nanowires making the application of TERS in harsh operation conditions possible as shown in our previous work on gold coated silver nanowires.[13] In literature, noble-metal nanocrystals have already received considerable interest for their promising applications in areas such as plasmonics, catalysis, sensing, imaging and medicine.[14] There are quite a few studies on enriching silver nanocubes with a second noble metal such as gold, platinum and palladium forming core-shell or core-frame structures,[15-19] but not much special attention has been paid to enriching silver nanowires with another chemical stable noble metal for silver nanowire based scanning probes. A major point to consider is that although a layer of more stable noble metal can protect the silver nanowire against oxidative etching, the propagation loss would also increase. When preparing silver nanowires with a second noble metal shell, special attention needs to be paid to control the shell thickness to minimize propagation loss. In this chapter, we demonstrate the feasibility of infusing ultra-sharp silver nanowires with a second noble metal such as platinum and palladium at room temperature with tunable shell thickness while suppressing galvanic replacement. Besides noble metal, transition metals such as copper and ruthenium can also be deposited to silver nanowire surface. The resulted Ag@M (Pt, Pd) core-shell nanowires showed increase stability against oxidation while maintaining the sharpness of silver nanowires which is crucial for high spatial resolution in TERS scanning. In addition, the etching-free smooth surface of Ag@ M NWs showed low scattering of light during propagation ensure great tip emissions.

4.2 Experimental

4.2.1 Materials

Silver nitrate (>99.7%), ammonium carbonate (>30%), ethylene glycol, hydrogen peroxide and sodium hydroxide were purchased from Fisher Chemical. Polyvinylpyrrolidone (PVP, Mw~55000) and copper (II) chloride dihydrate (>99.0%), sodium tetrachloroplatinate (Na2PtCl4), sodium tetrachloropalladate (Na2PdCl4), L-Ascorbic acid were purchased from Sigma-Aldrich. All chemicals were used as received.

4.2.2 Synthesis of Ultra-Sharp Silver Nanowire

Ultra-sharp silver nanowires were synthesized with the modified method described elsewhere.[20] In a typical synthesis, 0.160 g silver nitrate and 0.164 g PVP was dissolved in 10 ml ethylene glycol separately. 5 ml ethylene glycol in a 50 ml pear-sharp flask was preheated at 172 °C in an oil bath and 40 μl 5 mM $CuCl_2$ was added. After preheating 150 μl silver nitrate solution was quickly injected to the flask, followed by dropwise adding PVP and $AgNO_3$ solutions at a rate of 150 μl/min for 45 minutes. 1 ml ammonium carbonate ethylene glycol solution was then added to the reaction solution for further oxidative etching. Magnetic stirring of 260 rpm was maintain throughout the whole process. At the end of synthesis, the reaction solution was quickly cooled down in ice-water and then washed and centrifuged with ethanol for 6 times. After washing the AgNWs were dispersed in 15 ml ethanol and stored in refrigerator.

4.2.3 Synthesis of Ag@ M Core-Shell NWs

Preparation of Pt growth solutions: 3 ml of Na_2PtCl_4 (10 mM), 60 ul of NaOH (1M) were added to 6.94 ml DI (18 MΩ) water. The solution was left undisturbed for at least 12 hours in refrigerator.

Preparation of Pd growth solutions: 1 ml of Na_2PdCl_4 (10 mM), 60 ul of NaOH (1M) were added to 6.94 ml DI (18 MΩ) water. The solution was left undisturbed for at least 12 hours in refrigerator.

Preparation of Ag@ M NWs: in a typical synthesis, 2 ml 10% PVP, 1 ml L-AA (0.1 M) and 0.75 ml NaOH (1 M) aqueous solutions were added to 2 ml DI water subsequently. 1 ml of above prepared ultra-sharp silver nanowires were then added to the solution under continuous stirring at a speed of 400 rpm. The above noble metal growth solution was then dropwisely added via a syringe pump at a rate of 30 ul/min. After the reaction is stopped, the resulted silver nanowires were purified with ethanol for 8 times and stored in refrigerator for further characterization and test.

4.2.4 Characterization

Scanning electron microscopy (SEM) was conducted on a NovaNanoSEM 450. Transmission electron microscopy (TEM), scanning transmission electron microscopy (STEM) and energy dispersive X-ray spectroscopy (EDS) were conducted on a ThermoFisher Scientific Titan Themis 300. UV-Vis spectra were measured with a VWR UV/Vis scanning UV-3100PC spectrophotometers.

4.2.5 Propagation Length Measurements

Propagation length measurements were conducted following similar method described in our previous works.[3, 13] A tapered optical fiber was placed un upright optical microscope (Nikon Eclipse Ni-U) with a 50× microscope objective having a numerical aperture of 0.6 and a black-illuminated CCD camera (Zyla 5.5, Andor, Belfast, UK). AgNWs and Ag@M NWs dispersed in ethanol were drop-cast on a PDMS film. The ethanol was evaporated slowly while the NWs drop was moved on the substrate using a nitrogen gun.

AgNWs were picked up with a tungsten probe mounted in a triple-axis micromanipulator (Sutter Instrument Co.) and put in contact with the optical fiber. Polarized 532 and 650 nm lasers were coupled to the NWs from the tapered optical fiber, yielding an output power at the fiber tip of a few microwatts. The intensity of the light at the tip of the NW was measured while the NWs were slid toward the end by controlling the tungsten probe. The light signals at the tip of the nanowire were collected by the CCD camera.

4.3 Result and Discussion

4.3.1 Core-Shell Ag@ M NWs

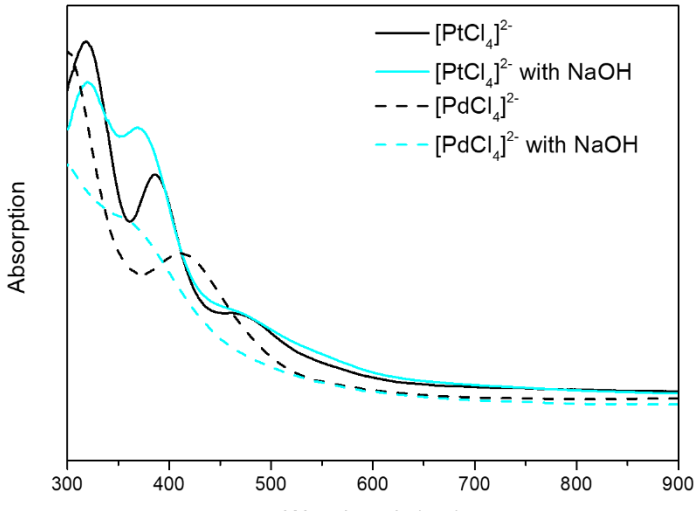

Figure 4.1 UV-Vis spectrum of $[PtCl_4]^{2-}$ and $[PdCl_4]^{2-}$ aqueous solutions and after ligand exchange with OH^-.

The synthesis of Ag@ M NWs followed a similar recipe reported in an early work of Suljo Linic *et al.*[21] with some modifications. When aqueous solution of $[PtCl_4]^{2-}$ and $[PdCl_4]^{2-}$ was added to aqueous mixture of AgNWs and the reducer L-AA, galvanic replacement happens immediately resulting etching to the silver nanowires since the reduction potential of of $[PtCl_4]^{2-}$ (0.755 V vs SHE) and $[PdCl_4]^{2-}$ (0.591 V vs SHE) are higher than that of AgCl (0.222 V vs SHE).[22, 23] To suppress the galvanic replacement, it

is desirable to form Pt and Pd metal complexes with lower reduction potential. With the addition of NaOH to the noble metal growth solutions, ligand exchange between Cl^- and OH^- can result lower reduction potential complex when the pH is tuned to be around 12. When NaOH solution is added, the color change in the growth solution indicates the ligand exchange between Cl^- and OH^-, which can be further confirmed with UV-Vis spectrum as shown in **Figure 4.1**. For both Pd and Pt cases, the addition of NaOH resulted a blue shift in the UV-Vis spectrum, suggesting formation of more stable complexes after Cl^- and OH^- ligand exchange.

Figure 4.2 shows the SEM images of the epitaxial Ag@ M NWs. The SEM images suggested after coating a layer of Pt and Pd to the silver nanowires, the results NWs are able to maintain reasonable smooth surface which is important to maintain low scattering loss during light propagation along the nanowires. Meanwhile, zoomed in SEM images at

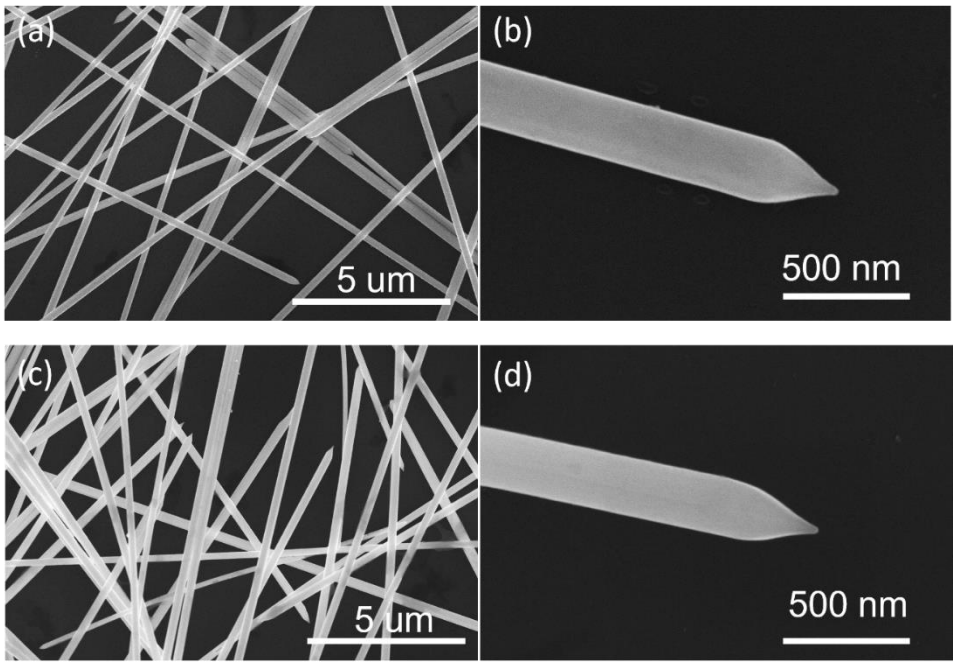

Figure 4.2 SEM images of Ag@ M NWs. (a,b) SEM images of Ag@ Pd NWs; (c, d) SEM images of Ag@ Pt NWs.

the tip region of the NWs shows with the preparation method mentioned earlier, with tuning the high pH to allow ligand exchange, galvanic replacement can be effectively suppressed that the sharpness of the silver nanowires is well protected which the major factor to achieve high spatial resolution in TERS measurement when the NWs are used in catalytic process studies.

While the SEM images showed that the resulted silver nanowires maintained smooth surface and sharp tips, we then conducted a series of characterization to verify the success of creating a core-shell structure. The product NWs were first drop-casted on silicon wafer and immersed into 2% H_2O_2 aqueous solution for 2 hours. After the silver is etched with hydrogen peroxide, smooth and contineous shell structure can be observed for both Ag@Pt and Ag@Pd NW prepared with the above mentioned method with SEM images shown in **Figure 4.3**.

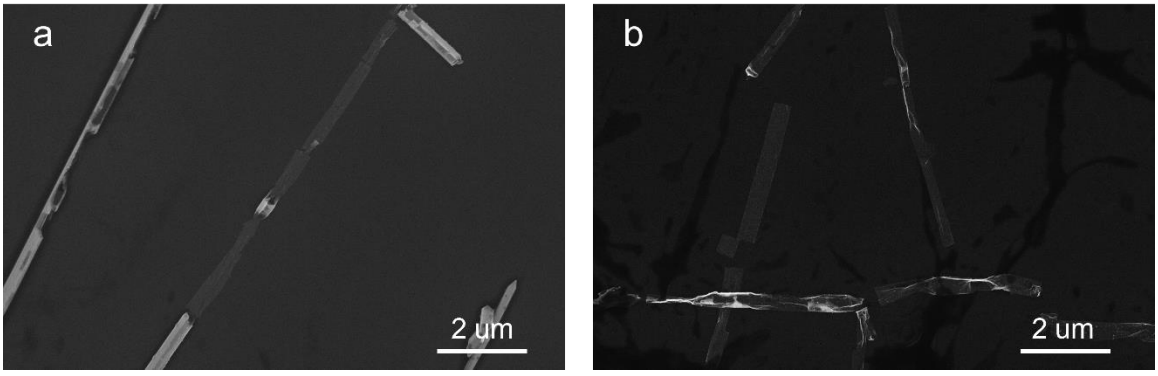

Figure 4.3 Ag@M NWs after etching with 2% H_2O_2 aqueous solution for 2 hours. (a) Ag@Pd NW; (b) Ag@Pt NW.

To confirm the elemental composition of the NWs, STEM-EDS measurements were conducted shown in **Figure 4.4** and **Figure 4.5**, a well-defined core-shell structure can be observed for both Ag@Pt and Ag@Pd NWs. The corresponding EDS maping images

suggest a uniform coating of Pt and Pd layer on to the silver nanowires both at the body and tip regions. The thickness of Pt and Pd shell can be controlled by varying the amount of growth solution added to the reaction mixture from syringes by adjusting the reaction time. With increasing of the reaction time, Pt and Pd shell thickness increases proved by the increased UV-Vis intensity and TEM images shown in **Figure 4.6** and **Figure 4.7**. The UV-Vis spectrums also show that during the synthesis, no nanoparticles of Pd and Pt was formed from homogeneous nucleation. By tuning the reaction time, we managed to control the Pt shell thickness from 3 to 9 nm and Pd shell thickness from 3 to 7 nm which can be tell from the TEM images. The high resolution TEM images zoom in at the shell area show epitaxial growth and single crystalline shell. The shell thickness of NWs propared at different conditions was also verified with EDS line scanning as shown in **Figure 4.8** and **Figure 4.9** agrees with TEM images.

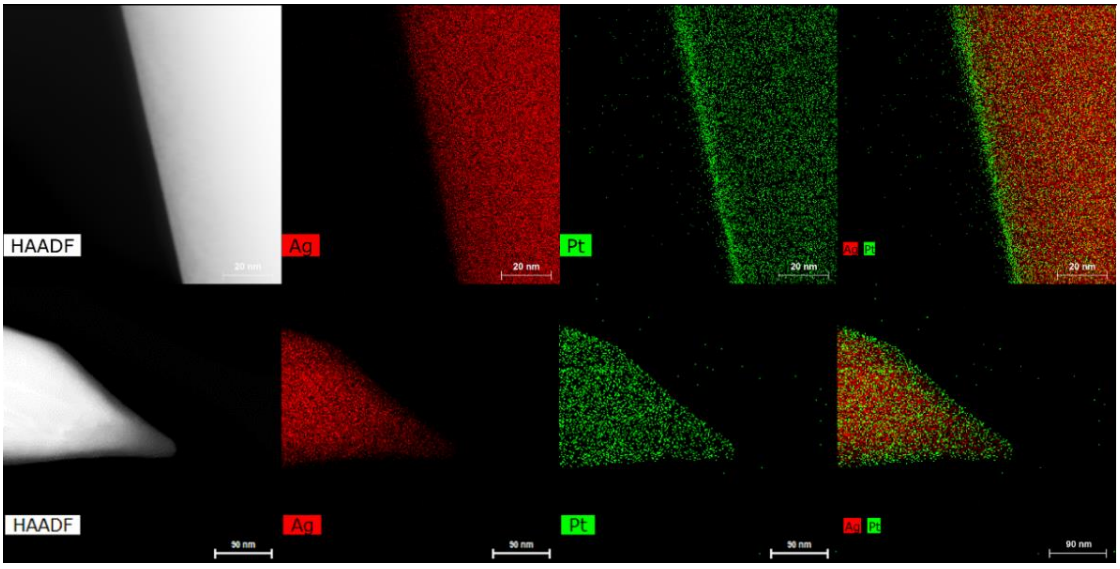

Figure 4.4 STEM-EDS images of sharp tip Ag@Pt NW.

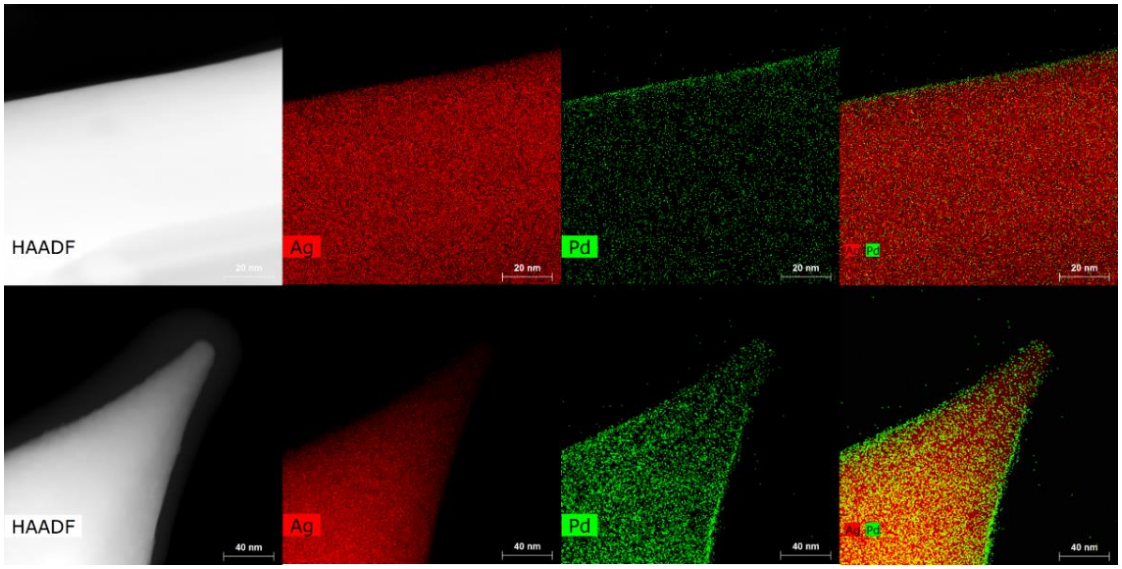

Figure 4.5 STEM-EDS images of sharp tip Ag@Pd NW.

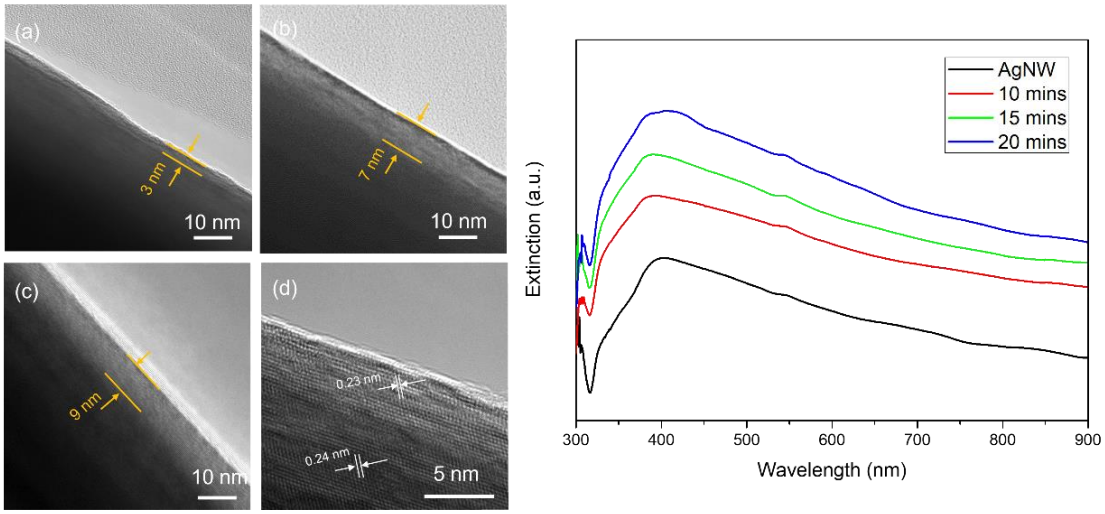

Figure 4.6 Tunable Pt shell thickness. (a~c)TEM images of Ag@Pt NWs synthesized with reaction time of 10 mins, 15 mins and 20 mins, respectively; (d) Zoom in TEM image at the shell core-shell interface; (e) UV-Vis extinction spectrum with corresponding reaction time.

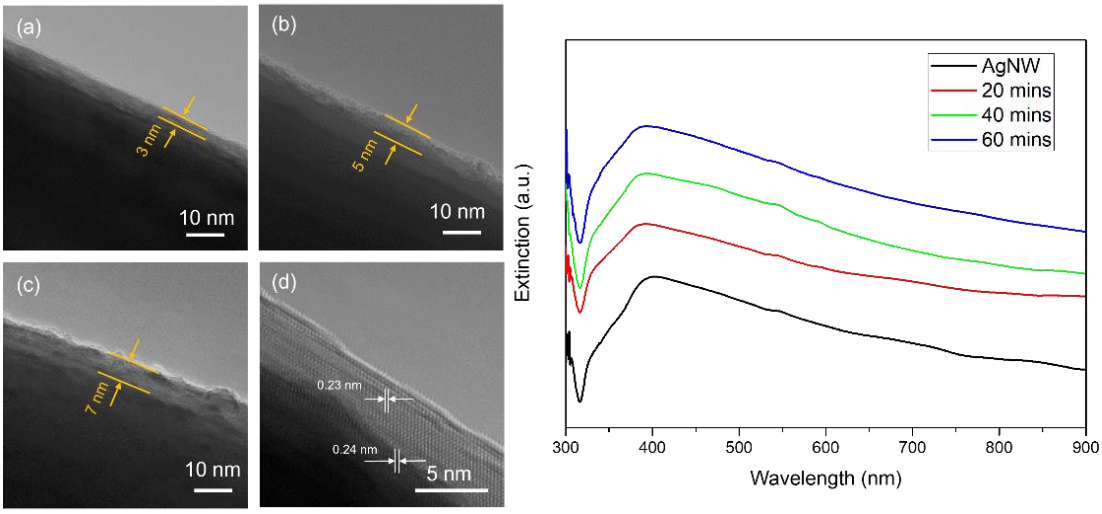

Figure 4.7 Tunable Pt shell thickness. (a~c)TEM images of Ag@Pd NWs synthesized with reaction time of 20 mins, 40 mins and 60 mins, respectively; (d) Zoom in TEM image at the shell core-shell interface; (e) UV-Vis extinction spectrum with corresponding reaction time.

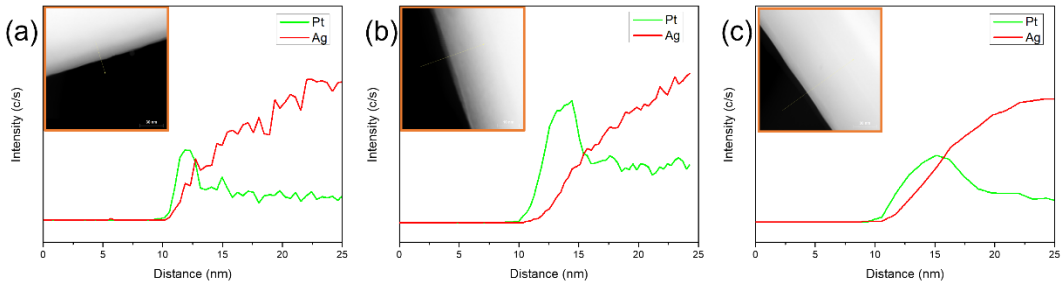

Figure 4.8 STEM-EDS line scan at the core-shell interface of Ag@Pt NWs prepared with different reaction time. (a) 10 minutes; (b) 15 minutes; (c) 20 minutes.

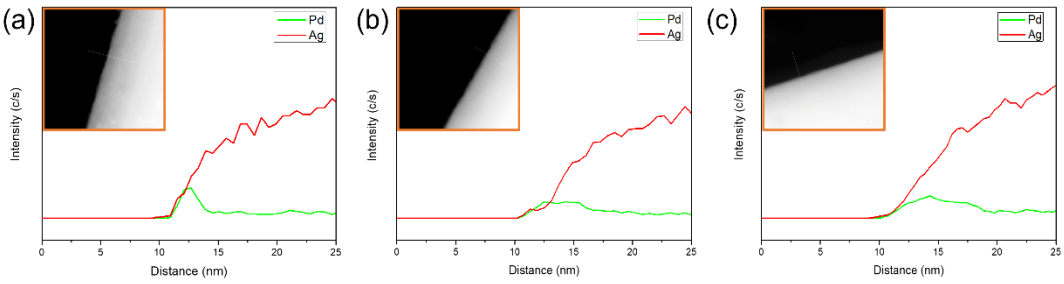

Figure 4.9 STEM-EDS line scan at the core-shell interface of Ag@Pd NWs prepared with different reaction time. (a) 20 minutes; (b) 40 minutes; (c) 60 minutes.

4.3.2 Ag@M NWs as Plasmonic Waveguide

To overcome diffraction limit of conventional Raman and confine light to sub-wavelength dimensions in the form of surface plasmon polaritons (SPPs), one-dimensional metallic nanostructures have been intensively studied among which silver nanowire is of special interest due to low ohmic loss and atomically smooth surface when silver nanowires are chemically synthesized.[24-29] A key factor that preventing the wide application of AgNW-based SPM probes is the fact that silver is sensitive and vulnerable to oxidation in harsh environments. While a thin smooth layer of Pt and Pd coating can significantly prolong the lifetime of AgNWs exposed to air, one needs to make sure that the Ag@M NWs do not compromise too much of the propagation length (L). With the method mentioned earlier, the propagation of both 532 nm and 650 nm laser light along pure AgNW, Ag@Pd NW and Ag@Pt NW are measured. The nanowires used for measurements have a diameter of 270 nm. In **Figure 4.10**, the tip emission intensity is calculated and plotted as a function of the propagation distance. While the intensity oscillates from the beating of different SPP mode, overall the intensity of light emission showed a decay trend for all the measurement.[3] The experimental propagation length was estimated when the intensity of light decays by a factor of 1/e.

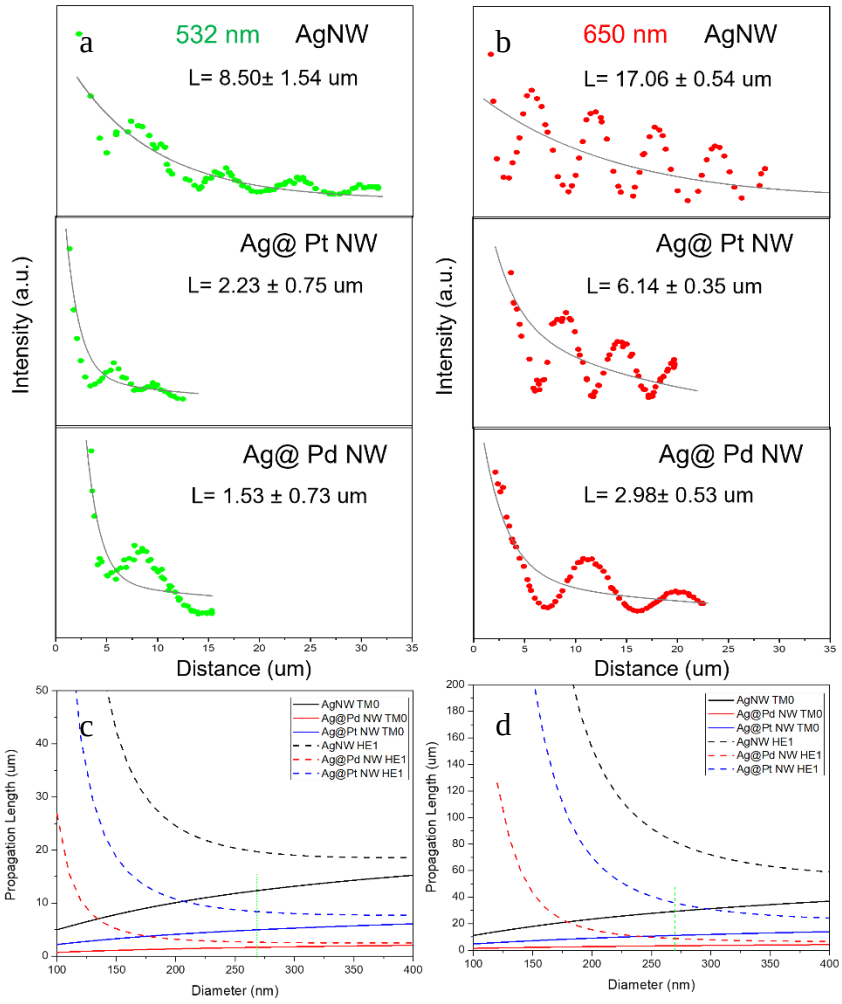

Figure 4.10 Measurement of SPP propagation length in free-standing nanowires. (a, b) Tip emission intensity of AgNW, Ag@Pt NW, Ag@Pd NW as a function of propagation distance with 532 nm and 650 nm excitation light. (c,d) Theoretical propagation length of fundamental mode and second order mode calculated for shell thickness of 3 nm.

From our estimation of 5 independent measurements of all type of nanowires and excitation wavelength, the propagation length of Ag@Pt NW and Ag@Pd NW at 532 nm and 650 nm all decreased when compared to that of pure AgNWs due to the fact that platinum and palladium have higher ohmic loss and the SPP propagation along the surface of metal waveguide while Ag@Pd NW showed greater decrease. For pure AgNW with a diameter of 270 nm, the propagation length was estimated to be 8.50 μm with 532 nm excitation and 17.06 μm with 650 nm excitation. Propagation length decreased to

2.23 μm, 1.53 μm with 532 nm excitation and 6.14 μm, 2.98 μm at 650 nm excitation for Ag@Pt NW and Ag@Pd NW, respectively. The decrease in propagation length was well expected and agrees with the simulation results shown in Figure 4.9 (c and d). The fact that the measured propagation lengths shorter than the simulation results can be attributed to stronger scattering loss in practical measurements.

Although coating a layer of a more stable noble metal over AgNWs could lead to decreased propagation length of light due to increased propagation loss, the resulted Ag@M NWs are still promising plasmonic waveguide to be used in TERS measurements especially considering that for practical scanning the protruding length is usually controlled well below 2 μm to increase scanning stability. As shown in **Figure 4.11**, when nanowires are mounted to a tapered optical fiber, strong light emission from the tip was observed with even 10 μm protruding length for both types of core-shell structured nanowires under 532 nm and 650 nm excitation. Meanwhile, no scattering was observed at the fiber and nanowire junction area, suggesting that when light is coupled into the nanowires, the coupling loss is low. All these findings proves that the Ag@Pt NW and Ag@Pd NW are promising plasmonic waveguides to be used in TERS measurements.

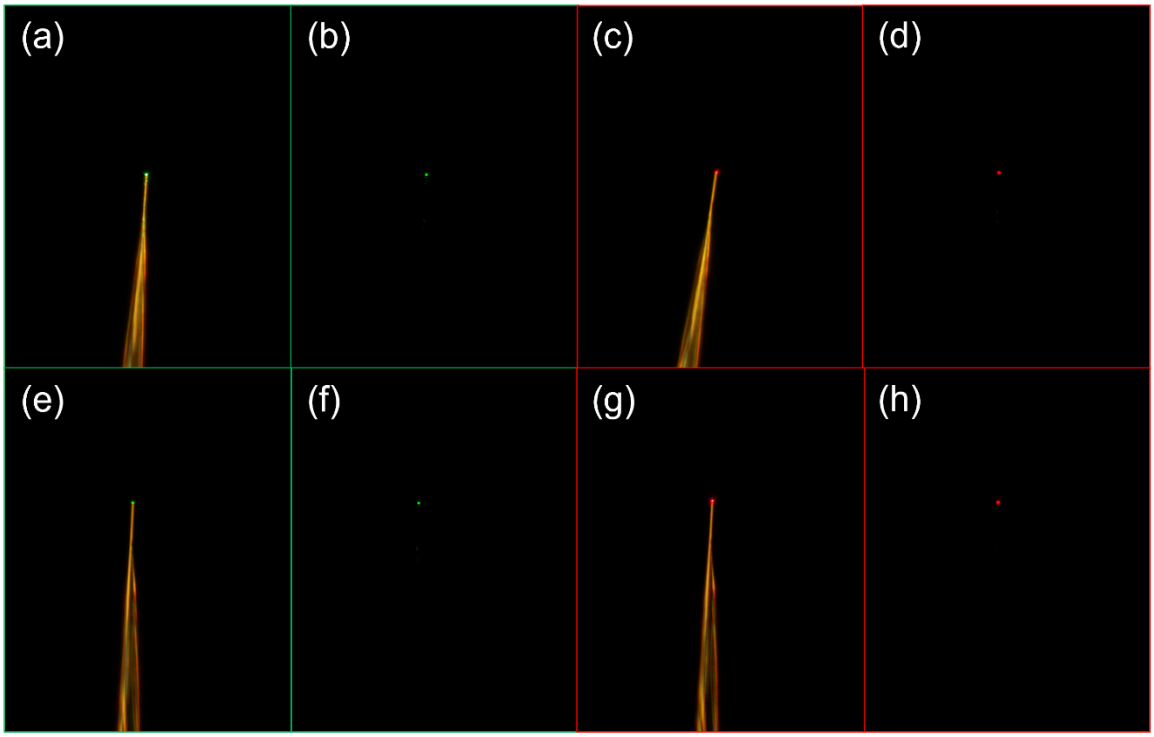

Figure 4.11 Light coupling and propagation along Ag@M NWs. (a) Ag@Pt NW with 532 nm laser (microscope light on); (b) Ag@Pt NW with 532 nm laser (microscope light off); (c) Ag@Pt NW with 650 nm laser (microscope light on); (d) Ag@Pt NW with 650 nm laser (microscope light off); (e) Ag@Pd NW with 532 nm laser (microscope light on); (f) Ag@Pd NW with 532 nm laser (microscope light off); (g) Ag@Pd NW with 650 nm laser (microscope light on); (h) Ag@Pd NW with 650 nm laser (microscope light off). Protruding length: 10 μm.

In summary, with the ultra-sharp silver nanowire we prepared in Chapter 3, we successfully infused a second noble metal layer to the sharp tip silver nanowires with epitaxial growth forming a well-defined core-shell structure by suppressing galvanic replacement via ligand exchange to the high reduction potential Pd and Pt precursors through a liquid phase room temperature synthesis method. By tuning the reaction time, the shell thickness can be controlled. The formation of core-shell structure was confirmed with STEM-EDS mapping and TEM images. With a uniform continuous shell structure of more stable noble metal over silver nanowires, the NWs are more robust against oxidation by air. While depositing a noble metal layer, the propagation length of SPP

along the NWs decreased significantly, the NWs mounted onto tapered optical fiber demonstrated great tip emissions even with 10 μm protruding length and minimal scattering loss suggesting the NWs are promising plasmonic waveguides to be used in TERS measurements. With a layer of Pt and Pd outside of the silver nanowires, the application of TERS in catalytic process can be significantly broadened to Pt and Pd catalyzed reactions in hasher environments.

4.4 References

1. Schmid, T.; Opilik, L.; Blum, C.; Zenobi, R., *Nanoscale Chemical Imaging Using Tip-Enhanced Raman Spectroscopy: A Critical Review*, *Angew Chem Int Edit*, **2013**, 52, (23), 5940-5954.

2. Blum, C.; Opilik, L.; Atkin, J. M.; Braun, K.; Kammer, S. B.; Kravtsov, V.; Kumar, N.; Lemeshko, S.; Li, J. F.; Luszcz, K.; Maleki, T.; Meixner, A. J.; Minne, S.; Raschke, M. B.; Ren, B.; Rogalski, J.; Roy, D.; Stephanidis, B.; Wang, X.; Zhang, D.; Zhong, J. H.; Zenobi, R., *Tip-enhanced Raman spectroscopy - an interlaboratory reproducibility and comparison study*, *J Raman Spectrosc*, **2014**, 45, (1), 22-31.

3. Kim, S.; Bailey, S.; Liu, M.; Yan, R. X., *Decoupling co-existing surface plasmon polariton (SPP) modes in a nanowire plasmonic waveguide for quantitative mode analysis*, *Nano Res*, **2017**, 10, (7), 2395-2404.

4. Qin, Q. Q.; Yin, S.; Cheng, G. M.; Li, X. Y.; Chang, T. H.; Richter, G.; Zhu, Y.; Gao, H. J., *Recoverable plasticity in penta-twinned metallic nanowires governed by dislocation nucleation and retraction*, *Nat Commun*, **2015**, 6.

5. Agapov, Rebecca L; Sokolov, Alexei P; Foster, Mark D. *Protecting TERS probes from degradation: extending mechanical and chemical stability*, *J Raman Spectrosc*, **2013**, 44, (5), 710-716.

6. Fujita, Yasuhiko; Chiba, Rie; Lu, Gang; Horimoto, Noriko N; Kajimoto, Shinji; Fukumura, Hiroshi; Uji-i, Hiroshi. *A silver nanowire-based tip suitable for STM tip-enhanced Raman scattering*, *Chem Commun*, **2014**, 50, (69), 9839-9841.

7. Chang, C. Y.; Batteas, J. D., *Novel and easy-to-use tip-enhanced Raman spectroscopy on opaque substrates with a micro-sized mirror and a silver-nanowire tip*, *Abstr Pap Am Chem S*, **2012**, 243.

8. Angel, S. M.; Gomer, N. R.; Sharma, S. K.; Mckay, C., *Remote Raman Spectroscopy for Planetary Exploration: A Review*, *Appl Spectrosc*, **2012**, 66, (2), 137-150.

9. Kim, Sanggon; Yu, Ning; Ma, Xuezhi; Zhu, Yangzhi; Liu, Qiushi; Liu, Ming; Yan, Ruoxue. *High external-efficiency nanofocusing for lens-free near-field optical nanoscopy*, *Nature Photonics*, **2019**.

10. Liu, Qiushi; Kim, Sanggon; Ma, Xuezhi; Yu, Ning; Zhu, Yangzhi; Deng, Siyu; Yan, Ruoxue; Zhao, Huijuan; Liu, Ming. *Ultra-sharp and surfactant-free silver nanowire for scanning tunneling microscopy and tip-enhanced Raman spectroscopy*, *Nanoscale*, **2019**, 11, (16), 7790-7797.

11. You, Yumeng; Purnawirman, NA; Hu, Hailong; Kasim, Johnson; Yang, Huanping; Du, Chaoling; Yu, Ting; Shen, Zexiang. *Tip -enhanced Raman spectroscopy*

using single-crystalline Ag nanowire as tip, *J Raman Spectrosc*, **2010**, 41, (10), 1156-1162.

12. Walke, Peter; Fujita, Yasuhiko; Peeters, Wannes; Toyouchi, Shuichi; Frederickx, Wout; De Feyter, Steven; Uji-i, Hiroshi. *Silver nanowires for highly reproducible cantilever based AFM-TERS microscopy: towards a universal TERS probe*, *Nanoscale*, **2018**, 10, (16), 7556-7565.

13. Zhu, Yangzhi; Kim, Sanggon; Ma, Xuezhi; Byrley, Peter; Yu, Ning; Liu, Qiushi; Sun, Xiaoming; Xu, Da; Peng, Sangshan; Hartel, Martin C.; Zhang, Shiming; Jucaud, Vadim; Dokmeci, Mehmet R.; Khademhosseini, Ali; Yan, Ruoxue. *Ultrathin-shell epitaxial Ag@Au core-shell nanowires for high-performance and chemically-stable electronic, optical, and mechanical devices*, *Nano Research*, **2021**.

14. Wu, Y. R.; Sun, X. J.; Yang, Y.; Li, J. M.; Zhang, Y.; Qin, D., *Enriching Silver Nanocrystals with a Second Noble Metal*, *Accounts Chem Res*, **2017**, 50, (7), 1774-1784.

15. Li, J. M.; Sun, X. J.; Qin, D., *Ag-Enriched Ag-Pd Bimetallic Nanoframes and Their Catalytic Properties*, *Chemnanomat*, **2016**, 2, (6), 494-499.

16. Sun, X. J.; Qin, D., *Co-titration of AgNO3 and HAuCl4: a new route to the synthesis of Ag@Ag-Au core-frame nanocubes with enhanced plasmonic and catalytic properties*, *J Mater Chem C*, **2015**, 3, (45), 11833-11841.

17. Liu, H. P.; Liu, T. Z.; Zhang, L.; Han, L.; Gao, C. B.; Yin, Y. D., *Etching-Free Epitaxial Growth of Gold on Silver Nanostructures for High Chemical Stability and Plasmonic Activity*, *Adv Funct Mater*, **2015**, 25, (34), 5435-5443.

18. Zhang, J. W.; Winget, S. A.; Wu, Y. R.; Su, D.; Sun, X. J.; Xie, Z. X.; Qin, D., *Ag@Au Concave Cuboctahedra: A Unique Probe for Monitoring Au-Catalyzed Reduction and Oxidation Reactions by Surface-Enhanced Raman Spectroscopy*, *Acs Nano*, **2016**, 10, (2), 2607-2616.

19. Wu, Y. R.; Zhang, J. W.; Winget, S.; Qin, D., *Ag@Au concave cuboctahedra for monitoring Au-catalyzed reduction and oxidation reactions by surface-enhanced Raman spectroscopy*, *Abstr Pap Am Chem S*, **2016**, 252.

20. Korte, K. E.; Skrabalak, S. E.; Xia, Y. N., *Rapid synthesis of silver nanowires through a CuCl- or CuCl2-mediated polyol process*, *Journal of Materials Chemistry*, **2008**, 18, (4), 437-441.

21. Aslam, U.; Linic, S., *Addressing Challenges and Scalability in the Synthesis of Thin Uniform Metal Shells on Large Metal Nanoparticle Cores: Case Study of Ag-Pt Core-Shell Nanocubes*, *Acs Appl Mater Inter*, **2017**, 9, (49), 43127-43132.

22. Xia, X. H.; Wang, Y.; Ruditskiy, A.; Xia, Y. N., *25th Anniversary Article: Galvanic Replacement: A Simple and Versatile Route to Hollow Nanostructures with Tunable and Well-Controlled Properties*, *Adv Mater*, **2013**, 25, (44), 6313-6333.

23. Yang, T. H.; Gilroy, K. D.; Xia, Y. N., *Reduction rate as a quantitative knob for achieving deterministic synthesis of colloidal metal nanocrystals*, *Chem Sci*, **2017**, 8, (10), 6730-6749.

24. Salandrino, A.; Wang, Y.; Zhang, X., *Nonlinear infrared plasmonic waveguide arrays*, *Nano Res*, **2016**, 9, (1), 224-229.

25. Pyayt, A. L.; Wiley, B.; Xia, Y. N.; Chen, A.; Dalton, L., *Integration of photonic and silver nanowire plasmonic waveguides*, *Nat Nanotechnol*, **2008**, 3, (11), 660-665.

26. Sanders, A. W.; Routenberg, D. A.; Wiley, B. J.; Xia, Y. N.; Dufresne, E. R.; Reed, M. A., *Observation of plasmon propagation, redirection, and fan-out in silver nanowires*, *Nano Lett*, **2006**, 6, (8), 1822-1826.

27. Knight, M. W.; Grady, N. K.; Bardhan, R.; Hao, F.; Nordlander, P.; Halas, N. J., *Nanoparticle-mediated coupling of light into a nanowire*, *Nano Lett*, **2007**, 7, (8), 2346-2350.

28. Yan, R. X.; Pausauskie, P.; Huang, J. X.; Yang, P. D., *Direct photonic-plasmonic coupling and routing in single nanowires*, *P Natl Acad Sci USA*, **2009**, 106, (50), 21045-21050.

29. Wei, H.; Zhang, S. P.; Tian, X. R.; Xu, H. X., *Highly tunable propagating surface plasmons on supported silver nanowires*, *P Natl Acad Sci USA*, **2013**, 110, (12), 4494-4499.

Chapter 5. Conclusion and Future Directions

While Raman is a powerful tool that can be used to identify chemicals in a mixed environment, two of the major issues significantly impede the wider application of Raman in research that the conventional Raman are weak signal intensity and low spatial resolution due to low ratio of inelastic scattering and diffraction limitation. To resolve these issues, surface and tip enhanced Raman spectroscopy has been developed that surface-enhanced Raman spectroscopy (SERS) mainly focused on solving the issue of weak Raman signal while tip-enhanced Raman can improve the spatial resolution overcoming the diffraction limit while enhancing Raman signal.

In this work, a one-pot synthesis method was developed for monodispersed silver nanocube with tunable size in a broad range from 60 to 180 nm. Allowing the synthesis solution to reflux for just a few minutes after stopping the precursor feeds, free Ag^{+} in the solution continues to be reduced, but the low concentration slowed down the growth rate which allows growth in more thermodynamically stable PVP passivated Ag (111) facets preventing the truncation at corners making large cube synthesis possible. SERS substrates were fabricated using LB assembly method from AgNCs with size of 100, 125, 140 nm, and the SERS measurement of 4-ATP absorbed on the corresponding substrates suggest the medium size AgNCs perform better as SERS substrate in terms of Raman signal enhancement.

TERS combines traditional Raman spectroscopy and near-field scanning optical microscopy that overcomes the diffraction limit, enabling to obtain Raman spectroscopy and topological image simultaneously at the nanoscale. Chemically synthesized silver nanowires (AgNWs) have been reported to be used as scanning probes. Specifically,

AgNW with sharp tips can significantly improve the Raman signals and spatial resolution. Here a two-step polyol synthetic method was developed to promote oxidative etching selectively to the ends of AgNWs, which eventually produce sharp tip AgNWs with over 96% selectivity and an average tip radius of 7.87 nm. Among atomic force microscope (AFM) probes fabricated by mounting silver nanowires with different tip sharpness onto commercial AFM cantilevers, the probe based on ultra-sharp AgNW showed significant improvement in spatial resolution in topographic scanning and enhancement factor of TERS tests over the same carbon nanotube sample compared to the probes based on AgNWs with regular pentagonal pyramid or rounded ends.

To broaden the application of TERS in catalysis field, a second noble metal (Pd, Pt) was successfully deposited onto ultra-sharp AgNWs creating a uniform core-shell structure with tunable shell thickness by varying the reaction time. With a thin shell of more stable noble metal, the NWs are more robust against oxidation compared with pure silver nanowires. Although with Pd and Pt shell, the SPP propagation length are significantly decreased especially for 532 nm excitation laser, these NWs are still promising to be used as TERS probes as there is minimal light scattering and strong tip emission when the NWs are mounted onto optical fiber under excitation light of 532 nm and 650 nm wavelength.

In my dissertation, I mainly focus on engineering the morphology of silver nanocrystals and demonstration of their performance in SERS and TERS to tackle the low signal and spatial resolution issues with normal Raman spectroscopy. While I have succeeded in preparing monodispersed AgNCs over a broad size range and achieved high yield ultra-sharp silver nanowires and demonstrated the feasibility of epitaxial growth of a second

noble metal (Pd, Pt) to the nanowires resulting core-shell nanowires suitable for TERS measurement in a harsher environment, more work could be done. The Pd and Pt coated silver nanowires can be tested in heterogeneous catalytic reactions with TERS if high spatial resolution is needed where normal Raman could not give desired resolution. Also, similar synthesis could be done to coat AgNCs with noble metal such as Au, Pd, Pt and the resulted NCs can be used as SERS substrate in an oxidative environment or reaction mechanism study such as detecting reaction intermediates in Pt and Pd catalyzed reactions.